

**Removal of Organic Pollutants Present in Water  
Using Inorganic-organic Hybrid Multifunctional  
Nanocomposites**

**by**

**Eric Jones**

A thesis submitted in partial fulfilment for the requirements for the degree of  
Master of Philosophy at the University of Central Lancashire

02/2017

## Table of Contents

Abstract .....	8
1. Literature Review .....	9
1.1. Dyes chemicals as organic pollutants .....	9
1.1.1. Methylene Blue .....	9
1.1.2. Congo Red .....	10
1.1.3 Allura Red AC .....	11
1.2 Adsorption and separation of organic pollutants. ....	12
1.3 Nano materials for organic pollutants reductions .....	14
1.3.1 Magnetic Nanoparticles .....	14
1.3.2 Carbon materials .....	16
1.4 Carbon Material Modification .....	24
1.4.1 Choosing a Photocatalyst - TiO <sub>2</sub> .....	24
1.4.2 Photocatalyst Optimisation .....	27
1.4.3 Photocatalytic Mechanism .....	29
1.4.4 Separation: Functionalization via the incorporation of iron oxide nanoparticles such as magnetite .....	32
1.4.5 Hybrid Ionic Liquid – Magnetic Nanocomposites .....	33
1.4.6 Selecting an Ionic Liquid for a hybrid nanocomposite .....	35
1.4.7 Ionic Liquid – Superparamagnetic Nanomaterial Hybrids .....	36
1.5 Adsorption kinetics of organic dyes by nanocomposites .....	37
1.6 Aims and Objectives .....	39
2. Materials and Methods .....	40
2.1 Chemicals .....	40
2.2 Nanocomposites synthesis .....	40
2.2.1. Superparamagnetic carbon based nanocomposites .....	40
2.2.2 Synthesis of Synthesis of Hybrid Ionic Liquid-Iron Oxide Nanocomposite .....	43
2.3 Physico-chemical characterisation .....	46
2.3.1 X-ray Diffraction .....	46
2.3.2 Fourier Transform Infra-Red Spectroscopy .....	47
2.3.3 Scanning Electron Microscopy/Energy Dispersive X-Ray Analysis .....	48
2.3.4 Nuclear Magnetic Resonance .....	50

2.4. Dye adsorption experiment .....	51
2.4.1 Methylene Blue .....	52
2.4.2 Congo Red.....	54
2.4.3 Allura Red AC.....	56
3. Results and Discussion.....	58
3.1 Adsorption of organic dyes by nanocomposites .....	58
3.1.1 Methylene Blue .....	58
3.1.2 Congo Red.....	63
3.1.3 Allura Red AC.....	68
3.2 Superparamagnetic carbon based nanocomposites .....	70
3.2.1 X-ray diffraction patterns.....	70
3.2.2 Fourier Transform Infra-red Spectra.....	72
3.2.3 Scanning Electron Microscope .....	79
3.2.4 Energy Dispersive Analysis using X-rays.....	80
3.3 Hybrid Ionic Liquid-Iron Oxide nanocomposites .....	82
3.3.1 Fourier Transform Infra-Red Spectra.....	82
3.3.2 Scanning Electron Microscope .....	83
3.3.3 Energy Dispersive Analysis using X-rays.....	84
3.4.1 Kinetics Methylene Blue.....	88
3.4.2 Kinetics Congo Red .....	90
3.4.3 Kinetics Allura Red AC .....	91
4. Conclusions and Future Work.....	93
References .....	95
Appendix .....	99

## List of Figures

Figure 1 Structure of Methylene Blue.....	9
Figure 2 Structure of Congo Red .....	10
Figure 3 Structure of Allura Red AC .....	11
Figure 4 Diagram of Activated Carbon pore distribution.....	16
Figure 5 Mechanism for synergistic enhancement in AC–TiO <sub>2</sub> composites. ....	17
Figure 6 Proposed Mechanisms of synergistic enhancement of TiO <sub>2</sub> -CNT .....	21
Figure 7 Mechanism of Photocatalysis .....	25
Figure 8 Enhancement of photocatalytic activity for TiO <sub>2</sub> , by MWCNTs. ....	29
Figure 9 TiO <sub>2</sub> Mechanism.....	31
Figure 10 Kinetics Rate Laws .....	37
Figure 11 Straight-Line Plot Graphs .....	38
Figure 12 Addition of a Thiol Group to SPION .....	43
Figure 13 Synthetic Step 2- Addition of Ionic Liquid to Iron Oxide.....	44
Figure 14 Figure 11. Iron Oxide-SIL-MPS-VOL .....	44
Figure 15 Schematic for XRD.....	47
Figure 16 Diagram of how an FT-IR functions .....	48
Figure 17 SEM-EDAX Diagram.....	49
Figure 18 Demonstration of excitation and relaxation of nucleus. ....	50
Figure 19 Methylene Blue Calibration Graph.....	53
Figure 20 Methylene Blue Starting Reagent Graph.....	54
Figure 21 Congo Red Calibration Graph .....	55
Figure 22 Allura Red AC Calibration Graph. ....	57
Figure 23 Methylene Blue Carbon + Iron Oxide Nanocomposites Data. ....	58
Figure 24. Methylene Blue Carbon/Iron Oxide/TiO <sub>2</sub> Nanocomposites Graph.....	59
Figure 25 Methylene Blue A against Ionic Liquid Nanocomposite Hybrid A, B, C and D Graph .....	61
Figure 26 Methylene Blue B against Ionic Liquid Nanocomposite Hybrid A, B, C and D Graph .....	62
Figure 27 Congo Red against Carbon/Iron Oxide/TiO <sub>2</sub> Graph.....	63
Figure 28 (a) Before Photocatalytic Test (b) After Photocatalytic Test .....	63
Figure 29 Congo Red A against Ionic Liquid Nanocomposite Hybrid A Graph. ....	65
Figure 30 Congo Red B against Ionic Liquid Nanocomposite Hybrid A Graph. ....	66

Figure 31 Allura Red AC (A) against Ionic Liquid Nanocomposite Hybrid A B C and D Graph .....	68
Figure 32 Allura Red AC (B) against Ionic Liquid Nanocomposite Hybrid A B C and D Graph .....	69
Figure 33 Iron Oxide-Activated Charcoal X-Ray Diffraction Pattern.....	70
Figure 34 Iron Oxide-Carbon Nanotube X-Ray Diffraction Pattern .....	71
Figure 35 FT-IR Methylene Blue Solution B 1.5 Absorbance (After removal of CNT/FeO/TiO <sub>2</sub> nanocomposite). .....	72
Figure 36 FT-IR Methylene Blue Solution A 0.5 Absorbance (After removal of CNT/FeO/TiO <sub>2</sub> nanocomposite). .....	72
Figure 37 Congo Red Solution B 1.5 Absorbance (After removal of CNT/FeO/TiO <sub>2</sub> nanocomposite). .....	73
Figure 38 Congo Red Solution A 0.5 Absorbance (After removal of CNT/FeO/TiO <sub>2</sub> nanocomposite) .....	74
Figure 39 Allura Red AC Solution B 1.5 Absorbance (After removal of CNT/FeO/TiO <sub>2</sub> nanocomposite). .....	74
Figure 40 Allura Red AC Solution A 0.5 Absorbance (After removal of CNT/FeO/TiO <sub>2</sub> nanocomposite). .....	75
Figure 41 Methylene Blue Solution B 1.5 Absorbance (After removal of AC/FeO/TiO <sub>2</sub> nanocomposite). .....	75
Figure 42. Methylene Blue Solution A 0.5 Absorbance (After removal of AC/FeO/TiO <sub>2</sub> nanocomposite). .....	76
Figure 43 Congo Red Solution B 1.5 Absorbance (After removal of AC/FeO/TiO <sub>2</sub> nanocomposite). .....	76
Figure 44 Congo Red Solution A 0.5 Absorbance (After removal of AC/FeO/TiO <sub>2</sub> nanocomposite). .....	77
Figure 45 Allura Red AC Solution B 1.5 Absorbance (After removal of AC/FeO/TiO <sub>2</sub> nanocomposite). .....	77
Figure 46 Allura Red AC Solution A 0.5 Absorbance (After removal of AC/FeO/TiO <sub>2</sub> nanocomposite). .....	78
Figure 47 (a) Carbon Nanotube-Iron Oxide Nanocomposites (b) Activated Charcoal-Iron Oxide Nanocomposite (c) Carbon Nanotube/Iron Oxide/Titanium Dioxide Nanocomposite (d) Activated Charcoal/Iron Oxide/Titanium Dioxide Nanocomposite.....	79
Figure 48 EDAX of AC-FeO-TiO <sub>2</sub> nanocomposite.....	80
Figure 49 EDAX of MWCNT-FeO-TiO <sub>2</sub> .....	81
Figure 50 Hybrid B (Ionic Liquid-Iron Oxide Hybrid B). .....	82

Figure 51 (a) Ionic Liquid-Iron Oxide Hybrid, (b) Image of porous Ionic Liquid-Iron Oxide Hybrid (c) Ionic Liquid-Iron Oxide Hybrid (d) Ionic Liquid-Iron Oxide Hybrid .....	83
Figure 52 EDAX of Ionic Liquid-Iron Oxide Hybrid A .....	84
Figure 53 EDAX of Ionic Liquid-Iron Oxide Hybrid B .....	85
Figure 54 EDAX of Ionic-Iron Oxide Hybrid C .....	86
Figure 55 EDAX of Ionic Liquid-Iron Oxide Hybrid D .....	87

## List of Tables

Table 1 Methylene Blue Calibration data .....	53
Table 2 Congo Red Calibration Data .....	55
Table 3 Allura Red Calibration Data .....	56
Table 4 Degradation kinetics of Methylene Blue Solution A with various carbon nanocomposites.....	88
Table 5 Degradation kinetics of Methylene Blue with ionic-liquid hybrid nanocomposites.....	88
Table 6. Degradation kinetics of Methylene Blue Solution B with ionic-liquid hybrid nanocomposites.....	89
Table 7. Degradation kinetics of Congo Red Solution A with ionic-liquid hybrid nanocomposites.....	90
Table 8. Degradation kinetics of Congo Red solution A with ionic-liquid hybrid nanocomposites.....	90
Table 9. Degradation kinetics of Congo Red solution B with ionic-liquid hybrid nanocomposites.....	91
Table 10. Degradation kinetics of Allure Red AC solution A with ionic-liquid hybrid nanocomposites.....	92
Table 11. Degradation kinetics of Congo Red solution B with ionic-liquid hybrid nanocomposites.....	92

## **Abstract**

Multifunctional Nanocomposites were synthesised with magnetic nanoparticles, photocatalyst (titanium dioxide) embedded into commercial carbon based nanomaterials such as activated charcoal and multi-walled carbon nanotubes. Novel hybrid Magnetic Ionic-liquid-nanocomposites were synthesised with silica coated magnetic nanoparticles and ionic-liquid.

These nanocomposites were characterised with scanning electron microscopy (SEM), fourier transform infrared spectroscopy (FTIR), x-ray diffraction (XRD), energy dispersive x-ray spectroscopy (EDAX) and nuclear magnetic resonance (NMR – Proton and Carbon). Their affinity for water purification was measured by, the decomposition and removal of three organic dyes (Methylene Blue, Congo Red and Allura Red) in controlled water samples. This was characterised with an ultraviolet-visible spectrometer. The rate at which dyes were adsorbed and broken down was measured by the relationship between concentration and absorbance. The UV-Vis data showed that the titanium dioxide-carbon based magnetic nanocomposites and novel magnetic ionic-liquid-nanocomposites have the capacity to reduce organic dye pollutants from water samples. However, kinetics data showed that the ionic-liquid-nanocomposites work at approximately half the efficiency of titanium dioxide-magnetic nanocomposites.

# 1. Literature Review

## 1.1. Dyes chemicals as organic pollutants

### 1.1.1. Methylene Blue

This research intends to evaluate the photocatalytic degradative ability/adsorption of magnetic nanocomposites against organic dyes.

Methylene blue is one of the most common to be tested against; it is frequently used in the textile industry. This dye has been subject to thousands of scientific papers worth of research – it is a staple in testing the adsorptive/degradative properties of nanocomposites.

Research reports that Methylene blue is a cationic dye; in the textile industry, it is commonly used for colouring paper, temporary hair colorant, dyeing cotton wools etc. [1] Its adsorption wavelength is in the range of 660-669nm.

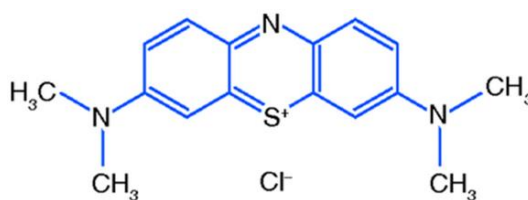


Figure 1 Structure of Methylene Blue (C<sub>16</sub>H<sub>18</sub>ClN<sub>3</sub>S) [2]

The decomposition of Methylene Blue has become a degradation standard due to its universal use and presence in factory wastewater.

Methylene Blue is not considered a toxic dye; however, it is known to cause harmful effects on living beings (Example causes nausea, vomiting and diarrhoea). [1]

### 1.1.2. Congo Red

Congo Red is another effluent in the dye industry. Congo Red dye (1-Naphthalenesulfonic acid, 3, 3'-(4, 4' biphenylene bis (azo) bis 4-amino) di sodium salt) is known to metabolize to benzedene, a known human carcinogen.

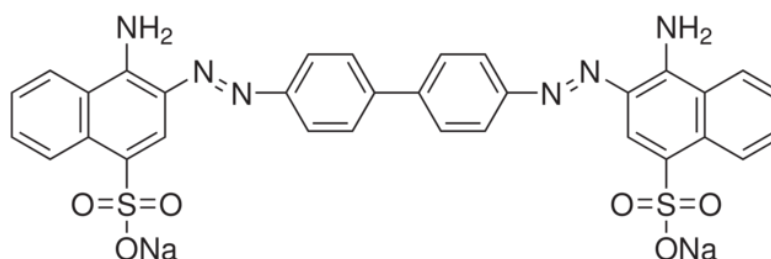


Figure 2 Structure of Congo Red [3]

Exposure to the dye has been known to cause allergic reactions (and possibly anaphylactic shock). The removal of dyes from industrial waste before they are discharged into the water bodies is important from health and hygiene point of view and for environmental protection. Its adsorption wavelength is in the range of 490-500nm. [4]

### 1.1.3 Allura Red AC

Allura Red AC is a waste product present in food industry wastewater. As the photo degradation of the organic dye Allura Red AC has not been thoroughly researched, this research aims to have novel research in the remove of this pollutant from water.

Allura Red AC is a red dye used as a food additive, it is known as E129.

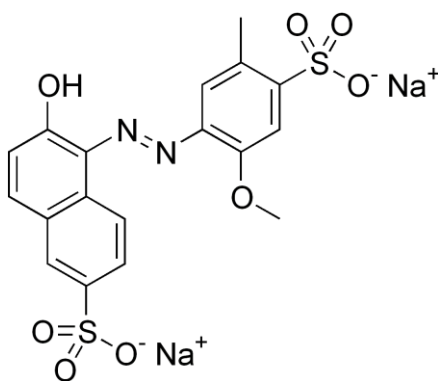


Figure 3 Structure of Allura Red AC [5]

Allura Red AC Additive is in the form of dark red powder, granule or red aqueous solution. It is used in pastry, confectionery and some drinks. When heated to decomposition it emits very toxic fumes of nitrogen and sulphur oxides. It is also a suspected carcinogen. Its adsorption wavelength is in the range of 504-510nm.

## 1.2 Adsorption and separation of organic pollutants.

A common method of monitoring and measuring photocatalysis; is measuring the degradation of organic compounds by use of a UV-Vis spectrophotometer.

The transmittance measured by the spectrophotometer is a function of the sample concentration per the Beer-Lambert Law; ( $A = \log_{10} P_0 / P$  [No units]). [6]

The Absorbance equation is as follows =  $e L c$ .

$e$  is the molar absorptivity (Adsorption coefficient) with units of  $L \text{ mol}^{-1} \text{ cm}^{-1}$ .

$L$  is the path length of the cuvette in which a sample is confined. (Commonly represented as 1cm, due to standardisation of cuvettes being the same size.)

$C$  is the concentration of the compound in solution, expressed in  $\text{mol L}^{-1}$ . [6]

To determine the concentration of compounds using a UV-Vis spectrometer, a calibration curve must be first generated from producing a series of standard solutions, i.e. producing a series of varied concentrations of the target dye against their absorbance. [6]

The adsorption coefficient (in regards to the formula the adsorption coefficient is equal to  $eL$ , in regards to the graph, this is the line of best fit) is determined experimentally at a specified wavelength through the construction of a calibration curve using the standard samples of the target dye.' [6] In this case, the specified wavelength will be around 663 – 670nm due that being the wavelength in Methylene absorbs light, 490-500nm for Congo Red and 504-510 for Allura Red AC. [1] [7] [8]

After calculating the adsorption coefficient ( $eL$  or line best-fit), together with the absorbance, it is possible to calculate the concentration for that solution.

This allows for the calculation of unknown concentrations of solutions to be calculated (if the absorbance is known). To calculate Concentration this simple calculation can be used: **Concentration = Absorbance / Slope**. [6]

Degradation of methylene blue should not only lead to a colour change; there should be a substantial decrease in the adsorption of light. This is due to the breakdown of MB's structure; MB can no longer absorb light produced by the UV-Vis spectrometer.

For degradation experiments, concentrations of  $1.5 \times 10^{-5}$  M seem to be a great starting point for research; due to a reflection of real world concentrations of effluents and the fact that higher concentrations of MB can affect the absorbency of UV-Vis spectrometers. [1] [9]

In the photocatalytic tests of the materials to be produced in this research, methylene blue, Congo Red and Allura will be used as the target "Pollutant" compounds. This is due to the fact these materials will be tested against a real world common effluent of the textile industry and food; therefore, these results will be comparable to other works in this field of research.

## **1.3 Nano materials for organic pollutants reductions**

### **1.3.1 Magnetic Nanoparticles**

Magnetic nanoparticles as the name suggests magnetic particles in the nanoscale ( $10^{-9}$  m). The most commonly used magnetic nanoparticle is magnetite (Iron Oxide) due to its availability, stability, relative inertness (not dangerous) and high magnetic susceptibility. An interesting trait that magnetite possess is superparamagnetism. This attribute occurs when the size of the nanoparticles is below a critical value around the range of 10–20 nm.

Superparamagnetism is the instance where the material does not have a permanent magnetic moment but can be magnetized via an external magnetic field. This is characterised as when a nanoparticle has a fast response to an applied magnetic field with negligible residual magnetism and coercivity (i.e. the field required to bring the magnetisation to zero).

Magnetic nanoparticles have been an interesting area of research for different sectors and applications. [10] In water purification, magnetic nanoparticles act as simple and effective separation agents via magnet; after its embedded catalyst, has broken down or captured the target impurity (for example capture of heavy metals or the photocatalytic breakdown of organic compounds. [10]

Other applications include the following:

In water purification, the magnetic nanoparticles act as a mode of removal i.e. after the nanocomposite has completed its task, it can simply be removed from the water

source by a magnet. [10] In drug delivery, an external magnetic field can control and guide a drug to a targeted area. [10] In hyperthermia, magnetic particles can be heated selectively by application of high frequency magnetic field in treatment of cancer. [11] Magnetic nanoparticles can also be employed as contrast agents for magnetic resonance imaging. [10]

Magnetic nanocomposites consisting of a mesoporous silica shell surrounding a magnetic core are an interesting class of nanocomposites. [12] The addition of mesoporous silica allows for enhanced surface functionalisation due to the presence of surface oxide groups and Sen et al has produced a method for synthesising

## 1.3.2 Carbon materials

### i) Activated Charcoal

Activated charcoal is also known as, activated carbon, active carbon and AC. Activated carbon is produced from burning coal, wood etc. It has a porous amorphous structure. It has a porosity which can span from the macro- (>25 nm), meso- (1–25 nm) and micro- (<1 nm) pore ranges. [13] [14]

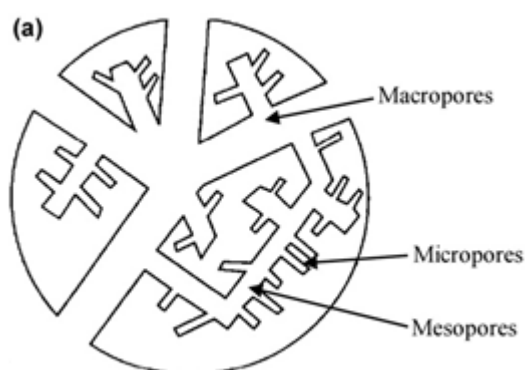


Figure 4 Diagram of Activated Carbon pore distribution. [65]

The amorphous nature of activated carbon provides a high-surface area structure. This is perfect for functionalisation as  $\text{TiO}_2$  particles may be distributed and immobilized. [14] [15]

AC- $\text{TiO}_2$  mixtures/composites are widely reported to yield improvements in photocatalytic activity over  $\text{TiO}_2$  alone. This is due to the porosity of the support; AC provides high adsorption capacity and ready passage of reacting species to the  $\text{TiO}_2$  particles.' [13] [16]

Activated carbon supports may play an active part in the mechanism of photocatalysis. This synergistic effect is due to the interaction between the support and the  $\text{TiO}_2$  particles, which enhances photocatalytic activity. [14] [17]

This has been demonstrated by Velasco et al. 2010 in regards to the degradation of phenol. During photocatalysis using AC– $\text{TiO}_2$ , different intermediate products were detected compared to the intermediates produced during the use of  $\text{TiO}_2$  alone. [13]

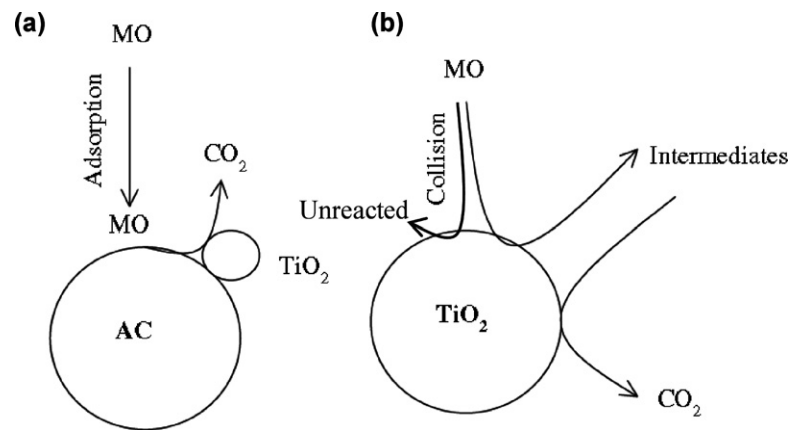


Figure 5 Mechanism for synergistic enhancement in AC– $\text{TiO}_2$  composites. [17]

Proposed mechanism of synergistic enhancement in AC– $\text{TiO}_2$  composites.

- (a) Adsorption onto the AC provides a high concentration of reactants near to the  $\text{TiO}_2$ , which may then be photo catalysed, possibly passing through intermediate stages. [18]
- (b) Without a highly adsorbent AC support, reactants must collide with the  $\text{TiO}_2$  by chance, and remain in contact for the photocatalysis to proceed. When this fails, the reactants or intermediate products will pass back into solution and can only react further when they collide with  $\text{TiO}_2$  again. [18]

Zhang et al. 2005 Figure 5 shows the photo-induced mineralisation of methyl orange (MO) to emphasise the retention of intermediate products by AC; hence chain photocatalytic reactions are likely to proceed more easily than for TiO<sub>2</sub> alone. [18]

On (b) the arrow labelling unreacted MO is to highlight the fact that not all the reactants colliding with TiO<sub>2</sub> will be adsorbed. This is due to the limited surface area. When compared to image (a), adsorption of MO to AC is more likely due to abundant surface adsorption sites. [18]

Due to its properties as a catalyst support, being inert, cheap and easy to manufacture, activated charcoal is a highly attractive support option for commercial nanocomposites. [19]

Conversely even though activated charcoal can enhance the formation of smaller nanosize TiO<sub>2</sub> particles [20] and contains nanosize pores, analysis from Velasco et al. 2010 and Lee et al. 2004 suggests that the smaller pores are rarely permeated with TiO<sub>2</sub>; as TiO<sub>2</sub> remains on the outer macropores. [13] [21]

Hence, this potentially leaves much of the nanopores and nanoscale phenomena in activated charcoal supports underexploited. [14]

Additionally, the need for band-gap tuning of the TiO<sub>2</sub> remains as activated charcoal as a support does not chemically interact with the TiO<sub>2</sub>; this can only be overridden by including additional constituents are added to the system. [14]

## **ii) Carbon Nanotube Support (CNT's)**

Carbon nanotubes are allotropes of carbon with a cylindrical structure. CNTs can be in two main forms, single walled nanotubes (SWCNTs) and multi walled nanotubes

(MWCNTs). Multiwalled CNT's are formed from the combination of two or more single walled CNT's.

Differences between SWCNT's; the total specific surface area of SWCNT's is normally between the regions of 400–900 m<sup>2</sup> g<sup>-1</sup>. The total specific surface area of MWCNTs is between the regions of 200-400 m<sup>2</sup> g<sup>-1</sup>. [14] [16]. The surface area of solids is calculated using Brunauer-Emmett-Teller theory, also known as BET.

The specific surface area of a solid is determined by physical adsorption of a gas on the surface of the solid including the pore size distribution. By calculating the amount of adsorbate gas, corresponds to a monomolecular layer on the surface.

Physical adsorption results from relatively weak forces (van der Waals forces) between the adsorbate gas molecules and the adsorbent surface area of the test powder. The procedure is carried out at the temperature of liquid nitrogen. This information predicts the dissolution rate, as this rate is proportional to the specific surface area.

Single walled carbon nanotubes have greater surface areas than multi-walled nanotubes; however, MWCNT's are much cheaper and are more resistant to chemical change. For this area of research, the focus will be multi-walled carbon nanotubes.

Carbon nanotubes have the potential to provide reactive surface areas like nanocomposites that use activated carbon as a host. Reports say that CNTs provide scope for greater control of morphology, and varieties of different structural forms of CNT–TiO<sub>2</sub> photo catalysts. These include TiO<sub>2</sub> nanoparticles on SWCNTs and MWCNTs. [22] [23]

Carbon nanotubes are highly attractive as potential TiO<sub>2</sub> supports as they have the potential to increase the semiconductors photocatalytic activity. [22] [24]

This is due to their high-surface area, quality active sites and the potential to impede electron–hole recombination (by means of altering and modifying the band-gap of TiO<sub>2</sub>) which allows for visible light catalysis. [25] [10]

Carbon Nanotubes have a high efficiency for adsorption organic molecules. Their high adsorption largely comes from their high surface area, however in the aqueous phase CNT's can form loose aggregates due to the hydrophobicity of the graphite surface. [26]

This leads to a reduced effective surface area. Conversely, this isn't a major hindrance as carbon nanotubes also contain interstitial spaces and grooves; these are areas of high adsorption for organic molecules. [26]

Carbon nanotubes have the advantage of a much higher adsorption capacity for bulky organic molecules (I.e. they contain a pore which are accessible to by bulky organic molecules such as industrial effluents, pharmaceuticals, heavy metals etc.) than activated carbon.

Another advantages Carbon nanotubes have over activated carbon; they have a higher affinity for low molecular weight polar organic compounds. This is due to the different interactions that can occur between carbon nanotubes and potential industrial effluents, i.e. effluents can absorb via hydrogen bonding, covalent bonding, electrostatic interactions etc. [27]

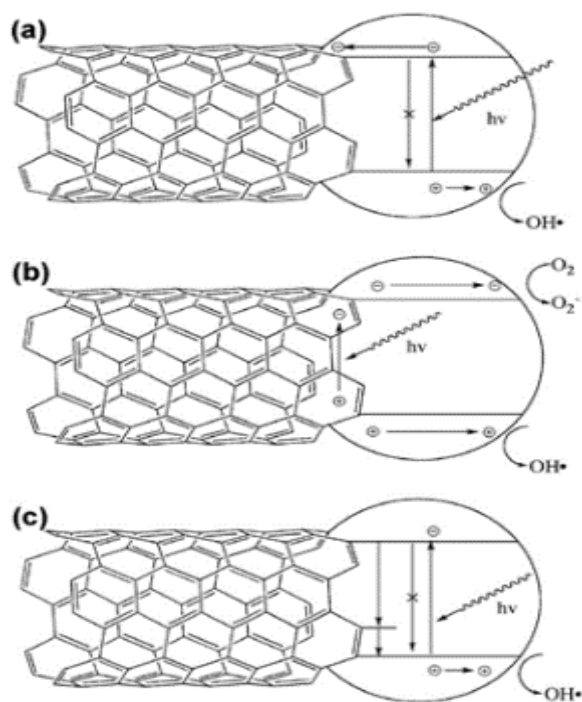


Figure 6 Proposed Mechanisms of synergistic enhancement of TiO<sub>2</sub>-CNT (a) (b) (c) [14]

Carbon Nanotubes have electron rich surface areas. This allows pep interactions between organic molecules with C=C double bonds, or aromatic rings (e.g. benzene, polycyclic aromatic, polar aromatic compounds i.e. organic waste products). [28] Organic compounds containing COOH, OH and NH<sub>2</sub> functional groups can form hydrogen bonds with the electron rich CNT surfaces (i.e. the graphite like surface). [29]Electrostatic attractions enable the adsorption of positively charged organic chemicals. [30]

TiO<sub>2</sub> is an n-type semiconductor, but in the presence of CNTs, photo generated electrons may move freely towards the CNT surface, which may have a lower Fermi level. [14] [31]

Figure 6 Produced by Leary & Westwood 2011: Diagram shows three proposed mechanisms of synergistic enhancement in TiO<sub>2</sub>-CNT nanocomposites. [14]

Diagram (a) proposes that the CNTs inhibit recombination by acting as sink for photo-generated electrons in TiO<sub>2</sub>. [32]

Diagram (b) proposes that a photosensitizing mechanism; which is based on electron–hole pair generation in the CNT. Depending on the relevant positions of the bands, the electron or hole may be injected into the TiO<sub>2</sub>, generating O<sub>2</sub><sup>-</sup> or ·OH species.” (Mechanism proposed by Wang et al. 2005). [14] [23]

Diagram (c) proposes that CNTs act as impurities through the Ti–O–C bonds (Mechanism proposed by Woan et al. 2009). [33]

It is theorised from diagram (a) that carbon nanotubes act as an electron sink. This leaves an excess of holes in the valence band of the TiO<sub>2</sub>, which can migrate to the surface and react; the TiO<sub>2</sub> therefore behaves as a p-type semiconductor. [32]

Carbon Nanotubes have characteristic properties such as high electrical conductivity [1] and high electron storage capacity (one electron for every 32 carbon atoms) [4]. Therefore, CNTs may act as extremely effective electron sinks. Kang et al. 2006 has shown that generating nanoscale TiO<sub>2</sub> morphologies with high aspect ratio play a role in retardation of electron–hole recombination. [34]

It is theorised from diagram (b) from Wang et al. 2005 second proposed mechanism, the photo generated electron in the CNT is transferred into the conduction band of the TiO<sub>2</sub>. This allows reduction to take place i.e. the formation of superoxide radicals by adsorbed molecular oxygen. The positively charged carbon nanotube then removes an electron from the valence band of the TiO<sub>2</sub>, leaving a hole. The positively charged TiO<sub>2</sub> can then take part in an oxidation process; for example, with water to form hydroxyl radicals. [32]

It is theorised from diagram (c) that Woan et al. 2009 proposes that CNT–TiO<sub>2</sub> systems may be more complex. The nanocomposites enhanced photocatalytic activity is due to two distinct effects leading to enhanced [33] [35]. The first effect is the presence of the C-O-Ti bond, which extends light adsorption to longer wavelengths. Woan et al. also proposes that this mechanism works like that of Carbon Doped TiO<sub>2</sub>. [36]

The second effect is a result from the electronic configuration of the CNTs; with greater numbers of mid band-gap states introduced by defects results in a higher photocatalytic activity. [33] [37]

According to research, the electronic-band structure of the CNT is more important for photocatalytic activity than the bond between the CNT and TiO<sub>2</sub>. [33]

Woan et al. 2009 also suggests that during photocatalysis, some degree of CNT oxidation is predicted to occur. Oxidised portions of CNTs may firstly permit defect states, which allows for enhanced photo- generation of electron–hole pairs. [33]

TiO<sub>2</sub>-CNT nanocomposites have been reported by various papers (Such as Yao et al. 2008, Yu et al. 2005, Ahmmad et al. 2008 etc), synergistically enhance the photocatalytic activity of TiO<sub>2</sub> through the retardation of electron–hole recombination. [39] [40]

CNT-TiO<sub>2</sub> Nanocomposites produced in these papers produced composites that were capable of adsorption light in the visible spectrum (I.e. Results showed that pure TiO<sub>2</sub> required UV light for positive results, whereas CNT-TiO<sub>2</sub> nanocomposites broke down target dye without the need of UV light). [38] [41]

## 1.4 Carbon Material Modification

### 1.4.1 Choosing a Photocatalyst - TiO<sub>2</sub>

TiO<sub>2</sub> is an ideal photocatalyst due to its low cost, stability and chemical properties. It offers the potential for simple and cheap methods for removing organic pollutants from polluted water sources, primarily industrial wastewaters. [10] [42]

Its application is normally restricted to ultraviolet (UV) environments due to its high band gap (3.2 eV) (Note this only occurs when in the Anatase phase). For TiO<sub>2</sub> nanomaterials to have applications as photo catalysts in visible light environments, its band gap must be lowered. [43] [44]

TiO<sub>2</sub> photocatalytic ability works via photocatalytic oxidation. Photocatalytic oxidation is an advanced oxidation process (AOP). AOP's remove organic materials in water and wastewater by oxidation through reactions with hydroxyl radicals ( $\cdot\text{OH}$ ). [45]

TiO<sub>2</sub> nanoparticles absorb ultraviolet light of 390 nm or less and generate active oxygen such as hydroxyl radicals and superoxide anions, after which this active oxygen with a strong oxidant activity can decompose organic materials. The mechanism is shown in Figure 7. [46]

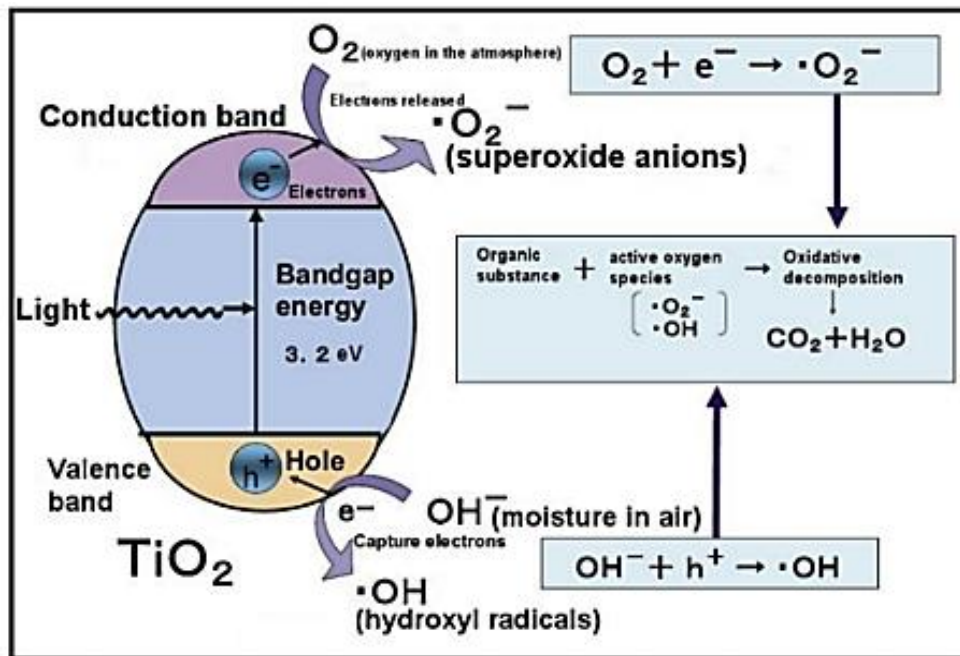


Figure 7 Mechanism of Photocatalysis [46]

$\text{TiO}_2$  absorbs UV radiation from a source such as Sunlight, UV lamps etc., this produces electrons and holes in the conduction and valence bands. [46]

These electrons of the valence band in  $\text{TiO}_2$  then become excited. The excess energy excites the electron and promotes it into the conduction band of  $\text{TiO}_2$ ; this is seen in the purple section of figure 7. This creates a state known as a semiconductor; i.e. negative electron ( $e^-$ ) in the conduction band and a positive-hole ( $h^+$ ) in the valence band. [46]

When Titanium dioxide is absorbing UV radiation in water, the positive-hole of titanium dioxide breaks apart water molecules to form hydrogen gas and a hydroxyl radical. This is seen in the green section of Figure 7. The negative electron reacts with oxygen molecule to form a super oxide anion. This cycle will continue if ultraviolet light is present. [46]

The energy difference between the valence band and the conduction band is known as the 'Band Gap'. Wavelength of the light necessary for photo-excitation is:  $1240$  (Planck's constant,  $h$ ) /  $3.2$  eV (band gap energy) =  $388$  nm. [13]

The use of  $\text{TiO}_2$  also makes it possible to degrade organic molecules that are resistant to oxidation, since the electrons in the conduction band can potentially reduce them. [32]

Hydroxyl radicals are very powerful reactive species and can virtually decompose any organic pollutant present in water; including pollutants that are highly chemically stable and resistant to mineralisation (E.g. organic dyes from the textile industry such as methylene blue). [37] [47]

The primary reaction pathways of hydroxyl radicals with organic compounds include hydrogen abstraction from aliphatic carbons, addition to double bonds and aromatic rings, and electron transfer. [21]

‘These reactions then go onto generate organic radicals as intermediates, which then undergo further reactions, eventually resulting in final products corresponding to the net oxidative degradation of the starting molecule.’ These organic compounds can degrade into much less harmful natural products such as  $\text{CO}_2$ ,  $\text{CH}_4$ ,  $\text{H}_2\text{O}$  etc. (I.e. mineralisation products). [21]

## 1.4.2 Photocatalyst Optimisation

Photo activity of nanosize  $\text{TiO}_2$  can be enhanced by adjusting particle size and shape, reducing negative electron ( $e^-$ ) and positive-hole ( $h^+$ ) pair ( $e^-/h^+$ ) recombination via metal doping, and enhancing contaminant adsorption. [48]

Titanium dioxide has two main forms, anatase and rutile. Both crystal forms possess substantial photocatalytic ability. [48]

When considering characteristics such as toxicity, resistance to photo corrosion, availability, catalytic efficiency and cost; the anatase form is the more favoured crystal structure. [48]

The anatase form is less thermodynamically stable than rutile; it is converted to rutile phase at high temperatures. However, this only occurs at very high temperatures  $>600^\circ\text{C}$ . The use of anatase  $\text{TiO}_2$  catalysts will be used at room temperature so there is no chance of conversion to other phases via temperature. [15] [16] [23]

The anatase form has a higher Fermi level over rutile by 0.2 eV. This leads to a lower oxygen affinity and a higher level of hydroxyl groups on the surface. These hydroxyl groups contribute to improving its photocatalytic ability. [15] [16] [23]

Note: that the Fermi level of anatase equals to 3.2 eV; Rutile Fermi level equals 3.0 respectively. [49]

This means that the anatase form of  $\text{TiO}_2$  can only be excited under irradiation of UV light at wavelengths lower than 380 nm; while rutile can be excited at wavelengths above  $>410$  nm, which is in the visible light spectrum. [50]

The advancement of research in regards of photo catalysts capable of adsorption light in the visible region of the spectrum is of great interest. This requires engineering the band-gap to less than 3.0 eV. [43]

Due to the advantages of anatase  $\text{TiO}_2$  a lot of recent research regarding  $\text{TiO}_2$  nanocomposites seem to favour the anatase phase in their synthesis e.g., Wang et al. 2005, Zhao et al. 2013 and Zhan et al. 2014.

$\text{TiO}_2$  in nanotube form have been found to be more efficient than  $\text{TiO}_2$  nanoparticles in the decomposition of organic compounds. [52]

This greater photocatalytic activity has been accredited to a shorter carrier-diffusion path in the tube walls and faster mass transfer of reactants toward the nanotube surface. [52]

Reports say, modifying  $\text{TiO}_2$  with a carbonaceous substance on the surface can induce visible-light responsive activity. [53] [54] [55]

### 1.4.3 Photocatalytic Mechanism

Zhao et al. 2013 proposed that MWCNTs can enhance the photocatalytic activity of  $\text{TiO}_2$  in two aspects specifically  $e^-$  transportation and adsorption. [37]

The results from Zhao et al. confirm that the MWCNT/ $\text{TiO}_2$  can induce the formation of hydroxyl radical under visible-light irradiation ( $\lambda > 450$ ). [37]

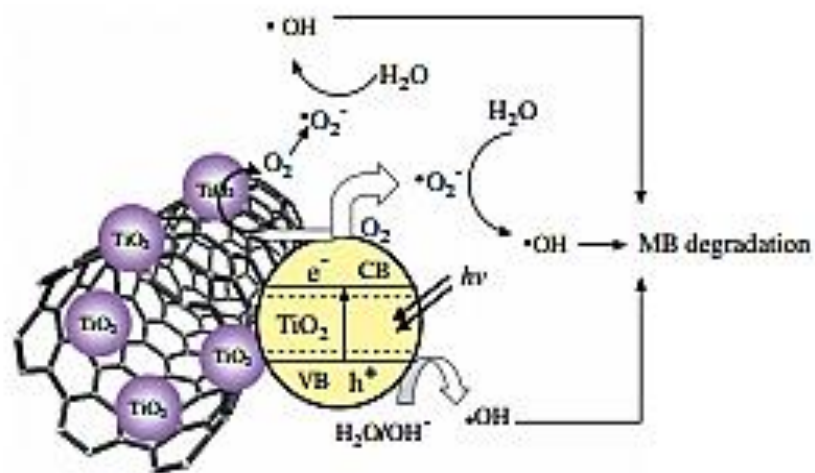


Figure 8 Enhancement of photocatalytic activity for  $\text{TiO}_2$ , by MWCNTs. [37]

Photocatalytic ability relies on the hole of the joint system, being positioned near the  $\text{TiO}_2$  valence band, as it needs 2.4 V versus normal hydrogen electrode to drive the hydroxyl radical formation. [37]

Under UV light radiation, electrons ( $e^-$ ) are excited from the valence band (VB) to the conduction band (CB) of  $\text{TiO}_2$ , creating a charge valency or hole ( $h^+$ ), in the valence band. [37]

Without MWCNT's, most of these charges recombine without doing any chemistry. Typically, only a small number of electrons (<1%) and hole are trapped and participate in photocatalytic reactions, resulting in low reactivity. [39]

Li & Gray 2007 reports that the conduction band position of anatase is about -4.21 eV using vacuum level as a reference, with a band gap of about 3.2 eV. [39]

When TiO<sub>2</sub> nanoparticles are in close contact with MWCNTs, the position of the MWCNT conduction band allows for the transfer of electrons from TiO<sub>2</sub> surface; this allows for charge separation, stabilization, and recombination. [37] [39]

Excited electrons are then shuttled freely along the conducting network of MWCNTs and then transferred to the surface to react with water and oxygen to yield hydroxyl radical, which oxidises methylene blue. [37]

The longer-lived holes on TiO<sub>2</sub>, give details for the higher activity of the MWCNT/TiO<sub>2</sub> photocatalyst. Additionally, the adsorption ability of TiO<sub>2</sub> bound to MWCNTs is greatly increased due to the increased available active sites on the surfaces of MWCNTs. [37]

O<sub>2</sub> may be adsorbed on the surfaces of MWCNTs, the e<sup>-</sup> in the MWCNTs react with O<sub>2</sub> and finally forms •OH, which oxidizes the adsorbed MB directly on the surfaces. [37]

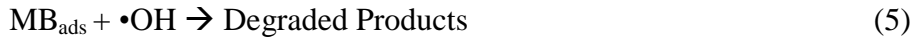
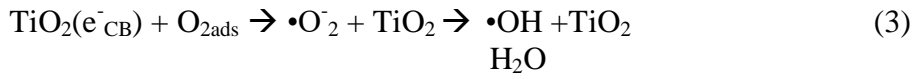
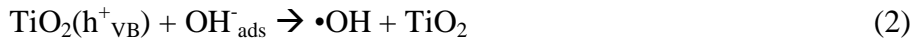
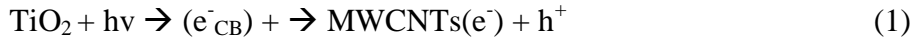


Figure 9 TiO<sub>2</sub> Mechanism [37]

Figure 9 describes the Hydroxyl free radical formation and photo degradation methylene Blue.

Yu et al [37] reported that the amount of  $\bullet\text{OH}$  formed in the system; with TiO<sub>2</sub> bound to MWCNTs is more than that with TiO<sub>2</sub> alone as a photocatalyst. Methylene blue molecules can re-allocate from the solution to the catalyst's surfaces. Which are then adsorbed with offset face-to-face orientation by p-p conjugation. Therefore, absorptivity of methylene blue on MWCNTs increases compared to that of methylene blue on bare TiO<sub>2</sub>. Therefore, CNT/TiO<sub>2</sub> nanocomposite materials have higher efficiencies as photo catalysts, compared to stand alone TiO<sub>2</sub> catalysts. Zhao et al. 2013 research has produced MWCNT/TiO<sub>2</sub> in the anatase phase. Their nanocomposite material can absorb a high amount of photo energy in the visible-light region, producing effective photochemical degradation reactions. [37]

Photochemical characterization of their MWCNT/TiO<sub>2</sub> confirmed that the origin of photocatalytic activity under visible-light is due to a direct optical charge transition involving both TiO<sub>2</sub> and MWCNTs, keeping the high reactivity of the photo generated electron and hole.

#### **1.4.4 Separation: Functionalization via the incorporation of iron oxide nanoparticles such as magnetite**

The application of TiO<sub>2</sub>/Carbon Nanocomposites for water treatment experiences a common obstacle; separation of such miniscule particles from large volumes of water requires additional expenditure on utilising modern water purification techniques makes almost makes the nanomaterial redundant, for example, purifying wastewater into drinking water in third world countries. The need for clean water in developing worlds is of the utmost importance. There is no point adding nanomaterials into polluted water with the intention to purify – with no way to remove the nanomaterials. Any leftover nanomaterials will be left over making the water unsanitary thereby making the nanomaterials redundant.

This research proposes a way to get around this problem, by synthesising a structure of compromising of TiO<sub>2</sub> (photo catalyst) and Iron Oxide (superparamagnetic). This method eliminates the separation problem of TiO<sub>2</sub> while retaining its photo catalytic ability.

Magnetic colloids allow for a very convenient recovery of the catalyst under an external magnetic field.

The incorporation of Iron Oxide magnetic particles into TiO<sub>2</sub> matrix also has the potential to block the aggregation of nanoparticles during renewal and can increase the durability of the catalysts. [40] [52]

A problem arises from directly bonding of TiO<sub>2</sub> on magnetic Iron Oxide decreases photocatalytic efficiency due to photo dissolution of Iron Oxide and the transfer of electron holes from TiO<sub>2</sub> to the core. [52]

To prevent the effects of photo dissolution, Carbon Nanotube/Activated Carbon acts as the support. CNT-Iron Oxide / AC-Iron Oxide nanocomposites will be synthesised first, then TiO<sub>2</sub> is added during another step. The photocatalytic efficiency of titanium dioxide does not decrease and the superparamagnetic properties of magnetite are retained. [56]

#### **1.4.5 Hybrid Ionic Liquid – Magnetic Nanocomposites**

Ionic Liquids (ILs) are known as molten salts, composed of ions that are poorly coordinated, which results in these solvents being liquid below 100°C, or even at room temperature (room temperature ionic liquids, RTIL's). [56] IL's at room temperature are composed of large, asymmetrically shaped, flexible ions, with delocalization of the electrostatic charge, or a combination of these factors. [45] Ionic liquids are highly structured in comparison with most molecular liquids. [57] At least one ion has a delocalized charge and one component is organic. The ionic charges impose a characteristic structure dictated by electroneutrality. [58]

In an ionic liquid, four to six ions of opposite sign surround an ion and successively less ordered layers of ions of alternating charge. These local order effects imposed by Coulomb forces have a longer range than molecular liquids; these features contribute to hinder crystallisation. [58]

The organic cations usually appear as imidazolium, pyridinium, pyrrolidinium, ammonium or phosphonium and either organic or inorganic anions appear as acetate, trifluoroacetate, tetrafluoroborate, hexafluorophosphate or bromide anions. [56] IL's have many unique physicochemical properties such as enhanced thermal stability, liquid on a wide temperature range, high electrical conductivity and enlarged electrochemical window (Up to 6V). [52] [56] [57]

Being salts, they are non-volatile their vapour pressure is virtually zero at moderate temperatures). [57] Ionic liquids are also essentially insoluble in weakly polar organic phases and some are hydrophobic. [56] They are miscible with a wide range of organic solvents, have good extractability for many different organic, inorganic and organometallic compounds. [57]

It is possible to prepare ionic liquids by combining cations and anions of different families and by modifying functional groups in their chemical structures. These properties have led these compounds are considered as "designer solvents" with tuneable properties in view of applications. [58] They also offer recycling options because of their stability, non-volatility and immiscibility in other solvents. [89] Ionic liquids contain not only charged groups, but also non-polar alkyl chains that can reach significant lengths and induce medium and long-range heterogeneities. [58]

#### 1.4.6 Selecting an Ionic Liquid for a hybrid nanocomposite

Dr. Xiaoqiang Qiao of Hebei University most recent work entitled “Imidazolium embedded C<sub>8</sub> based stationary phase for simultaneous reversed-phase/hydrophilic interaction mixed-mode chromatography” has produced a very powerful separation Ionic Liquid technology. [59]

Dr. Xiaoqiang Qiao work has produced a SIL-MPS-VOL, (SIL = Silica, MPS =3-Mercaptopropyl) trimethoxy-silane, VOL = 1-Vinyl-3-Octylimidazolium) an ionic liquid embedded on a C<sub>8</sub> based stationary phase. [59]

His work has proposed that due to the introduction of the quaternary imidazolium group to the traditional C<sub>8</sub> stationary phase it has produced a column that demonstrates both reversed-phase liquid chromatography (RPLC) and hydrophilic interaction liquid chromatography (HILIC) retention mechanisms. [59]

His series of hydrophobic and hydrophilic tests were performed on this research, which included benzene homologues, anilines and positional isomers, nucleosides and nucleotides. These species were used to evaluate the developed SIL-MPS-VOL stationary phase. [59] A rapid separation time, high separation selectivity and planar selectivity was achieved compared to the commercially available C<sub>8</sub> column they had tested. [59]

### 1.4.7 Ionic Liquid – Superparamagnetic Nanomaterial Hybrids

Years of research has gone into the development of nanocomposites, for organic wastewater purification. For example, using different cores (such as Iron Oxide, SiO<sub>2</sub>, Graphene, MWCNT etc.) and different photo catalysts such as TiO<sub>2</sub>, ZnO, quantum dots etc. [10] However, Ionic Liquid Iron Oxide coated silica hybrids are an up and coming technology, as research for these types of compound is new. [60] [61] The most commonly used ionic liquids are imidazolium-based; these groups consist of a  $\pi$  conjugated system and an imidazole cation and can have multiple-interactions, such as electrostatic, dipole-dipole, hydrogen bonding, and  $\pi$  -  $\pi$  interaction. Hence, the potential for polar and non-polar compound interactions. [62]

The hydroxide groups of the SiO<sub>2</sub>, from the nanocomposite (Iron Oxide@ SiO<sub>2</sub>) act as a synthetic route point to attach an Ionic Liquid. By combining Sen et al<sup>3</sup> superparamagnetic silica nanocomposites and Qiao et al<sup>61</sup> Ionic Liquid technologies, in theory this allows for producing a novel compound with the following characteristics - magnetism (Mode of separation from water source i.e. collection), photocatalyst (Iron oxide may act as a photo catalyst under UV-Visible light) and organic polar/non-polar absorbent. [3] [61]

## 1.5 Adsorption kinetics of organic dyes by nanocomposites

The order of reaction gives an indication of the mechanism of degradation. For example, a zero-order reaction would not require the presence of nanocomposite.

First order reaction: the degradation is directly proportional to the presence of nanocomposite.

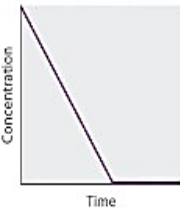
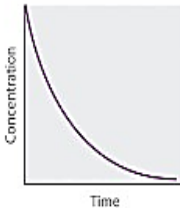
	Zeroth Order	First Order	Second Order
<b>Differential rate law</b>	Rate = $-\frac{\Delta[A]}{\Delta t} = k$	Rate = $-\frac{\Delta[A]}{\Delta t} = k[A]$	Rate = $-\frac{\Delta[A]}{\Delta t} = k[A]^2$
<b>Concentration vs. time</b>			
<b>Integrated rate law</b>	$[A] = [A]_0 - kt$	$[A] = [A]_0 e^{-kt}$ or $\ln[A] = \ln[A]_0 - kt$	$\frac{1}{[A]} = \frac{1}{[A]_0} + kt$

Figure 10 Kinetics Rate Laws

Above are the corresponding graphs we should obtain for each reaction order mechanism. The calibration graphs are of importance as they show the absorbance with respect to the concentration. This is especially useful for calculating unknown concentrations of known absorbance.

After producing the concentration vs. time graphs for each nanocomposite, it is possible to determine the reaction order for each nanocomposite, by producing a straight-line plot. By plotting graphs for the natural log (ln) of Concentration against time it can be determined if a reaction is 1<sup>st</sup> order. A 2<sup>nd</sup> order reaction can be determined by plotting 1/Concentration against time.

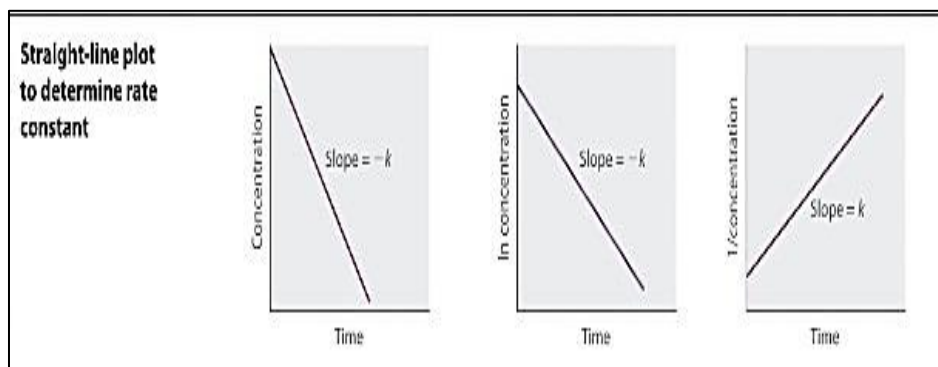


Figure 11 Straight-Line Plot Graphs

The rate constant (k) for each nanocomposite can be determined with this equation:

$$\ln(C) = \ln(C_0) - kt.$$

(Note: See Appendix for rate constant graphs and equations)

## 1.6 Aims and Objectives

### **Aims:**

This research aims to synthesize novel multifunctional organic/inorganic hybrid nanocomposites for purifying organic dye polluted water.

This research also aims to compare the efficiency and effectiveness of the various nanocomposites against one another; against several different coloured dyes at various concentrations.

### **Objectives:**

The objectives were as follows:

**Objective i)** Synthesis of multifunctional nanocomposites using commercially available carbon nanotubes and activated charcoal as a base matrix. Addition of multifunctional properties such as superparamagnetism (Source, Iron Oxide) and photo-catalysis (Source, Titanium Dioxide) to the nanocomposites.

**Objective ii)** Synthesis of novel hybrid superparamagnetic nanocomposites using silica-coated iron oxide nanoparticles with ionic liquids.

**Objective iii)** Assessing the ability of adsorption / photo-degradation of several organic compounds presence in water as model experiments using the materials developed in objective i) with one step magnetic separation and reuse of the material.

**Objective iv)** Assessing the ability of adsorption of small organic pollutants presence in water using the materials developed in objective ii) with one step magnetic separation.

## 2. Materials and Methods

### 2.1 Chemicals

Organic Dyes for Testing – Common Water Pollutants: Congo Red and Allura Red AC both purchased from (Sigma Aldrich UK). Methylene Blue was purchased from (Alfa Aesar UK).

Multi-Walled Carbon Nanotube  $\geq 98\%$  (with dimensions  $10 \text{ nm} \pm 1 \text{ nm} \times 4.5 \text{ nm} \pm 0.5 \text{ nm} \times 3\text{--}6 \mu\text{m}$ ) was ordered from Sigma Aldrich.

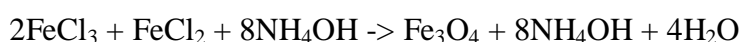
Activated Charcoal, Ammonia, Nitric Acid, Iron (II) chloride tetra hydrate, Titanium Isopropoxide, 1-Chlorooctane, 1-Vinylimidazole, 2,2'-Azobis(2-Methyl-Propionitrile), Anhydrous Toluene 99.85%, Chloroform, Isopropanol 99.5% and (3-Mercaptopropyl) trimethoxy-silane were all purchased from (Sigma Aldrich UK)

Iron (III) chloride hexahydrate, purchased from Alfa Aesar, UK.

### 2.2 Nanocomposites synthesis

#### 2.2.1. Superparamagnetic carbon based nanocomposites

##### i) Synthesis of Iron Oxide Nanoparticles



Iron Oxide nanocomposites were synthesised by a co-precipitation method by reacting Iron (II) Chloride Tetra hydrate ( $\text{FeCl}_2 \cdot 4\text{H}_2\text{O}$ ) and Iron (III) Chloride hexahydrate ( $\text{FeCl}_3 \cdot 6\text{H}_2\text{O}$ ) in a strong base (Ammonia Hydroxide).

## **ii) Carbon Nanotube (CNT) Functionalisation with Iron Oxide**

Weigh out 0.846g of Iron (II) Chloride Tetra hydrate ( $\text{FeCl}_2 \cdot 4\text{H}_2\text{O}$ ) and 2.162g of Iron (III) Chloride hexahydrate ( $\text{FeCl}_3 \cdot 6\text{H}_2\text{O}$ ) into a conical flask. Add 50mL of deionised water and stir for 30 minutes. After 30 minutes, add 1.00g of MWCNTs. Stir solution for an additional. After stirring is complete, filter black solid.

After filtering, move black solid to conical flask. Add 50mL of 1.6M of  $\text{NH}_4$  to conical flask and stir for 30 minutes.

Magnetic response test: Add a small amount of black solution to an eppendorf tube. Place eppendorf tube into magnetic rack. A successful test shows the movement of black solid to the magnetic side, while the solution becoming clear.

## **iii) Activated Charcoal (AC) Functionalisation with Iron Oxide**

Weigh out 0.846g of Iron (II) Chloride Tetra hydrate ( $\text{FeCl}_2 \cdot 4\text{H}_2\text{O}$ ) and 2.162g of Iron (III) Chloride hexahydrate ( $\text{FeCl}_3 \cdot 6\text{H}_2\text{O}$ ) into a conical flask. Add 50mL of deionised water and stir for 30 minutes. After 30 minutes, add 1.00g of AC. Stir solution for an additional. After stirring is complete, filter black solid. After filtering, move black solid to conical flask. Add 50mL of 1.6M of  $\text{NH}_4$  to conical flask and stir for 30 minutes. Magnetic response test: Add a small amount of black solution to an eppendorf tube. Place eppendorf tube into magnetic rack. A successful test shows the movement of black solid to the magnetic side, while the solution becoming clear.

#### **iv) Synthesis of Carbon Nanotube/Iron Oxide/Titanium Dioxide Nanocomposite**

Preparation of pre-cursor solution: Add 5mL titanium isopropoxide to 15mL isopropanol (Note: titanium isopropoxide must be poured into isopropanol to avoid hydrolysis.)

Add 0.2g of MWCNT+Fe<sub>3</sub>O<sub>4</sub> stir solution for 30 minutes. Vacuum filter and dry.

Note: Do not washed with water, as hydrolysis of TiO<sub>2</sub> will occur. (This TiO<sub>2</sub> will not be embedded into the nanocomposite). Add solid to beaker to a 50mL of acidic water, stir for 30 minutes. Filter and dry black solid.

#### **v) Synthesis of Activated Charcoal/Iron Oxide/Titanium Dioxide**

Preparation of pre-cursor solution: Add 5mL titanium isopropoxide to 15mL isopropanol (Note: Addition of titanium isopropoxide must be done to isopropanol to avoid hydrolysis.)

Add 0.2g of AC+Fe<sub>3</sub>O<sub>4</sub> stir solution for 30 minutes. Vacuum filter and dry. Note: Do not washed with water, as hydrolysis of TiO<sub>2</sub> will occur. (This TiO<sub>2</sub> which will not be embedded into the nanocomposite). Add solid to beaker to a 50mL of acidic water, stir for 30 minutes. Filter and dry black solid.

## 2.2.2 Synthesis of Synthesis of Hybrid Ionic Liquid-Iron Oxide

### Nanocomposite

The full synthesis of Ionic liquid-superparamagnetic silica hybrids A, B, C and D is detailed in this section. (Iron Oxide-Silica-Mercaptopropyl trimethoxy-silane-Vinyl-Oxytlimidazolium)

#### i) Synthesis of ionic liquid

Measure out 8.5ml of 1-Chlorooctane and 4.5ml of 1-Vinylimidazole into a 100mL double-necked round bottom flask. Reflux mixture at 70°C for 24 hours under nitrogen atmosphere.

After 24 hours' product, should separate out into two layers (Orange layer is the product). Separate product by a filter funnel. Wash product with organic solvents 10ml x 3 Ethyl Acetate and 10ml x 3 diethyl ether to remove starting reagents. Remove solvent layers by rotary evaporation.

#### ii) Addition of a Thiol Group to SPION (Thiol used as a connector)

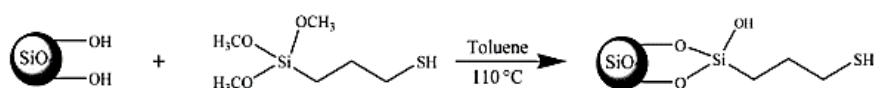


Figure 12 Addition of a Thiol Group to SPION (Thiol used as a connector) [59]

Note: In place of Silica, SPION [Silica-coated super paramagnetic iron oxide nanoparticles] is used instead. MPS = (3-Mercaptopropyl) trimethoxy-silane. Place 100mg of Iron Oxide-TEOS (Fine black powder) into 50mL double-necked round bottom flask. Suspend solid into a colourless solution of 10mL of dried toluene and 0.1mL of 3-mercaptopropyltrimethoxysilane (MPS). Reflux solution and

mechanically stir for 24 hours; at 110 degrees under nitrogen atmosphere. Leave solution to cool down to room temperature. Collect black solid and dry via vacuum filtration. Wash solid with methanol/water (1:1), then dried again for further use.

### iii) Addition of Ionic Liquid to Iron Oxide.



Figure 13 Synthetic Step 2- Addition of Ionic Liquid to Iron Oxide. [59]

Into a 50ml double-necked round bottom flask, suspend 3.0g of SIL-MPS into 20 mL of dried chloroform. Add 100 mg of AIBN and 3.0 g of 1-vinyl-3-octylimidazole (Ionic Liquid) reflux and mechanical stir for 48 hours, at 60°C, under nitrogen atmosphere. Cool solution to room temperature. Repeatedly wash black solid with methanol and methanol/water (1:1, v/v).

### iv) Final washing/drying steps to produce various products.

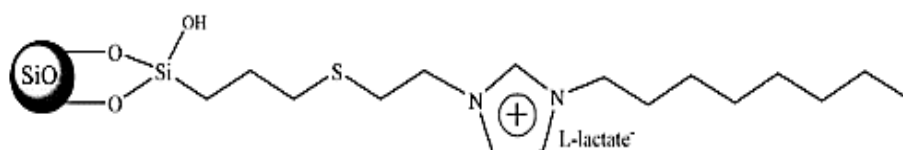


Figure 14. Iron Oxide-SIL-MPS-VOL [59]

Hybrid A Synthesis: Iron Oxide-MPS + Ionic Liquid. After synthesis, vacuum, dry and keep in glass vial.

Hybrid B Synthesis: Iron Oxide-MPS + Ionic Liquid. After synthesis vacuum, dry and keep in glass vial.

Hybrid C Synthesis: Iron Oxide-MPS + Ionic Liquid (Sample is suspended in methanol solution.) During this step: Reflux solution and mechanically stir for 24 hours; at 110 degrees under nitrogen atmosphere. Leave solution to cool down to room temperature. Collect black solid and dry via vacuum filtration. Wash solid with methanol/water (1:1), then dried again for further use. **Caution:** via vacuum filtration. Remove the solution via pipette and wash with 10mL x 3 acetone. Next, wash with 10mL x 3 of methanol and methanol/water (25ml/25ml). Product was then placed into plastic tube and suspended in 40mL of Methanol/water (1:1).

Hybrid D Synthesis: Iron Oxide-MPS + Ionic Liquid (Sample is suspended in acetone solution.) During this step: Reflux solution and mechanically stir for 24 hours; at 110 degrees under nitrogen atmosphere. Leave solution to cool down to room temperature. Collect black solid and dry via vacuum filtration. Wash solid with methanol/water (1:1), then dried again for further use. **Caution:** via vacuum filtration. Remove the solution via pipette and wash with 10mL x 3 acetone. Next, then wash with 10mL x 3 of methanol/water (25ml/25ml) then wash with 10mL x 3 of acetone, Product was then placed into plastic tube and suspended in 40mL of acetone.

## 2.3 Physico-chemical characterisation

### 2.3.1 X-ray Diffraction

X-ray diffraction (XRD) is the primary, non-destructive tool for identifying and quantifying the mineralogy and crystallinity of particulates. Every mineral or compound has a characteristic X-ray diffraction pattern whose 'fingerprint' can be matched against a database of over 250 000 recorded phases.

Computer-controlled diffraction systems can interpret the diffraction traces produced by individual constituents and highly complex mixtures.

XRD is an essential technique for identifying and characterising the nature of clay minerals, providing information, which cannot be determined by any other method. XRD works when monochromatic X-rays are projected onto a crystalline material at an angle ( $\theta$ ), diffraction occurs when the distance travelled by the rays reflected from successive planes differs by an integer ( $n$ ) of wavelengths ( $\lambda$ ). By varying the angle  $\theta$ , the Bragg's Law conditions [ $n\lambda = 2d \sin\theta$ ] are satisfied by different  $d$ -spacing's. Plotting the angular positions and intensities of the resultant diffracted peaks produces a characteristic pattern where different phases are present; the diffraction trace represents the sum of the individual patterns.

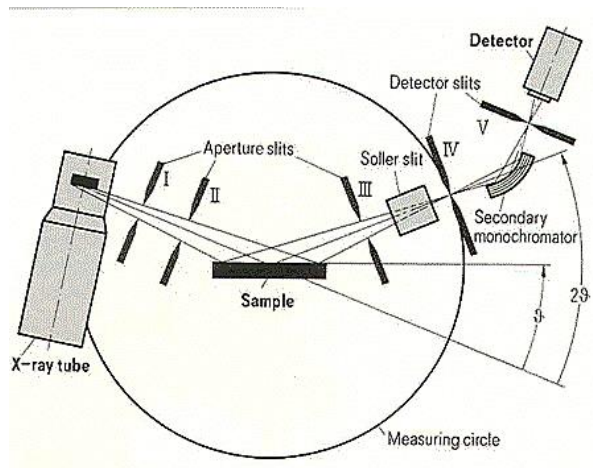


Figure 15 Schematic for XRD.] [63]

The X-ray diffraction patterns obtained with a Inel Equinox 2000 powder diffractometer equipment using  $\text{CuK}\alpha$  radiations ( $1.5418 \text{ \AA}$ ).

The samples were dried overnight in an oven set at  $80^\circ\text{C}$ . The dry samples were ground into a fine powder before X-ray diffraction study. Powders were packed into X-ray sample holder ensuring smooth surface with no visible cracks.

### 2.3.2 Fourier Transform Infra-Red Spectroscopy

FTIR spectra measured on an IR 200 Thermo Scientific spectrometer. FTIR spectra were processed and analysed using the software package Omnic 8.0 software. An FTIR device processes infrared radiation of sample against a wavelength. The infrared bands give the molecular structure and their bonding positions. A simple FTIR instrument consists of interferometer, source, sample compartment, detector and amplifier. An interferometer modulates the wavelength and the detector measures the transmitted/ reflected light.

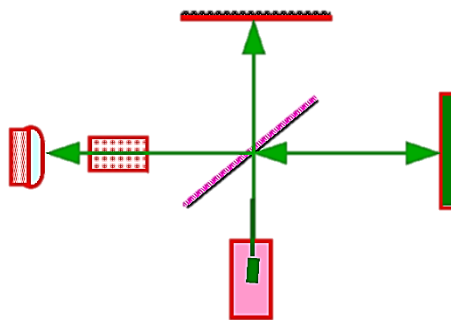


Figure 16 Diagram of how an FT-IR functions] [64]

For liquid samples: One drop of solution was pipetted onto the IR sensor and scanned. IR sensor was then washed with ethanol ready for next sample.

For solid: A small amount of solid was placed onto the IR sensor via a spatula and scanned. IR sensor was then washed with ethanol ready for next sample.

### 2.3.3 Scanning Electron Microscopy/Energy Dispersive X-Ray

#### Analysis

SEM images were recorded using FEI Quanta 200 (JEOL, Tokyo, Japan) operating at 20 kV, WD 10 mm with spot size 2.5 -5.0. Energy Dispersive X-Ray Analysis (EDX), also referred to as EDAX, is an x-ray technique used to identify the elemental composition of materials.

EDX systems are attachments to Electron Microscopy instruments (Scanning Electron Microscopy (SEM) or Transmission Electron Microscopy (TEM)) instruments where the imaging capability of the microscope identifies the specimen

of interest. The data generated by EDX analysis consist of spectra showing peaks corresponding to the elements making up the true composition of the sample being analysed. During SEM/EDX Analysis, the specimen is bombarded with an electron beam inside the scanning electron microscope. The bombarding electrons collide with the specimen atoms' own electrons, knocking some of them off in the process. A position vacated by an ejected inner shell electron, is eventually occupied by a higher-energy electron from an outer shell. To be able to do so, however, the transferring outer electron must give up some of its energy by emitting an X-ray. The amount of energy released by the transferring electron depends on which shell it is transferring from, as well as which shell it is transferring to. Additionally, the atom of every element releases X-rays with unique amounts of energy during the transferring process. Therefore, by measuring the amounts of energy present in the X-rays being released by a specimen during electron beam bombardment. The interaction of electron and sample depicts the information such as, morphology, orientation of individual materials making the sample, crystalline property and chemical compositions.

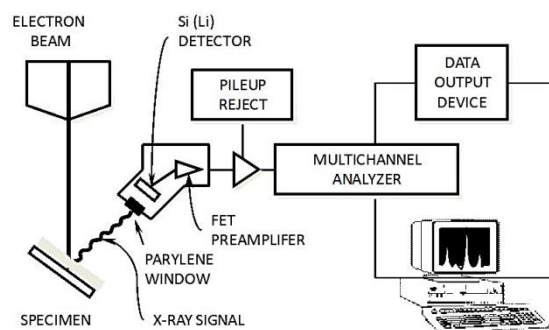


Figure 17 SEM-EDAX Diagram] [65]

### 2.3.4 Nuclear Magnetic Resonance

Nuclear Magnetic Resonance is a property of the nucleus of an atom, concerned with nuclear spin ( $I$ ). When a nucleus with  $I = 1/2$  is placed in a magnetic field, it can either align itself with the field (lower energy) or against it (higher energy). If radio waves are applied, nuclei in the lower energy state can absorb the energy and jump to the higher energy state. We can observe either the adsorption of energy, or the subsequent release of energy as the nucleus "relaxes" back to the lower energy state.

[81]

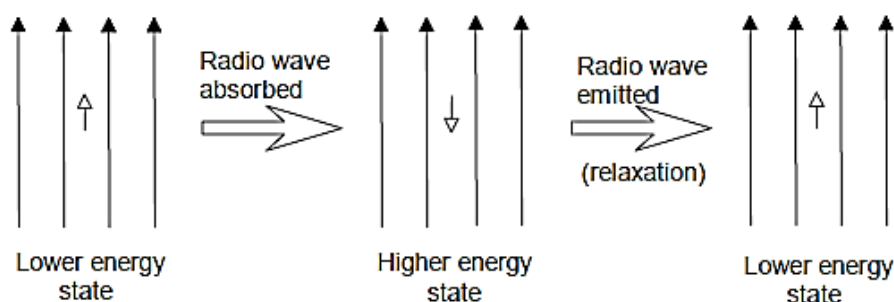


Figure 18 Demonstration of excitation and relaxation of nucleus. [66]

If radio waves are applied, nuclei in the lower energy state can absorb the energy and jump to the higher energy state. We can observe either the adsorption of energy, or the subsequent release of energy as the nucleus "relaxes" back to the lower energy state.

In a real molecule, the effective magnetic field "felt" by a nucleus ( $B_{\text{eff}}$ ) includes not only the applied field  $B_0$ , but also the magnetic effect of nearby nuclei and electrons. This causes the signal to absorb at a slightly different frequency than for a single atom; it is convenient to reference this resonant frequency to a standard

(usually tetramethylsilane, TMS, defined as zero). When we plot the output from this adsorption, we obtain a series of peaks known as an NMR spectrum (or "spectra" if you have more than one spectrum) such as the typical example shown in Figure. 2. The difference (in parts per million, ppm) from the zero point is referred to as the chemical shift ( $\delta$ ). A typical range for  $\delta$  is around 12 ppm for  $^1\text{H}$  and around 220 ppm for  $^{13}\text{C}$ . All ionic liquid product samples were prepared in an NMR tube with DMSO as the solvent. All starting reagents were prepared with  $\text{CDCl}_3$ .

## **2.4. Dye adsorption experiment**

This research produced two comparable solutions of three dyes, methylene blue, Congo Red and Allura red AC. These solutions had absorbencies in the range between 0.5 – 1.5. This is for two reasons; we have two comparable results, one being low concentration and the other high.

For this example, we will talk about methylene blue. We dissolved 0.01g in 50ml's of water yielding a concentration of  $6.25 \times 10^{-4}\text{M}$  (This original solution was used for to make all further standards – About, it will be labelled as MBS whenever it is being used. This concentration produced a very dark solution, it was so high that upon testing its absorbance the UV-Vis spectrophotometer could not read it properly i.e. Absorbance on the machine for this concentration was above  $>2.50$  and the peaks could not be read.

As previously stated in the literature review, dilutions of  $10^{-5}$  are a common pollutant concentration, which adds emphasis to the potential of these compounds. An initial calibration curve was plotted for methylene blue using Beer-Lambert law;  **$A = \epsilon Lc$** .

All tests were done with two solutions; Methylene Blue Solution A and B. Methylene Blue Solution A standard was prepared by using 6000uL (6mL of MBS) and 194000uL (194mL of Water), this was to ensure that there was enough of the solution for testing of the materials. Conversely Methylene Blue Solution B was prepared by using 12000uL (12mL of MBS) and 188000uL (188mL of water). In total 200mL of each solution was prepared to ensure that there was enough for all possible tests.

### **2.4.1 Methylene Blue**

#### **i) Methylene Blue Calibration Graph**

The calibration graph was prepared by plotting the absorbance values of methylene blue at a wavelength (665nm) against several known concentrations (As seen in Figure 16).

The absorbance measurements for the calibration graph were taken from a single wave length scan at 665nm. Before measuring each dilution of methylene blue, the spectrometer was blanked with samples of distilled deionised water.

For each degradation/adsorption test with Ionic-Iron Oxide Hybrid Nanocomposites, 0.02g of each solid is used. **Note: Methylene Blue Solution A and Methylene Blue B have respective concentrations of  $0.63 \times 10^{-5}$  and  $3.99 \times 10^{-5}$  mol/L.**

Table 1 Methylene blue calibration data

<b>Standard Dilutions of MB</b>	<b>Absorbance (Abs)</b>
Concentration (M) (mol/L ( $\times 10^{-5}$ ))	(665 nm)
0	0
0.63 (Solution A)	0.39
1.27	0.65
1.93	0.884
2.61	1.13
3.29	1.28
3.99 (Solution B)	1.47

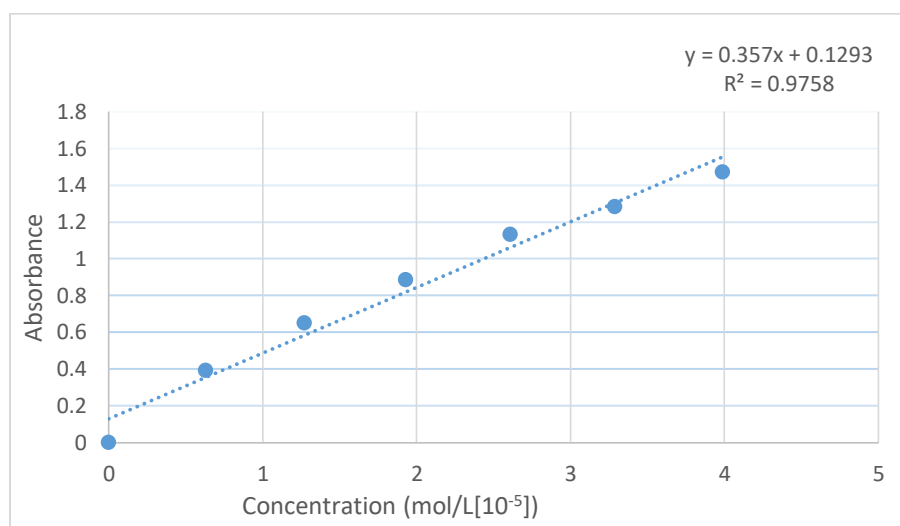


Figure 19 Methylene Blue Calibration Graph

The linear regression line of this calibration graph is 0.9758. 0.95 is considered the maximum threshold for a successful linear regression. This indicates an accurate for this calibration

**ii) Testing commercial base matrix against Methylene Blue:**

0.02g of AC and 0.02g of MWCNT were weighed out separately into 2 different glass vials containing 10mL of MB A. These solutions were stirred, the light blue colour was removed after 1 minute. When getting close to the minute mark, half a cuvette full was removed from the solution and its absorbance was tested. This was repeated four more times, for each passing minute.

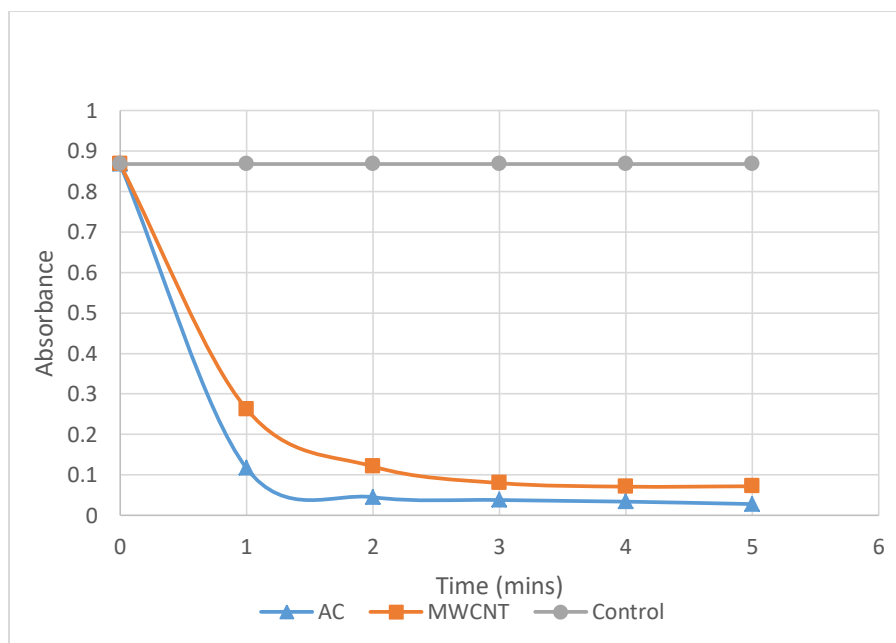


Figure 20 Methylene Blue Starting Reagent Graph (For data table refer to Appendix Table 2).

## 2.4.2 Congo Red

The calibration graph was prepared by plotting the absorbance values of Congo Red at a wavelength (490nm) against several known concentrations (Refer to table 2).

The absorbance measurements for the calibration graph were taken from a single wavelength scan at 490nm. Before measuring each dilution of Congo Red, the spectrometer was blanked with samples of distilled deionised water. For each degradation/adsorption test with Ionic-Iron Oxide Hybrid Nanocomposites, 0.02g of each solid is used. **Note: Congo Red Solution A and Congo Red Solution B have respective concentrations of  $0.29 \times 10^{-5}$  and  $5.06 \times 10^{-5}$  mol/L.**

Table 2 Congo Red Calibration Data

Standard Dilutions of CR Concentration (M) (mol/L ( $\times 10^{-5}$ ))	Absorbance
0	0
0.29 (Solution A)	0.198
0.88	0.372
1.51	0.809
3.19	1.12
5.06 (Solution B)	1.545

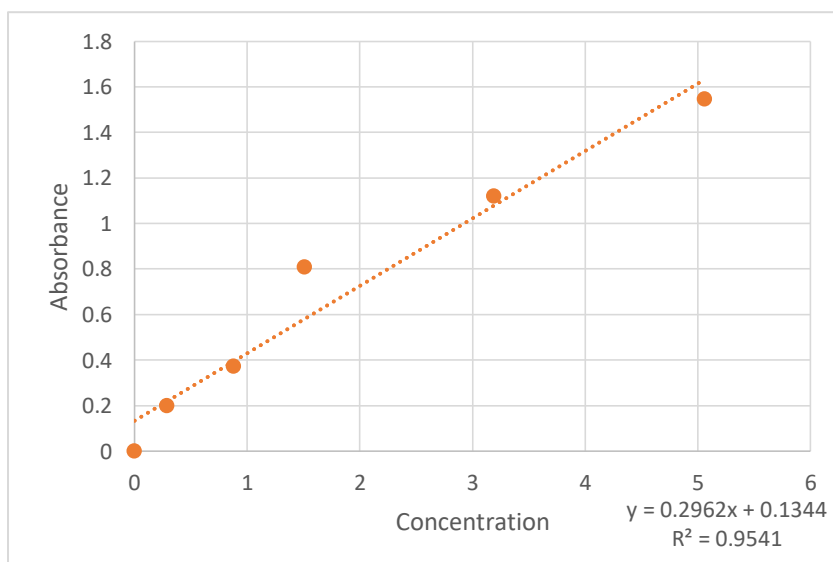


Figure 21 Congo Red Calibration Graph

The linear regression line is at 0.9521, which is considered the maximum threshold for a successful linear regression. This indicates a lack of accuracy for this calibration test. This lack of accuracy is most likely due to human error, as the slightest under measurement of solution/over measurement can greatly affect the concentration.

### 2.4.3 Allura Red AC

#### i) Allura Red Calibration Graph

The calibration graph was prepared by plotting the absorbance values of Allura Red at a wavelength (504nm-510nm) against several known concentrations (As seen in Figure C7A).

The absorbance measurements for the calibration graph were taken from a single wavelength scan at 490nm. Before measuring each dilution of Congo Red, the spectrometer was blanked with samples of distilled deionised water.

0.02g of each nanocomposite were weighed out separately into 4 differently labelled glass vials containing 10mL of Congo Red A. When getting close to the minute mark, half a cuvette full was removed from the solution and its absorbance was tested. **Note: Allura Red AC Solution A and Allura Red AC Solution B have respective concentrations of  $2.015 \times 10^{-5}$  and  $6.045 \times 10^{-5}$  mol/L.**

Table 3 Allura Red Calibration Data

<b>Standard Dilutions of AC</b>	<b>Absorbance</b>
Concentration (M) (mol/L ( $\times 10^5$ ))	505 nm
0	0
2.015 (Solution A)	0.505
3.023	0.762
4.03	1.018
5.038	1.31
6.045 (Solution B)	1.545

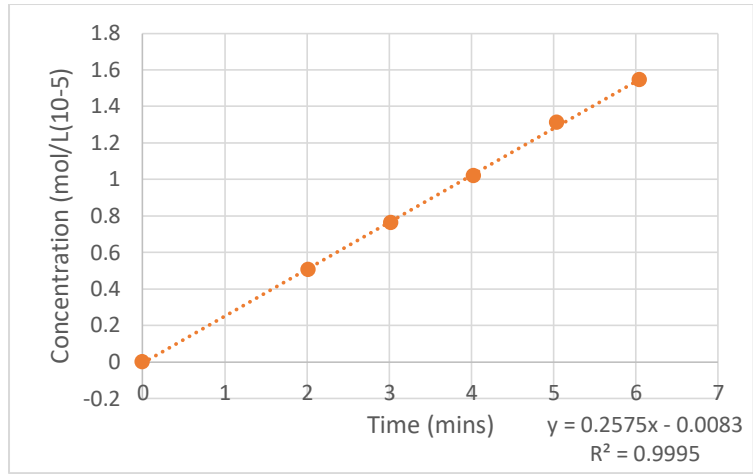


Figure 22 Allura Red AC Calibration Graph.

### 3. Results and Discussion

#### 3.1 Adsorption of organic dyes by nanocomposites

##### 3.1.1 Methylene Blue

###### i) Initial Degradation Test against Carbon + Iron Oxide Nanocomposites

0.02g of AC + Iron Oxide and 0.2g of MWCNT + Iron Oxide were weighed out separately into 2 different glass vials containing 10mL of MB A. These solutions were stirred, and again the blue colour was removed after 1 minute. When getting close to the minute mark, half a cuvette full was removed from the solution and its absorbance was tested. This was repeated four more times, for each passing minute.

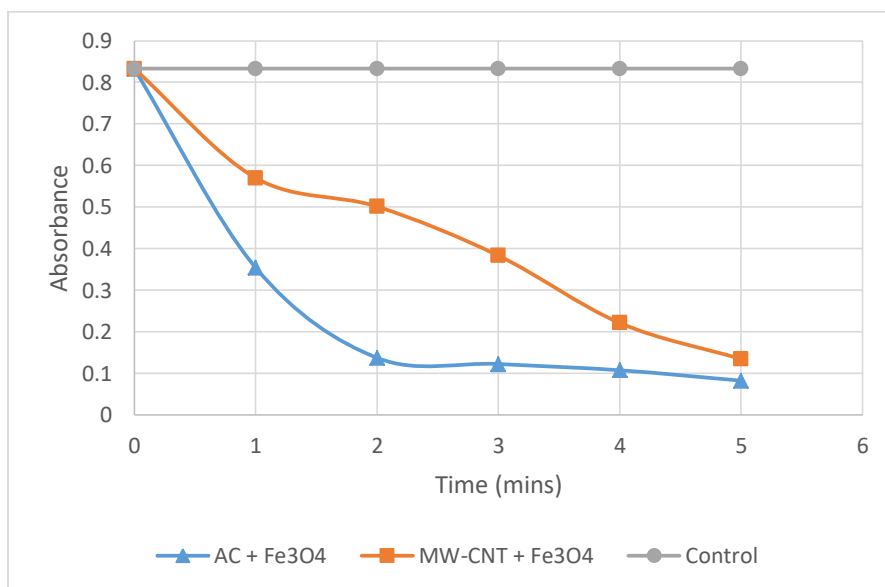


Figure 23 Methylene Blue Carbon + Iron Oxide Nanocomposites Data (For data table refer to Appendix Table A3).

The results show that, with the addition of the nanocomposites, the UV-Vis absorbance of methylene blue decreases. This indicates that the methylene blue dye is being adsorbed onto the surface of the nanocomposite and out of the water

solution. The results also show that the activated charcoal nanocomposite adsorbs more efficiently than the multi-walled carbon nanotubes.

## ii) Testing Carbon/Iron Oxide/TiO<sub>2</sub> Nanocomposites (Methylene Blue)

0.02g of each nanocomposite were weighed out separately into 4 differently labelled glass vials containing 10mL of MB A. When getting close to the minute mark, half a cuvette full was removed from the solution and its absorbance was tested. This was repeated four more times, for each passing minute.

Note: The MW-CNT Sample took the longest to lose its blue colour.

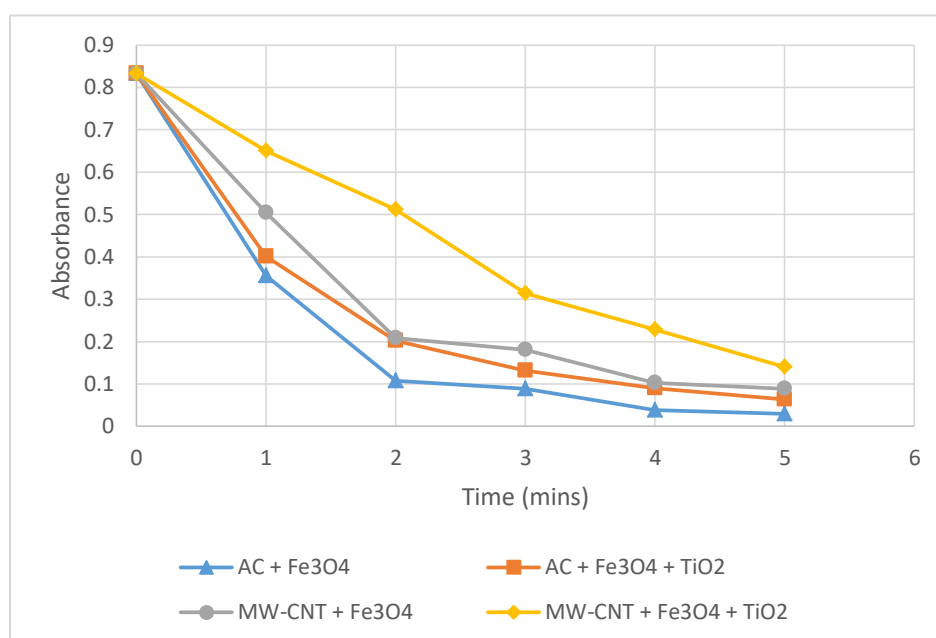


Figure 24. Methylene Blue Carbon/Iron Oxide/TiO<sub>2</sub> Nanocomposites Graph (For data table refer to Appendix Table A4).

For the data, four nanocomposite hybrids were tested against two different concentrations of methylene blue solution i.e.  $0.63 \times 10^{-5}$  (Solution A) and  $3.99 \times 10^{-5}$  (Solution B) mol/L (refer to section 2.4.1 for reference). It is expected that the nanocomposites embedded into multi-walled carbon nanotubes would have the fastest absorbance reduction.

These results show that that activated charcoal/magnetic nanocomposite reduced the absorbance of methylene blue faster than the multi-walled magnetic nanocomposite. It was expected that the multi-walled carbon nanotubes would adsorb the dye faster due to its greater surface area.

This is most likely due to the activated charcoal samples being a fine powder, which gave nanocomposites a greater surface area. The multiwalled nanocomposites were agglomerated i.e. the nanocomposites had clumped together, reducing surface area which reduced their effectiveness.

It was also presumed that the Titanium Dioxide samples would reduce the absorbance of the dye faster, due to its photocatalytic functionalisation. This was not the case, as the  $\text{TiO}_2$  samples took the longest out of the four samples. Due to the presence of  $\text{TiO}_2$  embedded into the carbon source, this most likely reduces surface area for adsorption which inhibits the rate of adsorption.

The solids were removed by placing a magnet under the glass vial, the nanocomposites in suspension where quickly attracted to the magnet and the solutions were extracted via a pipette.

## Hybrids against Methylene Blue Solution A

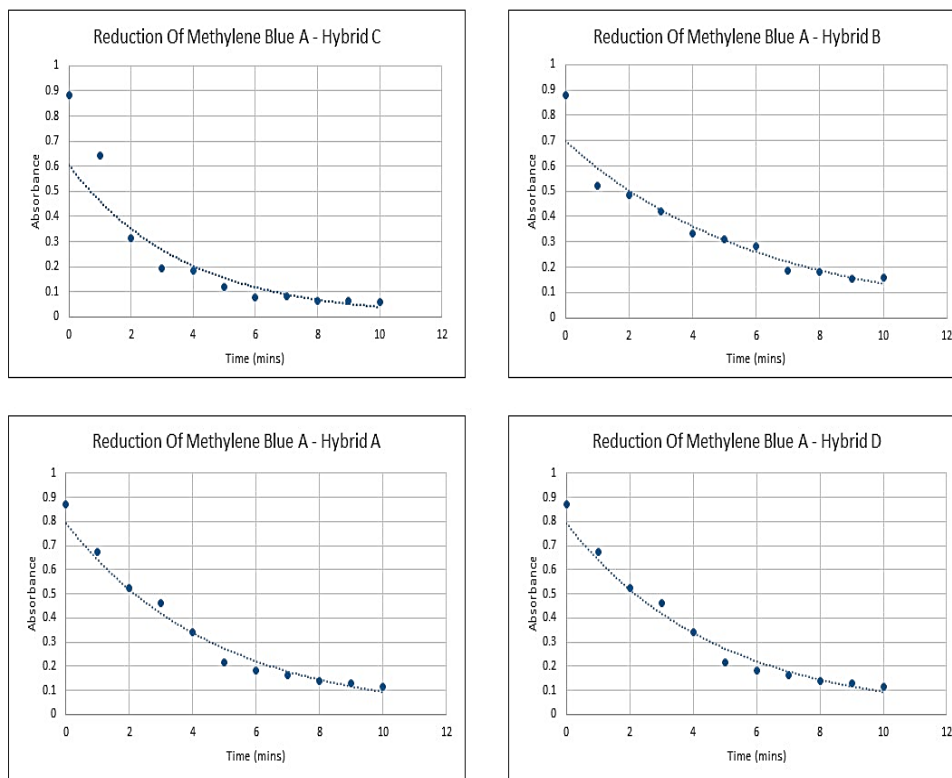


Figure 25 Methylene Blue A against Ionic Liquid Nanocomposite Hybrid A, B, C and D Graph (For data table refer to appendix tables A5-A8).

These results show that, with addition of a hybrid ionic-liquid nanocomposites the UV-Vis absorbance of methylene blue decreases. However, in comparison with the carbon-based nanocomposites, the reduction of methylene blue A takes twice as long. The carbon-based nanocomposites reduce the solution in five minutes rather than ten minutes, as shown with the ionic-liquid nanocomposite hybrids.

## Hybrid B against Methylene Blue Solution B

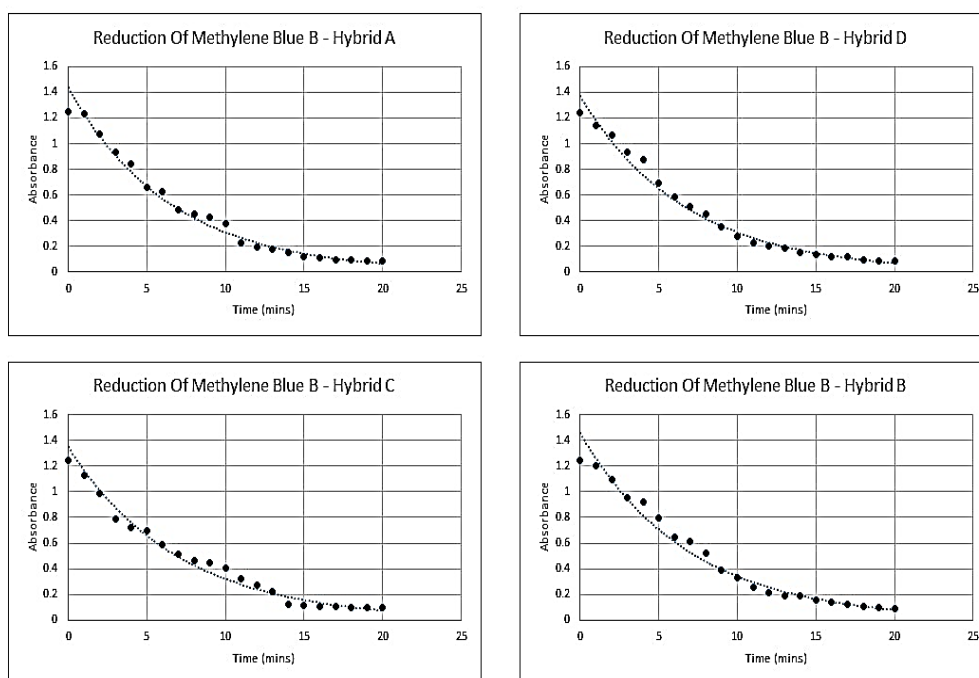


Figure 26 Methylene Blue B against Ionic Liquid Nanocomposite Hybrid A, B, C and D Graph (For data table refer to Appendix Table A9-A12)

The results show that the ionic-liquid hybrids successfully reduce the adsorbance of methylene blue solutions, however they are not on the level of the carbon based magnetic nanocomposites. The reduction of methylene blue B solution takes twice as long to adsorb/breakdown the dye. It is theorised that the imidazolium of the ionic liquid is interacting the pi bonding in the methylene blue, the octane group may also be attracting the polar the non-polar groups of the methylene blue. From the results, it can be assumed that the large surface area of the carbon nanocomposites provides a more efficient method of dye removal in comparison with the bonding that the ionic liquid group provide.

### 3.1.2 Congo Red

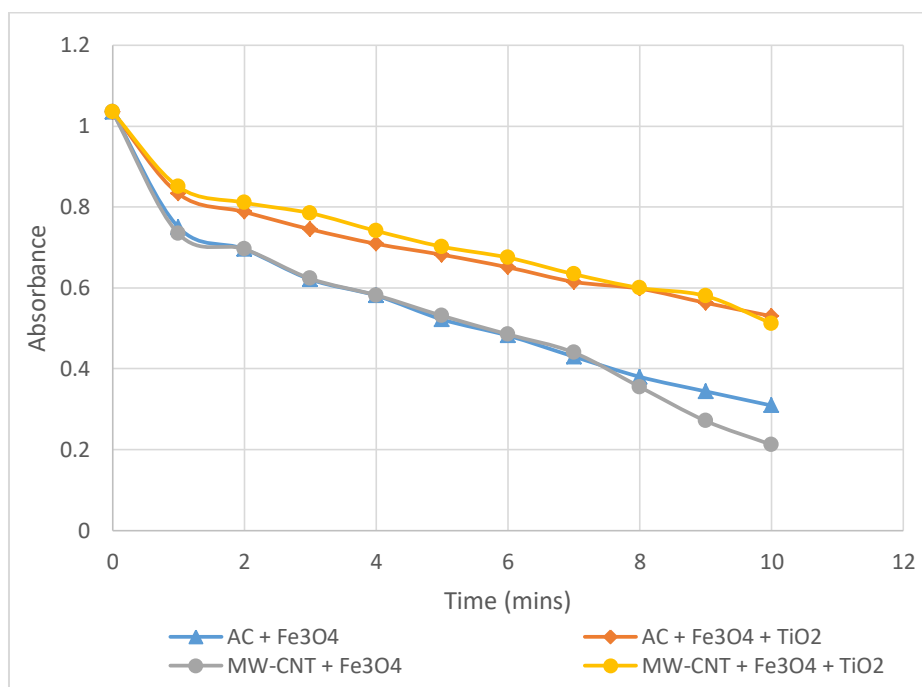


Figure 27 Congo Red against Carbon/Iron Oxide/TiO<sub>2</sub> Graph (For data table refer to Appendix Table A13).

0.02g of each nanocomposite were weighed out separately into 4 differently labelled glass vials containing 10mL of Congo Red A. When getting close to the minute mark, half a cuvette full was removed from the solution and its absorbance was tested. This was repeated nine more times, for each passing minute. (TiO<sub>2</sub> samples were done under a UV lamp covered in Tin Foil at 365nm).

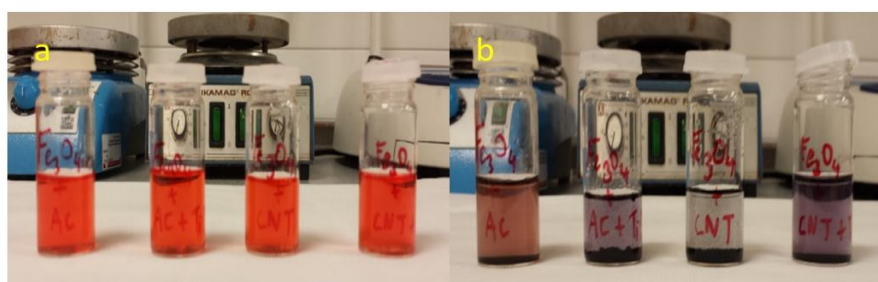


Figure 28 (a) Before Photocatalytic Test (b) After Photocatalytic Test

These results show that that activated charcoal/magnetic nanocomposite reduced the absorbance of Congo Red more efficiently than the multi-walled magnetic nanocomposite after ten minutes i.e. the UV absorbance of dye in the activated charcoal samples were lower than the carbon nanotubes. It was expected that the multi-walled carbon nanotubes would adsorb the dye faster due to its greater surface area.

As previously mentioned, this is most likely due to the activated charcoal samples being a fine powder in contrast to agglomerated less effective multi-walled nanocomposites. There is an interesting result here as the two samples with  $\text{TiO}_2$  have produced a blue/purple colour from the Congo Red. This is possibly a transition state caused by the addition of free radicals produced by  $\text{TiO}_2$  under UV light. This shows that the addition of  $\text{TiO}_2$  to the nanocomposite structure has photocatalytic properties. The solids were removed by placing a magnet under the glass vial, the nanocomposites in suspension were quickly attracted to the magnet and the solutions were extracted via a pipette.

## Hybrid A against Congo Red Solution A

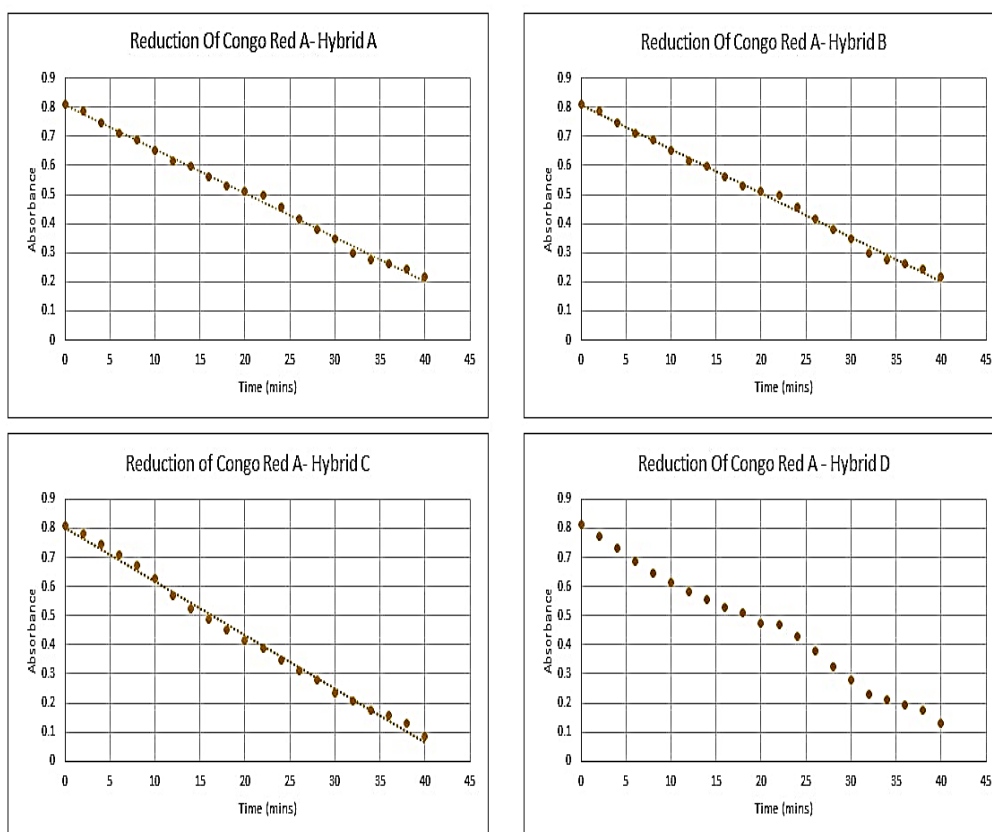


Figure 29 Congo Red A against Ionic Liquid Nanocomposite Hybrid A Graph (For data table refer to Appendix Table A14-A17).

These results show that, with addition of hybrid ionic-liquid nanocomposites the UV-Vis absorbance of Congo Red A decreases which indicates removal of dye from solution. However, in comparison with the carbon-based nanocomposites, the reduction of Congo Red A takes four times as long. The carbon-based nanocomposites reduce the solution in forty minutes rather than ten minutes, as shown with the ionic-liquid nanocomposite hybrids.

## Hybrid A against Congo Red Solution B

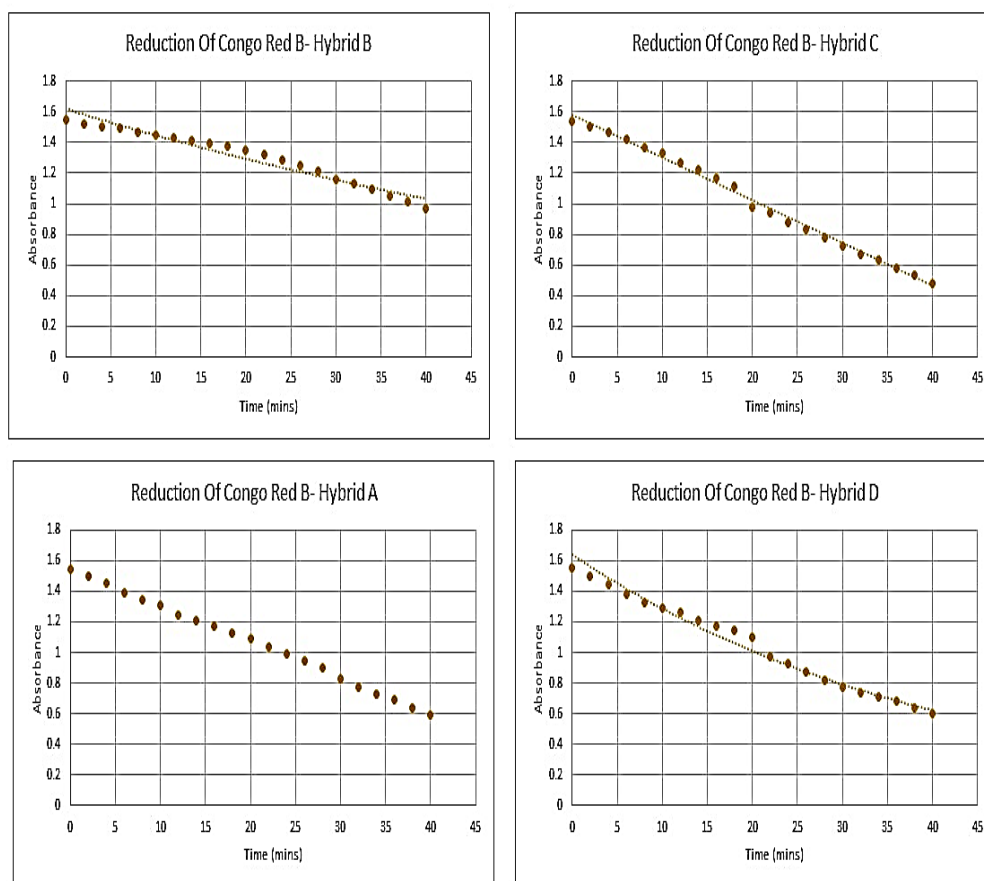


Figure 30 Congo Red B against Ionic Liquid Nanocomposite Hybrid A Graph (For data table refer to Appendix Table A18-A21).

These results show again that the ionic-liquid hybrids poorly reduce the adsorbance of Congo Red B solutions in comparison with the carbon-based nanocomposites. These nanocomposites took four times the amount of time to adsorb/breakdown the Congo Red B solution. It is theorised that the imidazolium of the ionic liquid is interacting the pi bonding azo group in of the Congo Red, the octane group may also be attracting the polar the non-polar.

It is of interest to note, the ionic-liquids hybrids were insufficient in the removal of Congo Red. The increase of concentration greatly inhibited the nanocomposites

ability to adsorb all the dye. This may be most likely because 0.01g of composite was used to remove the dye; as supply of nanocomposite was limited (In comparison with 0.02g of the carbon nanocomposite).

### 3.1.3 Allura Red AC

For this set of data I tested the four nanocomposite hybrids (refer to method for description) labelled A, B, C and D; against two different concentrations of Allura red solution labelled A and B (refer to method for description).

#### Hybrid A against Allura Red AC Solution A

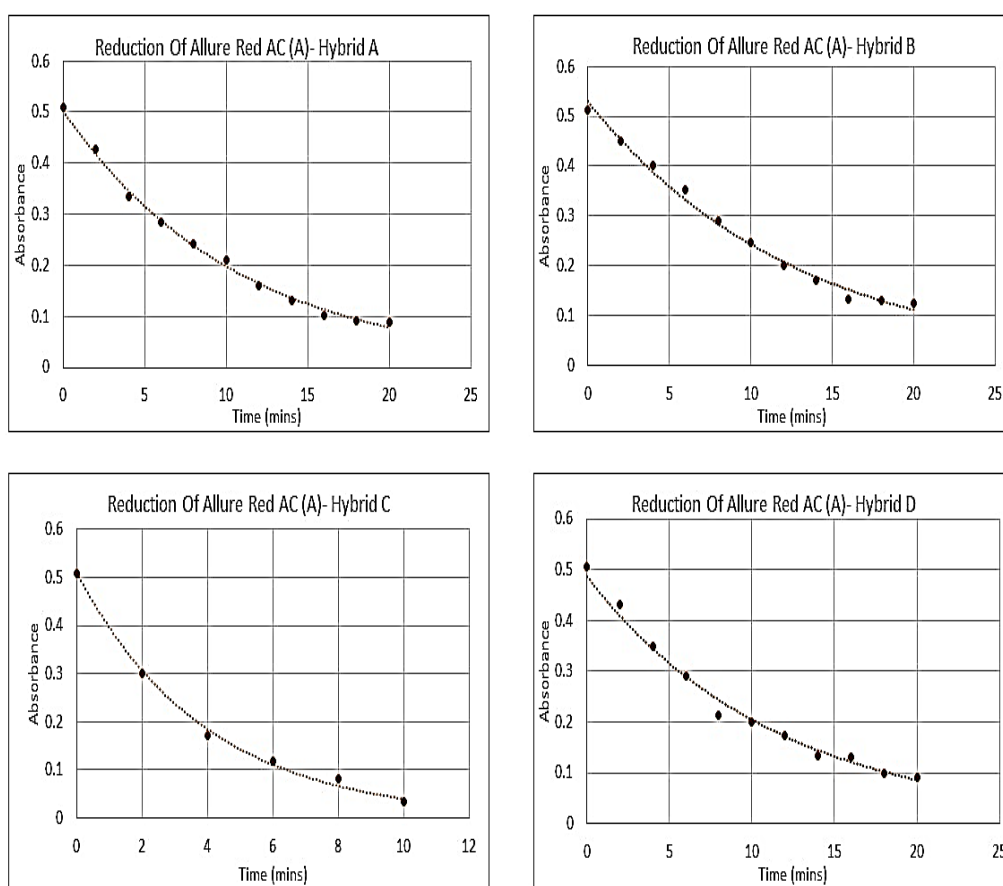


Figure 31 Figure 39. Allura Red AC (A) against Ionic Liquid Nanocomposite Hybrid A B C and D

Graph (For data table refer to Appendix Table A22-A25)

## Hybrid A against Allura Red AC Solution B

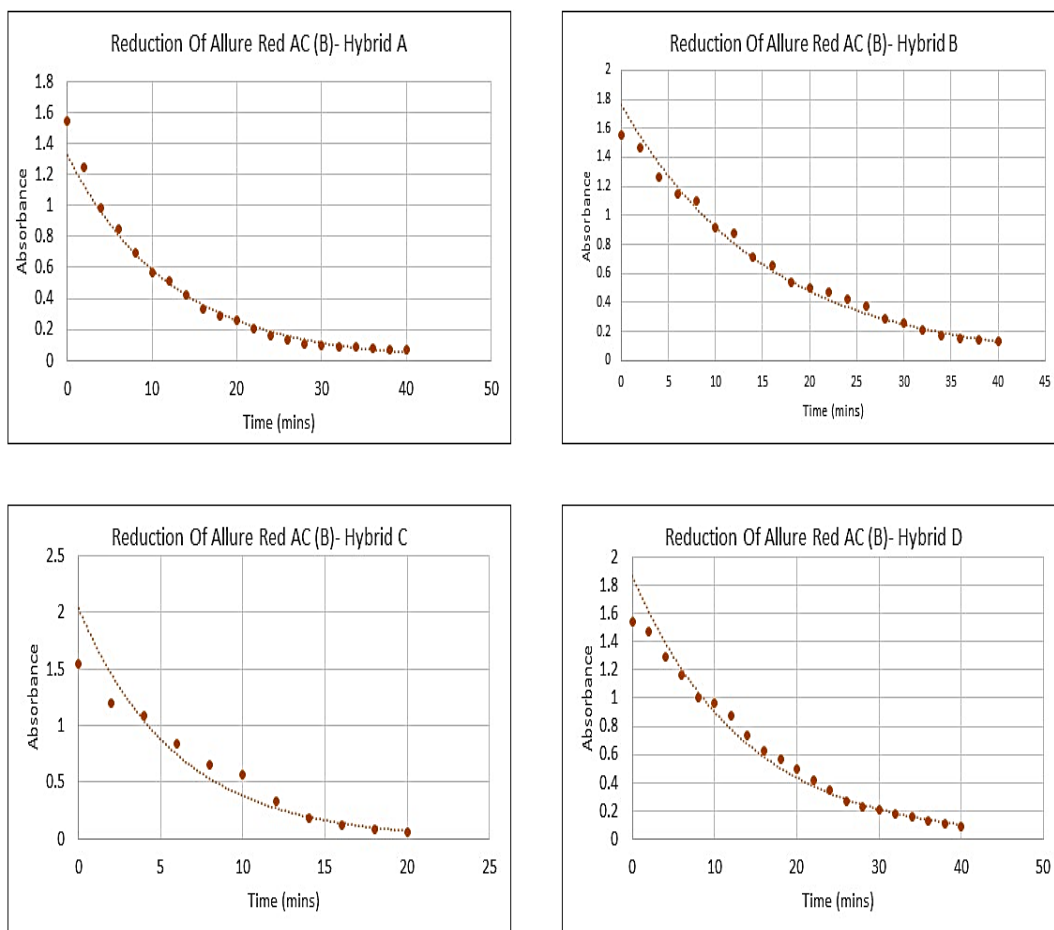


Figure 32 Allura Red AC (B) against Ionic Liquid Nanocomposite Hybrid A B C and D Graph (For data table refer to Appendix Table A26-A29)

Note: Only the Ionic-Liquid Hybrid nanocomposites were used to test against Allura Red AC due to time constraints. When considering the previous results (i.e. Methylene Blue and Congo Red), we can assume that carbon based nanocomposites would work superior to the hybrid nanocomposites. The ionic liquid hybrids show that they can successfully reduce the absorbance of Allura Red AC.

## 3.2 Superparamagnetic carbon based nanocomposites

### 3.2.1 X-ray diffraction patterns

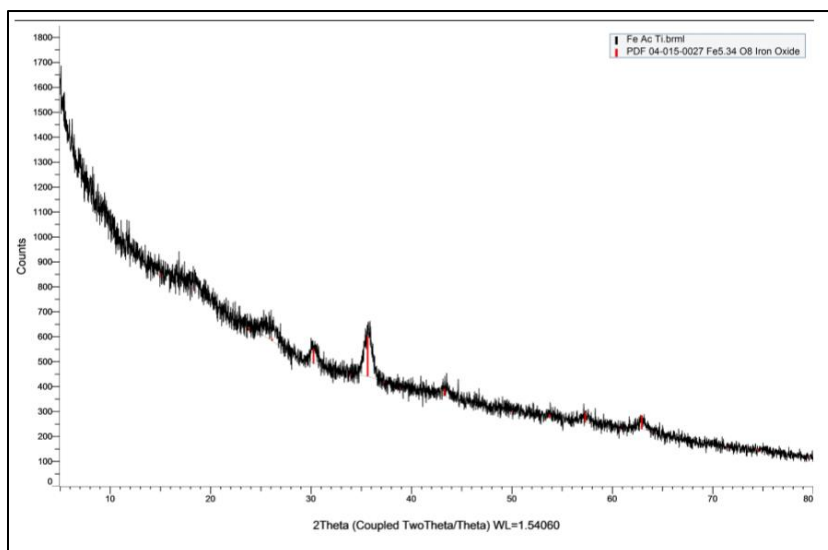


Figure 33 Iron Oxide-Activated Charcoal X-Ray Diffraction Pattern

The XRD was unable to determine the structure of this oxide i.e. the result came out as  $\text{Fe}_5.34\text{O}_8$  as seen in figure 33. However, the magnetic properties of these compounds are shown when separating the nanocomposites from dye solutions with a magnetic.

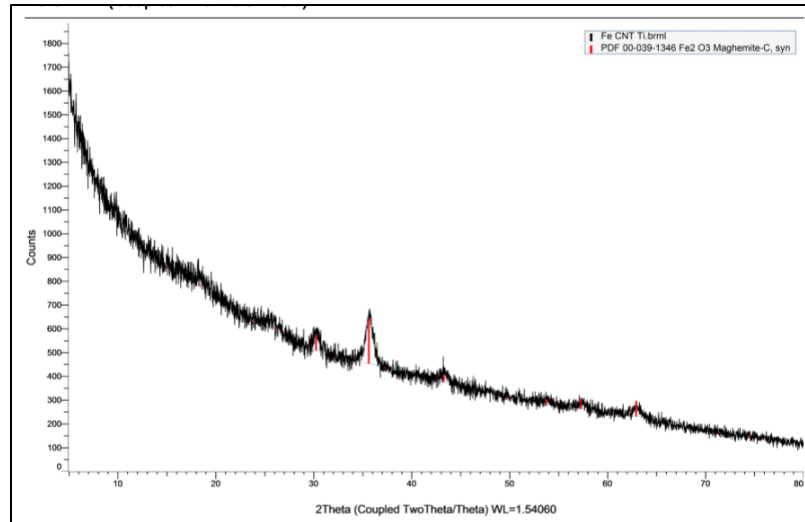


Figure 34 Iron Oxide-Carbon Nanotube X-Ray Diffraction Pattern

The XRD determined that the Iron Oxide present in this composite was Maghemite. Maghemite has the chemical formula of  $\text{Fe}_2\text{O}_3$ .

These AC-Iron Oxide compounds displayed magnetism during testing. This is because maghemite is ferrimagnetic; it has the same spinel ferrite structure as magnetite.

### 3.2.2 Fourier Transform Infra-red Spectra

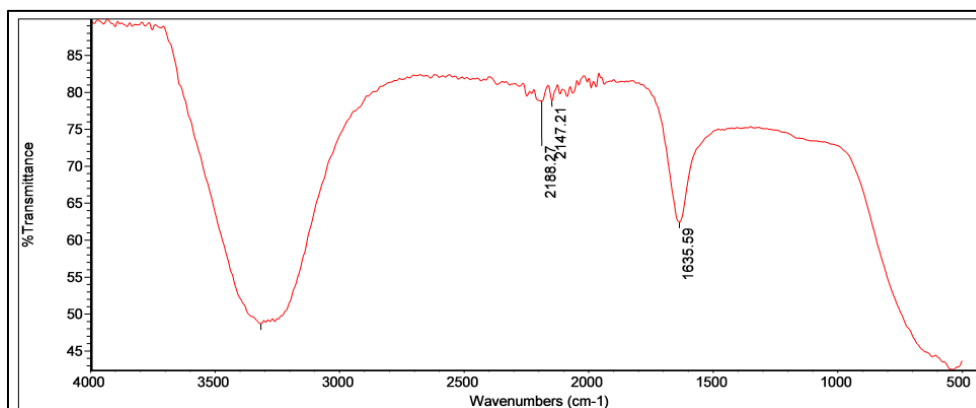


Figure 35 FT-IR Methylene Blue Solution B 1.5 Absorbance (After removal of CNT/FeO/TiO<sub>2</sub> nanocomposite).

Solution changed from a dark blue solution into a colourless solution after the addition of CNT/FeO/TiO<sub>2</sub> (after 5 minutes).

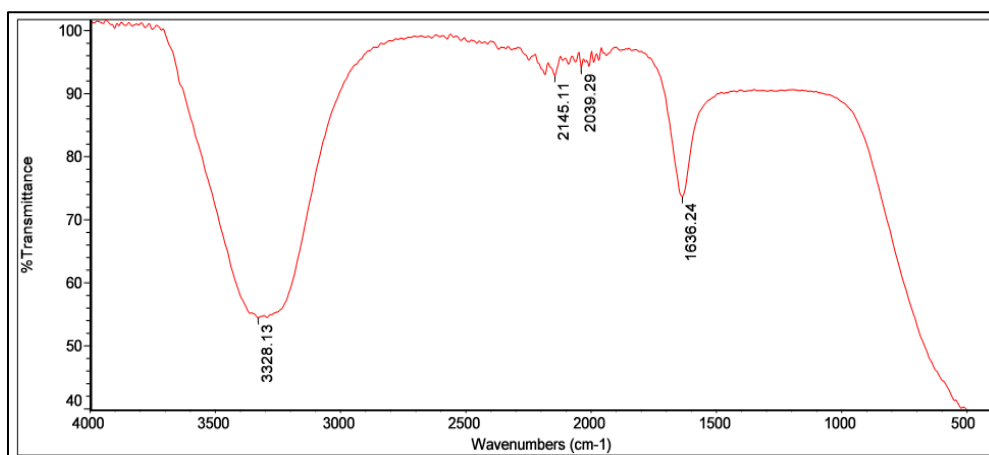


Figure 36 FT-IR Methylene Blue Solution A 0.5 Absorbance (After removal of CNT/FeO/TiO<sub>2</sub> nanocomposite).

Solution changed from a light blue solution into a colourless solution after the addition of CNT/FeO/TiO<sub>2</sub> (after 5 minutes).

The addition of new peaks is an indication of adsorbance onto the surface of nanocomposite.

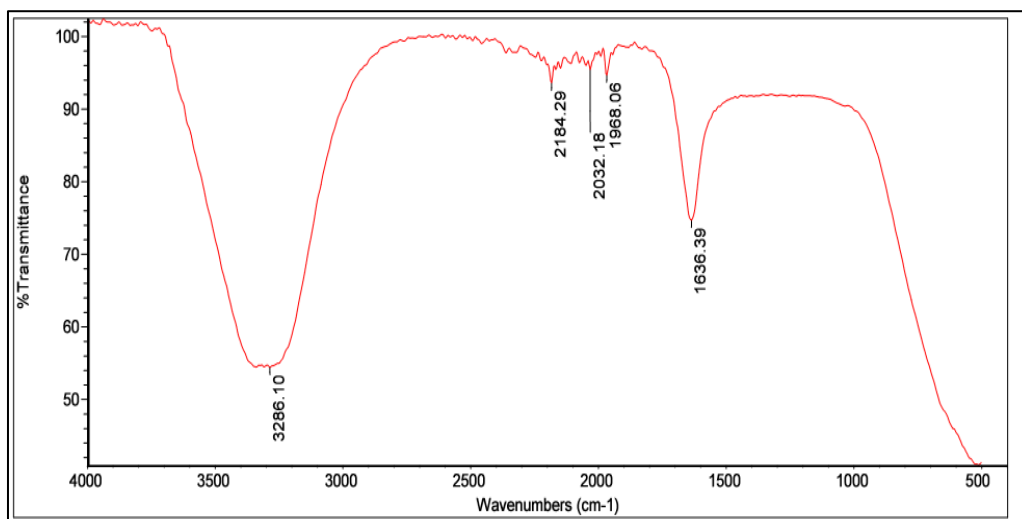


Figure 37 Congo Red Solution B 1.5 Absorbance (After removal of CNT/FeO/TiO<sub>2</sub> nanocomposite).

Reference to figure 57: Solution changed from a dark red solution into a colourless solution after the addition of CNT/FeO/TiO<sub>2</sub> (after 5 minutes).

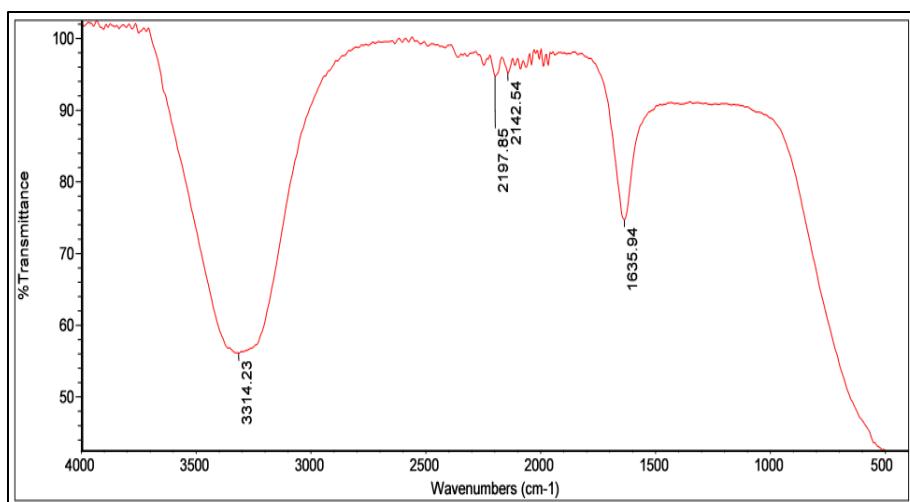


Figure 38 Congo Red Solution A 0.5 Absorbance (After removal of CNT/FeO/TiO<sub>2</sub> nanocomposite)

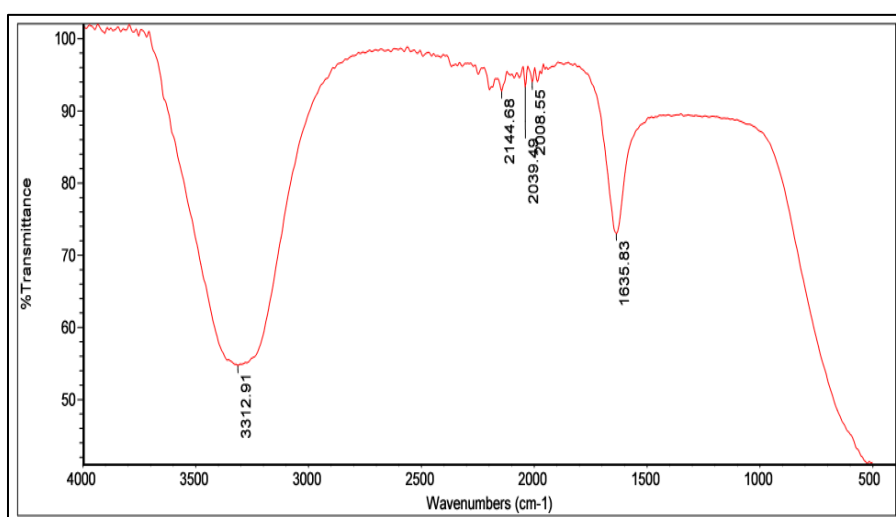


Figure 39 Allura Red AC Solution B 1.5 Absorbance (After removal of CNT/FeO/TiO<sub>2</sub> nanocomposite).

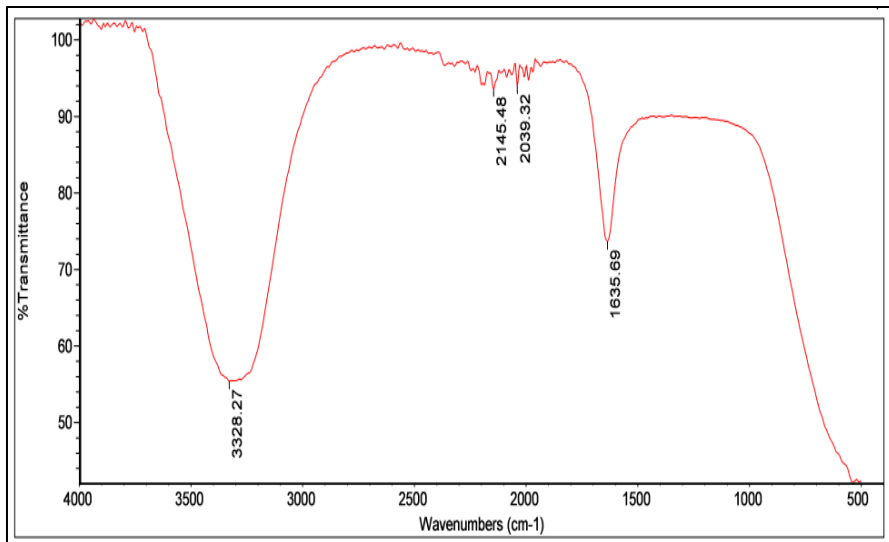


Figure 40 Allura Red AC Solution A 0.5 Absorbance (After removal of CNT/FeO/TiO<sub>2</sub> nanocomposite).

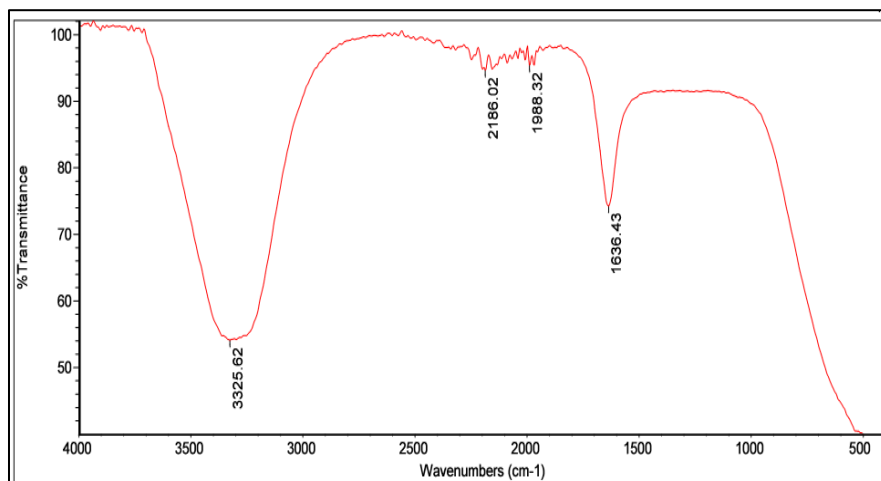


Figure 41 Methylene Blue Solution B 1.5 Absorbance (After removal of AC/FeO/TiO<sub>2</sub> nanocomposite).

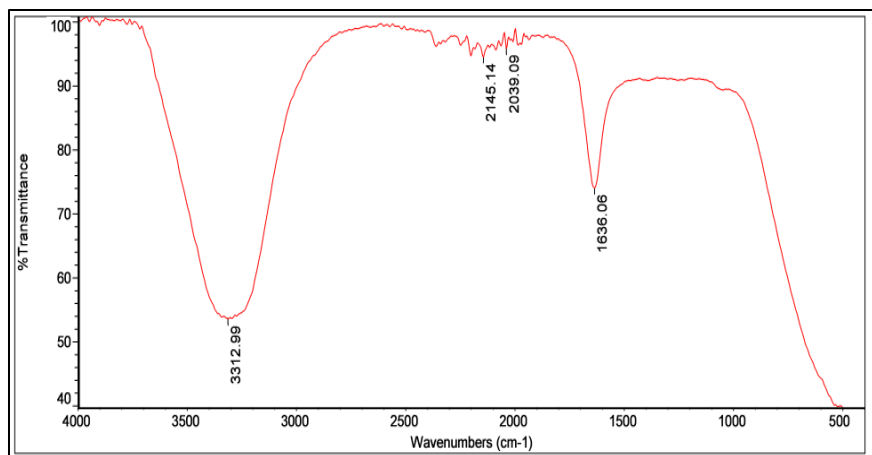


Figure 42. Methylene Blue Solution A 0.5 Absorbance (After removal of AC/FeO/TiO<sub>2</sub> nanocomposite).

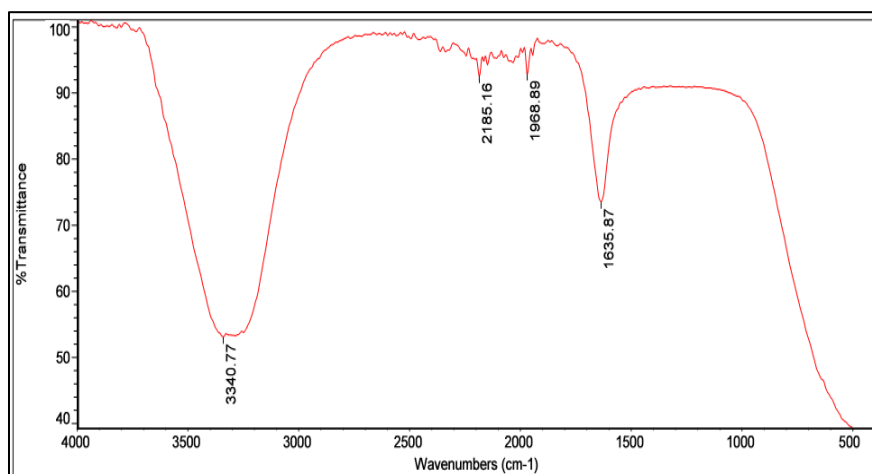


Figure 43 Congo Red Solution B 1.5 Absorbance (After removal of AC/FeO/TiO<sub>2</sub> nanocomposite).

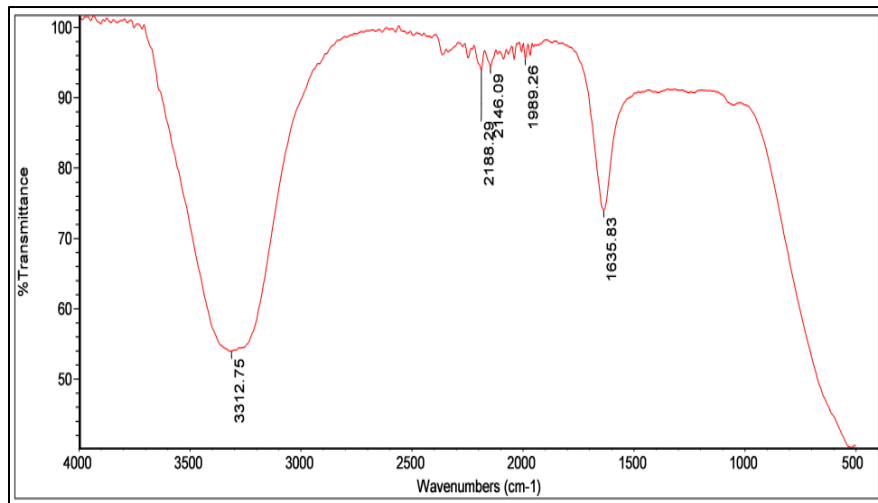


Figure 44 Congo Red Solution A 0.5 Absorbance (After removal of AC/FeO/TiO<sub>2</sub> nanocomposite).

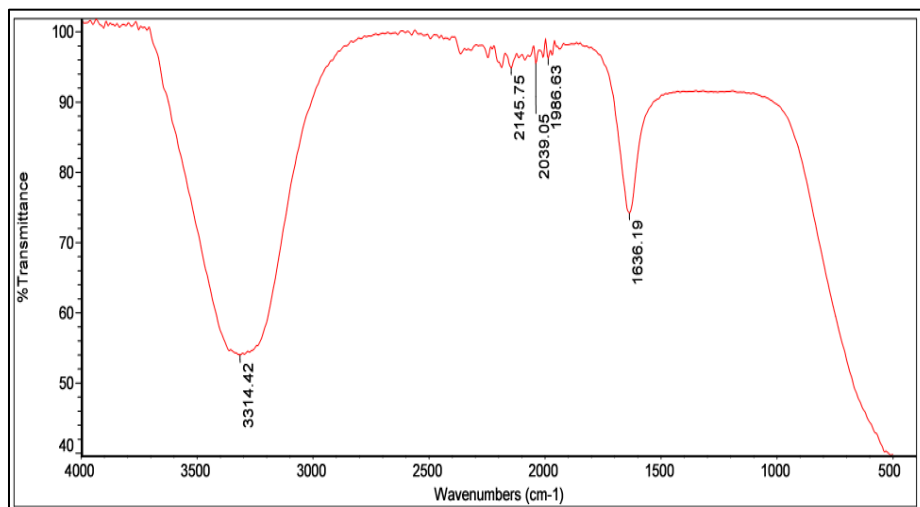


Figure 45 Allura Red AC Solution B 1.5 Absorbance (After removal of AC/FeO/TiO<sub>2</sub> nanocomposite).

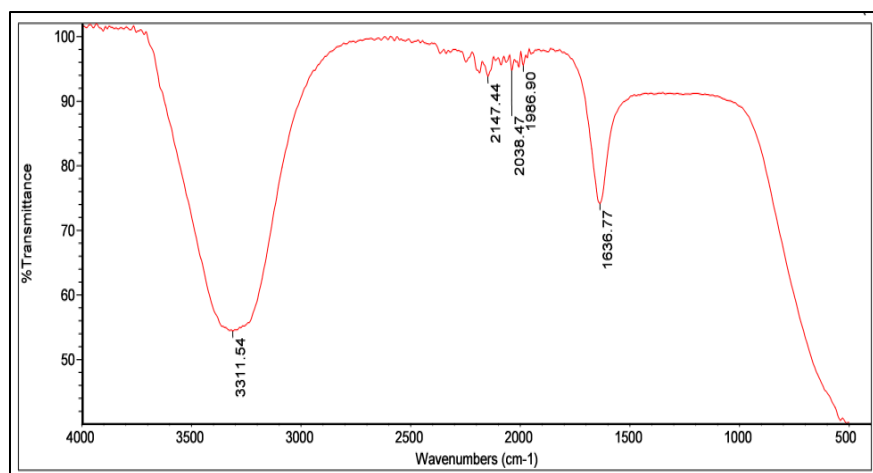


Figure 46 Allura Red AC Solution A 0.5 Absorbance (After removal of AC/FeO/TiO<sub>2</sub> nanocomposite).

### 3.2.3 Scanning Electron Microscope

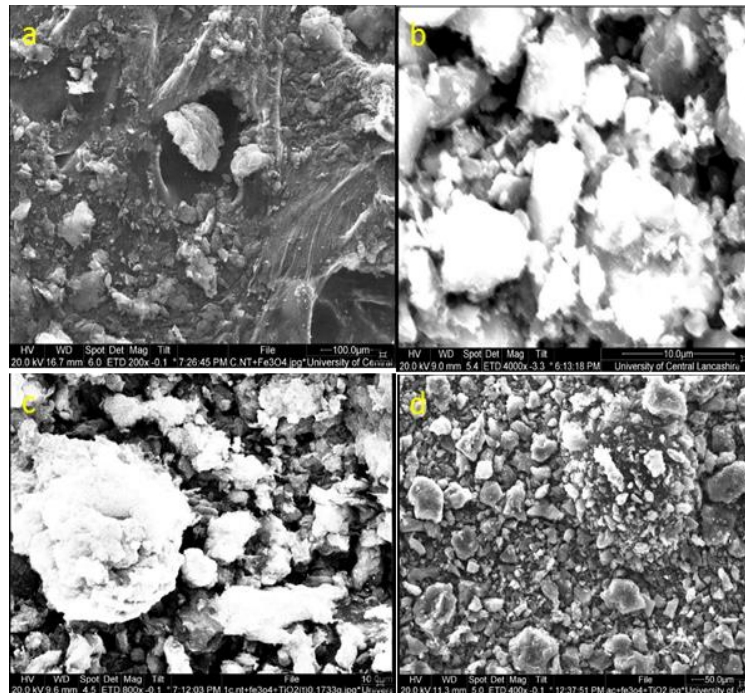


Figure 47 (a) Carbon Nanotube-Iron Oxide Nanocomposites (b) Activated Charcoal-Iron Oxide Nanocomposite (c) Carbon Nanotube/Iron Oxide/Titanium Dioxide Nanocomposite (d) Activated Charcoal/Iron Oxide/Titanium Dioxide Nanocomposite

SEM Image of (a) Carbon Nanotube and Iron Oxide. Image shows poly dispersive non-uniform material.

SEM Image of (b) Activated Charcoal and Iron Oxide. Image shows poly dispersive non-uniform material.

SEM Image of (c) Multi Walled Carbon Nanotubes/TiO<sub>2</sub>/Iron Oxide. Image shows a poly dispersive non-uniform material. Very difficult to see the fibre like structure of the CNT.

SEM Image of (d) Activated Charcoal/Iron Oxide/TiO<sub>2</sub>. Image shows poly dispersive non-uniform material

### 3.2.4 Energy Dispersive Analysis using X-rays

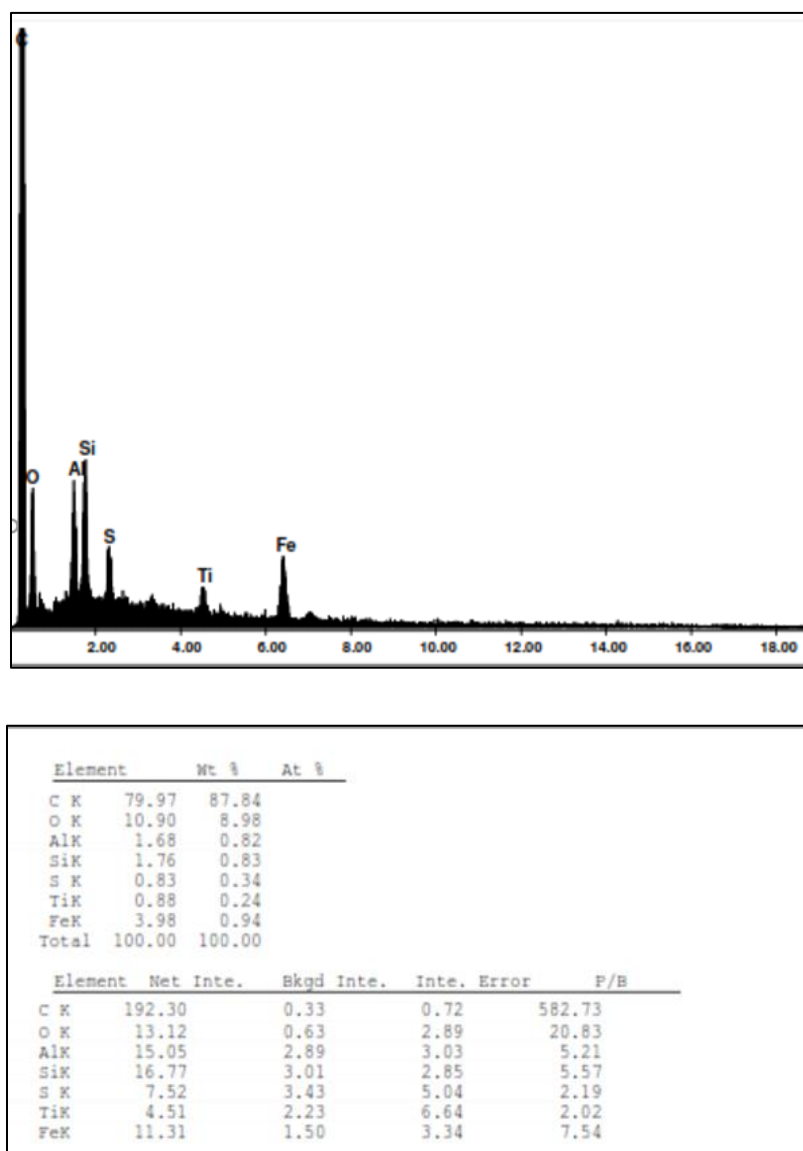


Figure 48 EDAX of AC-FeO-TiO<sub>2</sub> nanocomposite

EDAX confirms all the expected elements that should be present in this nanocomposite.

Titanium and oxygen due to TiO<sub>2</sub>, Iron and oxygen peak due iron oxide. Very high Carbon peak due to nanocomposite host material. Aluminium peak impurity due to improper cleaning of EDAX instrument.

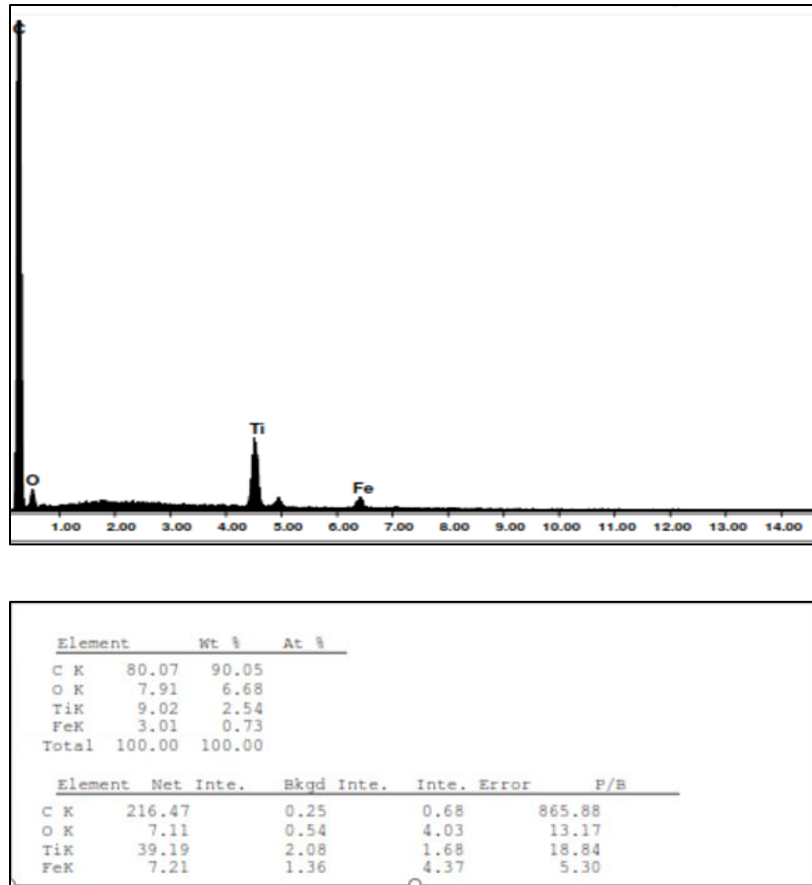


Figure 49 EDAX of MWCNT-FeO-TiO<sub>2</sub>

EDAX confirms all the expected elements that should be present in this nanocomposite. Titanium and oxygen due to TiO<sub>2</sub>, Iron and oxygen peak due iron oxide. Very high Carbon peak due to nanocomposite being the host material.

### 3.3 Hybrid Ionic Liquid-Iron Oxide nanocomposites

#### 3.3.1 Fourier Transform Infra-Red Spectra

##### Hybrid B:

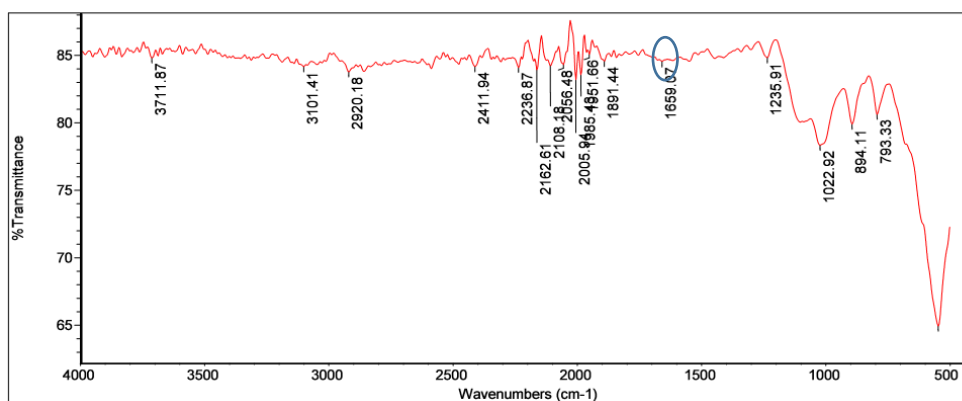


Figure 50 Hybrid B (Ionic Liquid-Iron Oxide Hybrid B).

The bands at  $2920.18\text{ cm}^{-1}$  are assignable to saturated and unsaturated C–H stretching vibrations of  $\text{CH}_2$  (From the octyl chain.) The band at  $3101.14\text{ cm}^{-1}$  is assignable to an H attached to Nitrogen (N–H) of the imidazole ring. The band at  $3711.02$  is assignable to an O–H band from water, as this solid was washed with water after synthesis. Sample must not have been dry.

For the imidazolium-IL the bands at  $2865\text{ cm}^{-1}$  is for the aliphatic C–H bending vibration, and  $1659$  are indicative of the imidazole ring skeleton. There appears to be a peak at around  $1400$  which would help indicate the presence of the imidazole ring, however the signal is either too weak or there was ‘noise’ preventing the machine picking the peak. The  $1022\text{ cm}^{-1}$  peak seems to indicate the imidazole ring C–H bond plane bending vibration.

### 3.3.2 Scanning Electron Microscope

**Ionic Liquid-Iron Oxide Nanocomposites:** These are characterized by SEM images, showing a sponge-like morphology. The morphology of these four nanocomposites is like one another other.

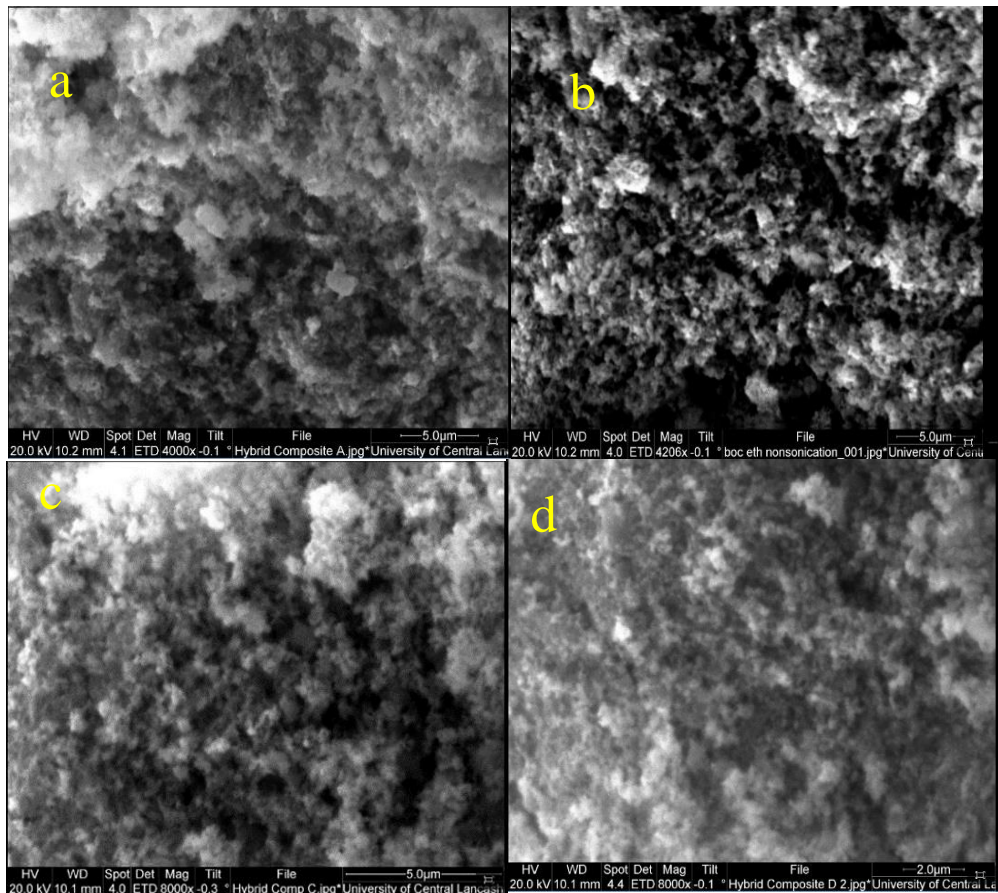


Figure 51 (a) Ionic Liquid-Iron Oxide Hybrid, (b) Image of porous Ionic Liquid-Iron Oxide Hybrid (c) Ionic Liquid-Iron Oxide Hybrid (d) Ionic Liquid-Iron Oxide Hybrid

### 3.3.3 Energy Dispersive Analysis using X-rays

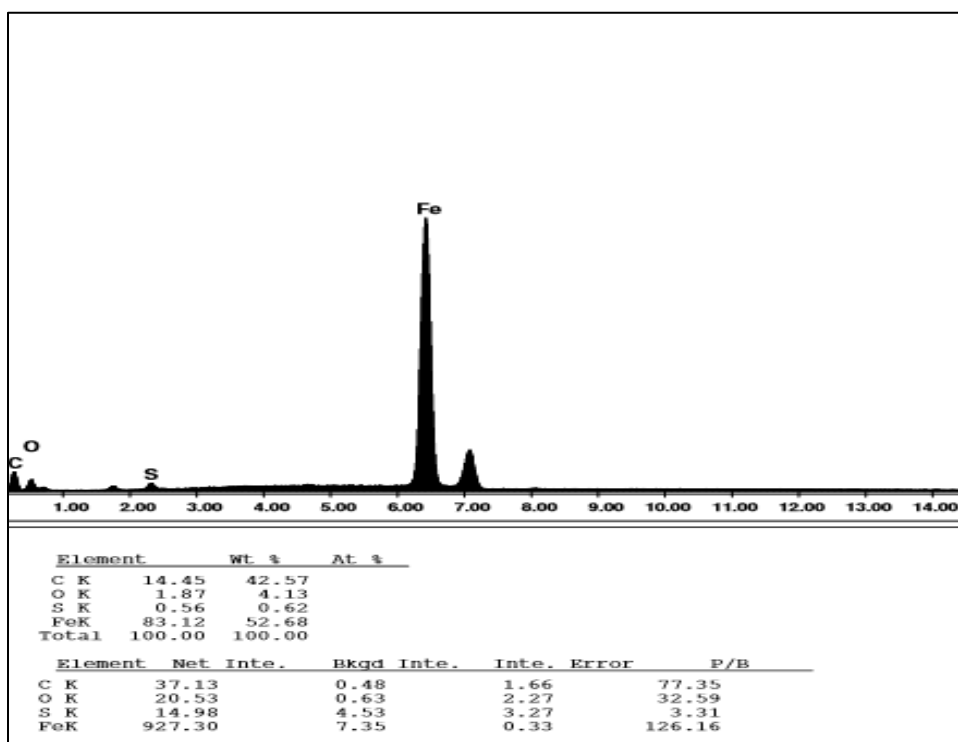


Figure 52 EDAX of Ionic Liquid-Iron Oxide Hybrid A

#### i) Ionic Liquid-Iron Oxide Hybrid Nanocomposite A

EDAX confirms all but one element that should be present in this nanocomposite. Carbon peak due to the presence of the octyl chain. Large Iron Peak due to core shell being Iron Oxide. Oxygen present due Iron Oxide, Sulphur present from Sulphur-Carbon Bond (S reacting with Alkene.) Nitrogen is an expected element due to the imidazole group, however peak did not turn up as the voltage of the SEM was not accelerated enough.

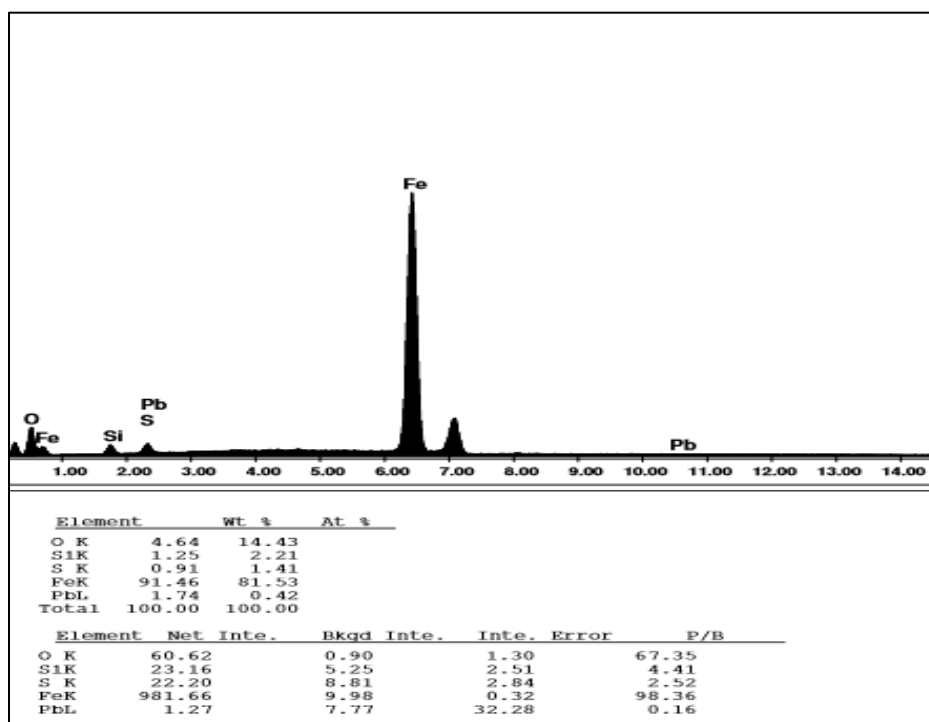


Figure 53 EDAX of Ionic Liquid-Iron Oxide Hybrid B

## ii) Ionic Liquid-Iron Oxide Hybrid Nanocomposite B

EDAX confirms all but one elements that should be present in this nanocomposite.

Nitrogen is missing as explained in Ionic Liquid-Iron Oxide Nanocomposite A.

Carbon peak due to the presence of the octyl chain.

Large Iron Peak due to core shell being iron oxide. Oxygen present due Iron Oxide,

Sulphur present from Sulphur-Carbon Bond (S reacting with Alkene.)

### iii) Ionic Liquid-Iron Oxide Hybrid Nanocomposite C

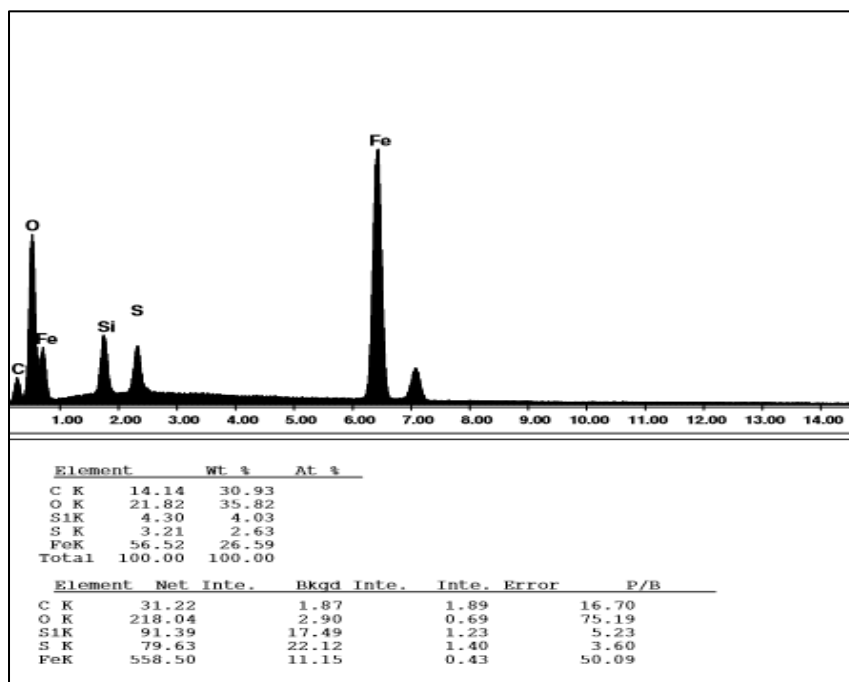


Figure 54 EDAX of Ionic-Iron Oxide Hybrid C

EDAX confirms all but one element that should be present in this nanocomposite.

Nitrogen is missing as explained in Ionic Liquid-Iron Oxide Nanocomposite A.

Carbon peak due to the presence of the octyl chain.

Large Iron Peak due to core shell being iron oxide. Oxygen present due Iron Oxide,

Sulphur present from Sulphur-Carbon Bond (S reacting with Alkene.)

#### iv) Ionic Liquid-Iron Oxide Hybrid Nanocomposite D

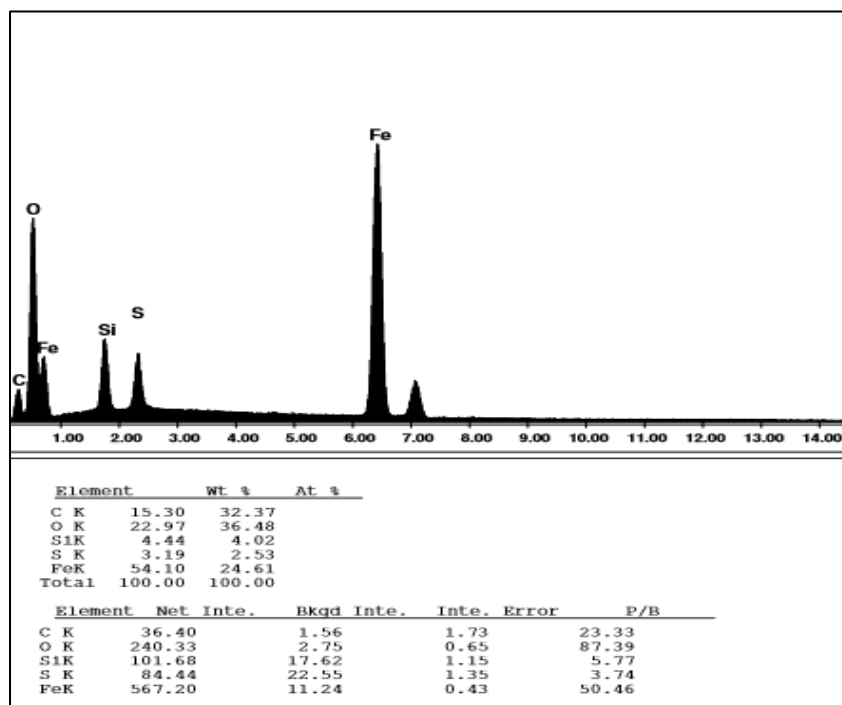


Figure 55 EDAX of Ionic Liquid-Iron Oxide Hybrid D

EDAX confirms all but one element that should be present in this nanocomposite.

Nitrogen is missing as explained in Ionic Liquid-Oxide Nanocomposite A.

Carbon peak due to the presence of the octyl chain.

Large Iron Peak due to core shell being iron oxide. Oxygen present due Iron Oxide,

Sulphur present from Sulphur-Carbon Bond (S reacting with Alkene.)

### 3.4.1 Kinetics Methylene Blue

The calibration graph data produced the following equations:

The equation for Methylene Blue =  $y = 0.357x + 0.1293$

With these equations, a graph showing time against concentration was created (Note:

See Appendix for Concentration vs. Time graphs).

Table 4 shows the degradation kinetics of Methylene Blue Solution A with various carbon nanocomposites. (Please refer to Table A61, A62, A63 and A64 in the appendix for values and plots.)

<b>Nanocomposite (Methylene Blue Solution A)</b>	<b>Rate Constant</b>
Iron Oxide + Activated Charcoal	$0.00857s^{-1}$
Iron Oxide + Activated Charcoal +TiO <sub>2</sub>	$0.00851s^{-1}$
Iron Oxide + Multi-Walled Carbon Nanotube	$0.00849s^{-1}$
Iron Oxide + Multi-Walled Carbon Nanotube + TiO <sub>2</sub>	$0.00844s^{-1}$

Table 5 shows the degradation kinetics of Methylene Blue with ionic-liquid hybrid nanocomposites,

(Please refer to Table A69, A70, A71 and A72 in the appendix for values and plots.)

<b>Nanocomposite (Methylene Blue Solution A)</b>	<b>Rate Constant</b>
Hybrid A	$k=0.00476s^{-1}$
Hybrid B	$k=0.00405s^{-1}$
Hybrid C (Anomalous Result)	$k=0.00916s^{-1}$
Hybrid D (Anomalous Result)	$k=0.00760s^{-1}$

Anomalous result due to - Reaction completed in 10 minutes, however results after 5 minutes produced a negative concentration on the calibration graph. Therefore, was impossible to plot onto the graph.

Table 6. Shows the degradation kinetics of Methylene Blue Solution B with ionic-liquid hybrid nanocomposites, (Please refer to Table A73, A74, A75 and A76 in the appendix for values and plots.)

<b>Nanocomposite (Methylene Blue Solution B)</b>	<b>Rate Constant</b>
Hybrid A	0.003096s <sup>-1</sup>
Hybrid B	0.00271s <sup>-1</sup>
Hybrid C	0.00262s <sup>-1</sup>
Hybrid D	0.00275s <sup>-1</sup>

From the concentration, vs time plots it can be concluded that the removal of dyes works via a first order reaction. I.e. The adsorbance of dye is directly proportional to the amount of nanocomposite present. From the concentration vs time plots, straight-line graphs were produced to determine the rate constants of the nanocomposites present in dye solution. The results clearly show that carbon based nanocomposites are twice as fast as the ionic liquid-nanocomposites e.g. carbon based nanocomposites have a rate constant of 0.00850s<sup>-1</sup> while hybrids have a rate constant of around 0.00400s<sup>-1</sup> in methylene blue solution A.

The carbon-based nanocomposites have an even greater efficiency in higher concentrations in comparison e.g. carbon-based nanocomposites have a rate constant of 0.00850s<sup>-1</sup> while hybrids have a rate constant of around 0.00275s<sup>-1</sup> in methylene solution B.

### 3.4.2 Kinetics Congo Red

The calibration graph data produced the following equations:

The equation for Congo Red =  $0.2962x + 0.1344$

With these equations, a graph showing time against concentration was created (Note:

See Appendix for Concentration vs. Time graphs).

Table 7. Shows the degradation kinetics of Congo Red Solution A with ionic-liquid hybrid nanocomposites. (Please refer to Table A65, A66, A67 and A68 in the appendix for values and plots.)

<b>Nanocomposite (Congo Red A)</b>	<b>Rate Constant</b>
Iron Oxide + Activated Charcoal	$0.00407s^{-1}$
Iron Oxide + Activated Charcoal +TiO <sub>2</sub>	$0.00396s^{-1}$
Iron Oxide + Multi-Walled Carbon Nanotube	$0.00416s^{-1}$
Iron Oxide + Multi-Walled Carbon Nanotube + TiO <sub>2</sub>	$0.00397s^{-1}$

Table 8. Shows the degradation kinetics of Congo Red solution A with ionic-liquid hybrid nanocomposites. (Please refer to Table A77, A78, A79 and A80 in the appendix for values and plots.)

<b>Nanocomposite (Congo Red A)</b>	<b>Rate Constant</b>
Hybrid A	$0.001036s^{-1}$
Hybrid B	$0.00106s^{-1}$
Hybrid C	$0.00116s^{-1}$
Hybrid D	$0.0011s^{-1}$

Table 9. Shows the degradation kinetics of Congo Red solution B with ionic-liquid hybrid nanocomposites. (Please refer to Table A81, A82, A83 and A84 in the appendix for values and plots.)

<b>Nanocomposite (Congo Red B)</b>	<b>Rate Constant</b>
Hybrid A	$0.001\text{s}^{-1}$
Hybrid B	$0.00098\text{s}^{-1}$
Hybrid C	$0.000888\text{s}^{-1}$
Hybrid D	$0.001\text{s}^{-1}$

The results show that carbon based nanocomposites are four times as fast as the ionic liquid-nanocomposites e.g. carbon based nanocomposites have a rate constant of  $0.00400\text{s}^{-1}$  while hybrids have a rate constant of around  $0.00100\text{s}^{-1}$  in Congo Red solution A and B.

The carbon-based nanocomposites have an even greater efficiency in higher concentrations in comparison e.g. carbon based nanocomposites have a rate constant of  $0.00850\text{s}^{-1}$  while hybrids have a rate constant of around  $0.00275\text{s}^{-1}$

### **3.4.3 Kinetics Allura Red AC**

The calibration graph data produced the following equations:

The equation for Allura Red AC =  $0.2575x - 0.0083$

With these equations, a graph showing time against concentration was created (Note: See Appendix for Concentration vs. Time graphs).

The ionic liquid hybrids did not have a problem with adsorption/degrading Allura Red AC. The carbon-based nanocomposites were not tested against Allura red at the time.

Table 10. Shows the degradation kinetics of Allure Red AC solution A with ionic-liquid hybrid nanocomposites. (Please refer to Table A85, A86, A87 and A88 in the appendix for values and plots.)

Nanocomposite (Allura Red AC A)	Rate Constant
Hybrid A	0.002059s <sup>-1</sup>
Hybrid B	0.002032s <sup>-1</sup>
Hybrid C	0.002127s <sup>-1</sup>
Hybrid D	0.002055s <sup>-1</sup>

Table 11. Shows the degradation kinetics of Congo Red solution B with ionic-liquid hybrid nanocomposites. (Please refer to Table A89, A90, A91 and A92 in the appendix for values and plots.)

Nanocomposite (Allura Red AC B)	Rate Constant
Hybrid A	0.001084s <sup>-1</sup>
Hybrid B	0.001061s <sup>-1</sup>
Hybrid C	0.001086s <sup>-1</sup>
Hybrid D	0.001074s <sup>-1</sup>

Standard Dilutions of MB	Absorbance (Abs)
Concentration (M) (mol/L (x10 <sup>-5</sup> ))	(665 nm)
0	0
0.63 (Solution A)	0.39
1.27	0.65
1.93	0.884
2.61	1.13
3.29	1.28
3.99 (Solution B)	1.47

## 4. Conclusions and Future Work

In this research, inorganic-organic nanocomposites were synthesised. All compounds synthesised and displayed a magnetic response. These materials showed adsorption of organic pollutant in aqueous environment. The studies were performed using a UV spectrophotometer. Novel materials were characterised using a variety of physicochemical properties. The XRD data shows that iron oxide is present in carbon nanocomposites. The XRD data confirms state of iron oxide in carbon nanotube is  $\text{Fe}_2\text{O}_3$  (maghemite). However, the state of Iron Oxide in activated charcoal composite could not be confirmed as either  $\text{Fe}_3\text{O}_4$  or  $\text{Fe}_2\text{O}_3$ . As these nanocomposites produced a magnetic response, they can separate the nanocomposites after adsorbing the environmental organic pollutants. The initial results from this work suggested the cost-effective methods for separation of organic compounds in water purification industry.

From the UV spectroscopy, data the novel hybrids nanocomposite synthesised have ability to successfully adsorb the organic pollutants. Meanwhile, using titanium dioxide, the organic pollutant can be degraded successfully. The ionic-liquid nanocomposites take almost two to four times (Depending on solution concentration) the amount of time to adsorb/interact/breakdown the dye solutions. The carbon-based nanocomposite has shown good cost and time effectiveness over ionic liquid based materials. The nanocomposite takes only 5 to 60 minutes to separate the organic pollutants; however, ionic liquids are still a novel functionalisation.

**Future work:** Further synthesis with other Ionic-Liquids (imidazolium's, pyridinium's, pyrrolidinium etc), and different lengths of polar chains (hexyl, heptyl, nonyl etc); to see whether this has an effect on rates of degradation of dyes. An extensive study on kinetics and adsorption of various dyes using novel nanocomposites could be worth investigating in order to have a clear understanding on the removal of organic dyes from water.

## References

- [1] N. P. Mohabansi, V. B. Patil, and N. Yenkie, "A comparative study on photo degradation of methylene blue dye effluent by advanced oxidation process by using TiO<sub>2</sub>/ZnO photo catalyst," *Rasayan J. Chem.*, vol. 4, no. 4, pp. 814–819, 2011.
- [2] J. J. A.-G. and P. Q.-O. Lidia Vilca-Quispe, Alejandro Castilla-Loeza, *Diffusion of Methylene Blue in Phantoms of Agar Using Optical Absorption Techniques, Advanced Biomedical Engineering*. 2011.
- [3] P. Zhang, J. Chen, and L. Jia, "N-Methylimidazolium-functionalized monolithic silica column for mixed-mode chromatography," *J. Chromatogr. A*, vol. 1218, no. 22, pp. 3459–3465, 2011.
- [4] A. Kongkanand and P. V. Kamat, "Electron storage in single wall carbon nanotubes. Fermi level equilibration in semiconductor–SWCNT suspensions," *ACS Nano*, vol. 1, no. 1, pp. 13–21, 2007.
- [5] Wikipedia, "Allura Red AC," 2017. [Online]. Available: [https://upload.wikimedia.org/wikipedia/commons/8/89/Allura\\_Red\\_AC.png](https://upload.wikimedia.org/wikipedia/commons/8/89/Allura_Red_AC.png). [Accessed: 09-Feb-2017].
- [6] C. Guide, "Beer Lambert Law," 2017. [Online]. Available: <http://www.chemguide.co.uk/analysis/uvvisible/beerlambert.html>. [Accessed: 09-Feb-2017].
- [7] bgs, "X-Ray Diffraction." [Online]. Available: [http://www.bgs.ac.uk/scienceFacilities/laboratories/mpb/xrd\\_tech.html](http://www.bgs.ac.uk/scienceFacilities/laboratories/mpb/xrd_tech.html). [Accessed: 09-Feb-2017].
- [8] Z. Rappoport, *The Chemistry of Phenols, 2 Volume Set*. John Wiley & Sons, 2004.
- [9] J. Cenens and R. A. Schoonheydt, "Visible spectroscopy of methylene blue on hectorite, laponite B, and barasym in aqueous suspension," *Clays Clay Miner.*, vol. 36, no. 3, pp. 214–224, 1988.
- [10] X. Qu, P. J. J. Alvarez, and Q. Li, "Applications of nanotechnology in water and wastewater treatment," *Water Res.*, vol. 47, no. 12, pp. 3931–3946, 2013.
- [11] A. Ito, M. Shinkai, H. Honda, and T. Kobayashi, "Medical application of functionalized magnetic nanoparticles," *J. Biosci. Bioeng.*, vol. 100, no. 1, pp. 1–11, 2005.
- [12] T. Sen, I. J. Bruce, and T. Mercer, "Fabrication of novel hierarchically ordered porous magnetic nanocomposites for bio-catalysis," *Chem. Commun.*, vol. 46, no. 36, pp. 6807–6809, 2010.
- [13] L. F. Velasco, J. B. Parra, and C. O. Ania, "Role of activated carbon features on the photocatalytic degradation of phenol," *Appl. Surf. Sci.*, vol. 256, no. 17, pp. 5254–5258, 2010.
- [14] R. Leary and A. Westwood, "Carbonaceous nanomaterials for the enhancement of TiO<sub>2</sub> photocatalysis," *Carbon N. Y.*, vol. 49, no. 3, pp. 741–772, 2011.
- [15] P. Serp, *Carbon nanotubes and nanofibers in catalysis*. John Wiley & Sons, Inc.: Hoboken, NJ, 2009.
- [16] P. Serp, M. Corrias, and P. Kalck, "Carbon nanotubes and nanofibers in catalysis," *Appl. Catal. A Gen.*, vol. 253, no. 2, pp. 337–358, 2003.
- [17] B. Tryba, A. W. Morawski, and M. Inagaki, "Application of TiO<sub>2</sub>-mounted activated carbon to the removal of phenol from water," *Appl. Catal. B Environ.*, vol. 41, no. 4, pp. 427–433, 2003.

- [18] X. Zhang, Mi. Zhou, and L. Lei, "Preparation of photocatalytic TiO<sub>2</sub> coatings of nanosized particles on activated carbon by AP-MOCVD," *Carbon N. Y.*, vol. 43, no. 8, pp. 1700–1708, 2005.
- [19] N. Satoh, T. Nakashima, K. Kamikura, and K. Yamamoto, "Quantum size effect in TiO<sub>2</sub> nanoparticles prepared by finely controlled metal assembly on dendrimer templates," *Nat. Nanotechnol.*, vol. 3, no. 2, pp. 106–111, 2008.
- [20] X. Zhang, M. Zhou, and L. Lei, "TiO<sub>2</sub> photocatalyst deposition by MOCVD on activated carbon," *Carbon N. Y.*, vol. 44, no. 2, pp. 325–333, 2006.
- [21] D.-K. Lee, S.-C. Kim, I.-C. Cho, S.-J. Kim, and S.-W. Kim, "Photocatalytic oxidation of microcystin-LR in a fluidized bed reactor having TiO<sub>2</sub>-coated activated carbon," *Sep. Purif. Technol.*, vol. 34, no. 1, pp. 59–66, 2004.
- [22] Y. Yao, G. Li, S. Ciston, R. M. Lueptow, and K. A. Gray, "Photoreactive TiO<sub>2</sub>/carbon nanotube composites: synthesis and reactivity," *Environ. Sci. Technol.*, vol. 42, no. 13, pp. 4952–4957, 2008.
- [23] B. Ahmmad, Y. Kusumoto, S. Somekawa, and M. Ikeda, "Carbon nanotubes synergistically enhance photocatalytic activity of TiO<sub>2</sub>," *Catal. Commun.*, vol. 9, no. 6, pp. 1410–1413, 2008.
- [24] B.-S. Huang, F.-Y. Chang, and M.-Y. Wey, "An efficient composite growing N-doped TiO<sub>2</sub> on multi-walled carbon nanotubes through sol–gel process," *J. Nanoparticle Res.*, vol. 12, no. 7, pp. 2503–2510, 2010.
- [25] R. H. Baughman, A. A. Zakhidov, and W. A. De Heer, "Carbon nanotubes—the route toward applications," *Science (80-. )*, vol. 297, no. 5582, pp. 787–792, 2002.
- [26] B. Pan and B. Xing, "Adsorption mechanisms of organic chemicals on carbon nanotubes," *Environ. Sci. Technol.*, vol. 42, no. 24, pp. 9005–9013, 2008.
- [27] K. Yang and B. Xing, "Adsorption of organic compounds by carbon nanomaterials in aqueous phase: Polanyi theory and its application," *Chem. Rev.*, vol. 110, no. 10, pp. 5989–6008, 2010.
- [28] W. Chen, L. Duan, and D. Zhu, "Adsorption of polar and nonpolar organic chemicals to carbon nanotubes," *Environ. Sci. Technol.*, vol. 41, no. 24, pp. 8295–8300, 2007.
- [29] R. Bauer and H. Fallmann, "The photo-Fenton oxidation—a cheap and efficient wastewater treatment method," *Res. Chem. Intermed.*, vol. 23, no. 4, pp. 341–354, 1997.
- [30] L. Ji, W. Chen, L. Duan, and D. Zhu, "Mechanisms for strong adsorption of tetracycline to carbon nanotubes: a comparative study using activated carbon and graphite as adsorbents," *Environ. Sci. Technol.*, vol. 43, no. 7, pp. 2322–2327, 2009.
- [31] Y. Chen, J. C. Crittenden, S. Hackney, L. Sutter, and D. W. Hand, "Preparation of a novel TiO<sub>2</sub>-based p–n junction nanotube photocatalyst," *Environ. Sci. Technol.*, vol. 39, no. 5, pp. 1201–1208, 2005.
- [32] W. Wang, P. Serp, P. Kalck, and J. L. Faria, "Visible light photodegradation of phenol on MWNT-TiO<sub>2</sub> composite catalysts prepared by a modified sol–gel method," *J. Mol. Catal. A Chem.*, vol. 235, no. 1, pp. 194–199, 2005.
- [33] K. Woan, G. Pyrgiotakis, and W. Sigmund, "Photocatalytic carbon-nanotube–TiO<sub>2</sub> composites," *Adv. Mater.*, vol. 21, no. 21, pp. 2233–2239, 2009.
- [34] S. Kang, Z. Xu, Y. Song, and J. Mu, "Photocatalytic activity of high aspect ratio TiO<sub>2</sub> nanorods," *J. Dispers. Sci. Technol.*, vol. 27, no. 6, pp. 857–859, 2006.
- [35] G. Pyrgiotakis, S.-H. Lee, and W. Sigmund, "Advanced photocatalysis with

- anatase nano-coated multi-walled carbon nanotubes,” in *MRS Proceedings*, 2005, vol. 876, pp. R5–7.
- [36] R. Asahi, T. Morikawa, T. Ohwaki, K. Aoki, and Y. Taga, “Visible-light photocatalysis in nitrogen-doped titanium oxides,” *Science (80-. )*, vol. 293, no. 5528, pp. 269–271, 2001.
- [37] D. Zhao, X. Yang, C. Chen, and X. Wang, “Enhanced photocatalytic degradation of methylene blue on multiwalled carbon nanotubes–TiO<sub>2</sub>,” *J. Colloid Interface Sci.*, vol. 398, pp. 234–239, 2013.
- [38] Y. Yu *et al.*, “Enhancement of adsorption and photocatalytic activity of TiO<sub>2</sub> by using carbon nanotubes for the treatment of azo dye,” *Appl. Catal. B Environ.*, vol. 61, no. 1, pp. 1–11, 2005.
- [39] G. Li and K. A. Gray, “The solid–solid interface: explaining the high and unique photocatalytic reactivity of TiO<sub>2</sub>-based nanocomposite materials,” *Chem. Phys.*, vol. 339, no. 1, pp. 173–187, 2007.
- [40] Z. Zhang, C.-C. Wang, R. Zakaria, and J. Y. Ying, “Role of particle size in nanocrystalline TiO<sub>2</sub>-based photocatalysts,” *J. Phys. Chem. B*, vol. 102, no. 52, pp. 10871–10878, 1998.
- [41] X.-H. Xia, Z.-J. Jia, Y. Yu, Y. Liang, Z. Wang, and L.-L. Ma, “Preparation of multi-walled carbon nanotube supported TiO<sub>2</sub> and its photocatalytic activity in the reduction of CO<sub>2</sub> with H<sub>2</sub>O,” *Carbon N. Y.*, vol. 45, no. 4, pp. 717–721, 2007.
- [42] A. Fujishima, K. Hashimoto, and T. Watanabe, *TiO<sub>2</sub> photocatalysis: fundamentals and applications*. BKC Incorporated, 1999.
- [43] Y. Fan, C. Ma, W. Li, and Y. Yin, “Synthesis and properties of Fe<sub>3</sub>O<sub>4</sub>/SiO<sub>2</sub>/TiO<sub>2</sub> nanocomposites by hydrothermal synthetic method,” *Mater. Sci. Semicond. Process.*, vol. 15, no. 5, pp. 582–585, 2012.
- [44] M. Ni, M. K. H. Leung, D. Y. C. Leung, and K. Sumathy, “A review and recent developments in photocatalytic water-splitting using TiO<sub>2</sub> for hydrogen production,” *Renew. Sustain. Energy Rev.*, vol. 11, no. 3, pp. 401–425, 2007.
- [45] J. Arana *et al.*, “TiO<sub>2</sub> activation by using activated carbon as a support: part I. Surface characterisation and decantability study,” *Appl. Catal. B Environ.*, vol. 44, no. 2, pp. 161–172, 2003.
- [46] J. Matos, J. Laine, and J.-M. Herrmann, “Effect of the type of activated carbons on the photocatalytic degradation of aqueous organic pollutants by UV-irradiated titania,” *J. Catal.*, vol. 200, no. 1, pp. 10–20, 2001.
- [47] C.-Y. Kuo, “Prevenient dye-degradation mechanisms using UV/TiO<sub>2</sub>/carbon nanotubes process,” *J. Hazard. Mater.*, vol. 163, no. 1, pp. 239–244, 2009.
- [48] Y. Ao, J. Xu, D. Fu, X. Shen, and C. Yuan, “Low temperature preparation of anatase TiO<sub>2</sub>-coated activated carbon,” *Colloids Surfaces A Physicochem. Eng. Asp.*, vol. 312, no. 2, pp. 125–130, 2008.
- [49] B. Sun and P. G. Smirniotis, “Interaction of anatase and rutile TiO<sub>2</sub> particles in aqueous photooxidation,” *Catal. Today*, vol. 88, no. 1, pp. 49–59, 2003.
- [50] S. X. Liu, X. Y. Chen, and X. Chen, “A TiO<sub>2</sub>/AC composite photocatalyst with high activity and easy separation prepared by a hydrothermal method,” *J. Hazard. Mater.*, vol. 143, no. 1, pp. 257–263, 2007.
- [51] J. Zhan, H. Zhang, and G. Zhu, “Magnetic photocatalysts of cenospheres coated with Fe<sub>3</sub>O<sub>4</sub>/TiO<sub>2</sub> core/shell nanoparticles decorated with Ag nanoparticles,” *Ceram. Int.*, vol. 40, no. 6, pp. 8547–8559, 2014.
- [52] J. M. Macak, M. Zlamal, J. Krysa, and P. Schmuki, “Self-Organized TiO<sub>2</sub>

- Nanotube Layers as Highly Efficient Photocatalysts,” *small*, vol. 3, no. 2, pp. 300–304, 2007.
- [53] M. Long and W. Cai, “Visible light responsive TiO<sub>2</sub> modification with nonmetal elements,” *Front. Chem. China*, vol. 6, no. 3, pp. 190–199, 2011.
- [54] Y. Choi, T. Umebayashi, and M. Yoshikawa, “Fabrication and characterization of C-doped anatase TiO<sub>2</sub> photocatalysts,” *J. Mater. Sci.*, vol. 39, no. 5, pp. 1837–1839, 2004.
- [55] L. Zhang, H. Fu, and Y. Zhu, “Efficient TiO<sub>2</sub> photocatalysts from surface hybridization of TiO<sub>2</sub> particles with graphite-like carbon,” *Adv. Funct. Mater.*, vol. 18, no. 15, pp. 2180–2189, 2008.
- [56] S. Keskin, D. Kayrak-Talay, U. Akman, and Ö. Hortaçsu, “A review of ionic liquids towards supercritical fluid applications,” *J. Supercrit. Fluids*, vol. 43, no. 1, pp. 150–180, 2007.
- [57] R. D. Rogers and K. R. Seddon, *Ionic liquids: industrial applications for green chemistry*. ACS Publications, 2002.
- [58] C. F. Poole and S. K. Poole, “Extraction of organic compounds with room temperature ionic liquids,” *J. Chromatogr. A*, vol. 1217, no. 16, pp. 2268–2286, 2010.
- [59] X. Qiao *et al.*, “Imidazolium embedded C8 based stationary phase for simultaneous reversed-phase/hydrophilic interaction mixed-mode chromatography,” *J. Chromatogr. A*, vol. 1400, pp. 107–116, 2015.
- [60] N. Azgomi and M. Mokhtary, “Nano-Fe<sub>3</sub>O<sub>4</sub>@ SiO<sub>2</sub> supported ionic liquid as an efficient catalyst for the synthesis of 1, 3-thiazolidin-4-ones under solvent-free conditions,” *J. Mol. Catal. A Chem.*, vol. 398, pp. 58–64, 2015.
- [61] S. M. Sadeghzadeh and M. Malekzadeh, “Synthesis of 1, 3-thiazolidin-4-one using ionic liquid immobilized onto Fe<sub>3</sub>O<sub>4</sub>/SiO<sub>2</sub>/Salen/Mn,” *J. Mol. Liq.*, vol. 202, pp. 46–51, 2015.
- [62] A. K. Mallik, H. Qiu, M. Takafuji, and H. Ihara, “Copolymer-grafted silica phase from a cation–anion monomer pair for enhanced separation in reversed-phase liquid chromatography,” *Anal. Bioanal. Chem.*, vol. 406, no. 14, pp. 3507–3515, 2014.
- [63] “KS Analytical,” 2016. [Online]. Available: <http://www.ksanalytical.com/images/I-XRD-Diagram.gif> on Friday 29th May at 09:30am. [Accessed: 10-Jan-2017].
- [64] Analyt, “Analytical Spectroscopy,” 2017. [Online]. Available: [http://www.analyticalspectroscopy.net/ap3\\_html\\_m4ead8c48.png](http://www.analyticalspectroscopy.net/ap3_html_m4ead8c48.png). [Accessed: 01-Jan-2017].
- [65] Intechopen, “Intechopen,” 2017. [Online]. Available: [http://www.intechopen.com/source/html/48083/media/image3\\_w.jpg](http://www.intechopen.com/source/html/48083/media/image3_w.jpg). [Accessed: 01-Jan-2017].
- [66] RSC, “RSC,” 2017. [Online]. Available: [http://www.rsc.org/learn-chemistry/wiki/Introduction\\_to\\_NMR\\_spectroscopy](http://www.rsc.org/learn-chemistry/wiki/Introduction_to_NMR_spectroscopy). [Accessed: 01-Jan-2017].

## Appendix

Table A1 Appendix Table 1. Methylene Blue Calibration Data.

Standard Dilutions of MB Concentration (M) (mol/L (x10 <sup>-5</sup> ))	Absorbance (Abs) (665 nm)
0	0
0.63	0.39
1.27	0.65
1.93	0.884
2.61	1.13
3.29	1.28
3.99	1.47

Table A2. Methylene Blue Starting Reagent Test

Methylene Blue A Solution	AC (Abs)	MWCNT (Abs)	Control (Abs)
Time (Min)	663 nm	663 nm	663 nm
0	0.868	0.868	0.868
1	0.117	0.263	0.868
2	0.045	0.121	0.868
3	0.038	0.08	0.868
4	0.034	0.071	0.868
5	0.028	0.072	0.868

Table A3. Methylene Blue Carbon + Iron Oxide Nanocomposites Data

Methylene Blue A Solution	AC + Iron Oxide	MW-CNT + Iron Oxide	Control
Time (Min)	663 nm	663 nm	663 nm
0	0.833	0.833	0.833
1	0.354	0.57	0.833
2	0.137	0.501	0.833
3	0.122	0.383	0.833
4	0.107	0.221	0.833
5	0.082	0.134	0.833

Table A4. Methylene Blue Carbon/ Iron Oxide /TiO<sub>2</sub> Nanocomposites Data

Methylene Blue A Solution	AC + Iron Oxide	AC + Iron Oxide + TiO <sub>2</sub>	MW-CNT + Iron Oxide	MW-CNT + Iron Oxide + TiO <sub>2</sub>	Control
Time (Min)	663 nm	663 nm	663 nm	663 nm	663 nm
0	0.833	0.833	0.833	0.833	0.833
1	0.356	0.401	0.504	0.65	0.833
2	0.107	0.202	0.208	0.512	0.833
3	0.089	0.132	0.18	0.314	0.833
4	0.038	0.09	0.102	0.228	0.833
5	0.03	0.063	0.089	0.14	0.833

Table A5. Methylene Blue A against Ionic Liquid Nanocomposite Hybrid A Data

Methylene Blue A Solution	Hybrid A	Control
Time (min)	665 nm	
0	0.873	0.873
1	0.674	0.873
2	0.522	0.873
3	0.462	0.873
4	0.341	0.873
5	0.215	0.873
6	0.182	0.873
7	0.163	0.873
8	0.139	0.873
9	0.128	0.873
10	0.115	0.873

Table A6. Methylene Blue A against Ionic Liquid Nanocomposite Hybrid B Data

Methylene Blue A Solution	Hybrid B	Control
Time (min)	665 nm	
0	0.878	0.884
1	0.52	0.884
2	0.484	0.884
3	0.42	0.884
4	0.335	0.884
5	0.31	0.884
6	0.282	0.884
7	0.186	0.884
8	0.18	0.884
9	0.155	0.884
10	0.16	0.884

Table A7. Methylene Blue A against Ionic Liquid Nanocomposite Hybrid C Data

Methylene Blue A Solution	Hybrid C	Control
Time (min)	665 nm	
0	0.884	0.884
1	0.645	0.884
2	0.315	0.884
3	0.192	0.884
4	0.185	0.884
5	0.121	0.884
6	0.08	0.884
7	0.082	0.884
8	0.065	0.884
9	0.063	0.884
10	0.062	0.884

Table A8. Methylene Blue A against Ionic Liquid Nanocomposite Hybrid D Data

Methylene Blue A Solution	Hybrid D	Control
Time (min)	665 nm	
0	0.883	0.883
1	0.62	0.883
2	0.308	0.883
3	0.218	0.883
4	0.175	0.883
5	0.153	0.883
6	0.122	0.883
7	0.105	0.883
8	0.101	0.883
9	0.1	0.883
10	0.098	0.883

Table A 9. Methylene Blue B against Ionic Liquid Nanocomposite Hybrid A Data

Methylene Blue B Solution	Hybrid A	Control
Time (min)	665 nm	
0	1.252	1.252
1	1.235	1.252
2	1.077	1.252
3	0.93	1.252
4	0.845	1.252
5	0.662	1.252
6	0.625	1.252
7	0.485	1.252
8	0.455	1.252
9	0.426	1.252
10	0.38	1.252
11	0.224	1.252
12	0.198	1.252
13	0.178	1.252
14	0.153	1.252
15	0.121	1.252
16	0.11	1.252
17	0.098	1.252
18	0.092	1.252
19	0.085	1.252
20	0.084	1.252

Table A10. Methylene Blue B against Ionic Liquid Nanocomposite Hybrid B Data

Methylene Blue B Solution	Hybrid B	Control
Time (min)	665 nm	
0	1.243	1.243
1	1.206	1.243
2	1.098	1.243
3	0.951	1.243
4	0.92	1.243
5	0.796	1.243
6	0.65	1.243
7	0.613	1.243
8	0.52	1.243
9	0.389	1.243
10	0.33	1.243
11	0.256	1.243
12	0.214	1.243
13	0.19	1.243
14	0.186	1.243
15	0.155	1.243
16	0.143	1.243
17	0.123	1.243
18	0.11	1.243
19	0.095	1.243
20	0.092	1.243

Table A11. Methylene Blue B against Ionic Liquid Nanocomposite Hybrid C Data

Methylene Blue B Solution	Hybrid C	Control
Time (min)	665 nm	
0	1.248	1.248
1	1.125	1.248
2	0.985	1.248
3	0.784	1.248
4	0.724	1.248
5	0.698	1.248
6	0.585	1.248
7	0.512	1.248
8	0.466	1.248
9	0.445	1.248
10	0.409	1.248
11	0.318	1.248
12	0.276	1.248
13	0.221	1.248
14	0.125	1.248
15	0.118	1.248
16	0.106	1.248
17	0.107	1.248
18	0.099	1.248
19	0.096	1.248
20	0.095	1.248

Table A12. Methylene Blue D against Ionic Liquid Nanocomposite Hybrid D Data

Methylene Blue B Solution	Hybrid D	Control
Time (min)	665 m,	
0	1.244	1.244
1	1.143	1.244
2	1.069	1.244
3	0.93	1.244
4	0.875	1.244
5	0.694	1.244
6	0.586	1.244
7	0.512	1.244
8	0.455	1.244
9	0.356	1.244
10	0.278	1.244
11	0.224	1.244
12	0.204	1.244
13	0.182	1.244
14	0.149	1.244
15	0.135	1.244
16	0.121	1.244
17	0.119	1.244
18	0.092	1.244
19	0.087	1.244
20	0.086	1.244

Table A13. Congo Red against Carbon/Iron Oxide/TiO<sub>2</sub> Data

Congo Red A Solution	AC + Iron Oxide	AC + Iron Oxide + TiO <sub>2</sub>	MW-CNT + Iron Oxide	MW-CNT + Iron Oxide + TiO <sub>2</sub>	Control
Time (min)	490 nm	490 nm	490 nm	490 nm	490 nm
0	1.035	1.035	1.035	1.035	1.035
1	0.75	0.833	0.734	0.85	1.035
2	0.696	0.788	0.696	0.811	1.035
3	0.621	0.745	0.623	0.785	1.035
4	0.581	0.709	0.582	0.741	1.035
5	0.522	0.682	0.531	0.702	1.035
6	0.482	0.651	0.485	0.675	1.035
7	0.43	0.615	0.44	0.634	1.035
8	0.38	0.598	0.355	0.6	1.035
9	0.344	0.563	0.271	0.58	1.035
10	0.309	0.53	0.212	0.512	1.035
After 24 Hours	0.097	0.53	0.056	0.124	1.035

Table A14. Congo Red A against Ionic Liquid Nanocomposite Hybrid A

Congo Red (A)	Product A	Control
Time (min)	491 nm	
0	0.811	0.811
2	0.788	0.811
4	0.745	0.811
6	0.709	0.811
8	0.682	0.811
10	0.651	0.811
12	0.615	0.811
14	0.598	0.811
16	0.563	0.811
18	0.53	0.811
20	0.512	0.811
22	0.497	0.811
24	0.456	0.811
26	0.418	0.811
28	0.381	0.811
30	0.348	0.811
32	0.299	0.811
34	0.274	0.811
36	0.262	0.811
38	0.246	0.811
40	0.218	0.811

Table A15. Congo Red A against Ionic Liquid Nanocomposite Hybrid A Data

Congo Red (A)	Product B	Control
Time (min)	491 nm	
0	0.812	0.812
2	0.788	0.812
4	0.745	0.812
6	0.709	0.812
8	0.682	0.812
10	0.651	0.812
12	0.615	0.812
14	0.598	0.812
16	0.571	0.812
18	0.557	0.812
20	0.538	0.812
22	0.531	0.812
24	0.496	0.812
26	0.473	0.812
28	0.45	0.812
30	0.439	0.812
32	0.421	0.812
34	0.377	0.812
36	0.356	0.812
38	0.336	0.812
40	0.327	0.812

Table A16. Congo Red A against Ionic Liquid Nanocomposite Hybrid C Graph

Congo Red (A)	Product C	Control
Time (Min)	491 nm	
0	0.809	809
2	0.783	809
4	0.746	809
6	0.707	809
8	0.675	809
10	0.629	809
12	0.57	809
14	0.522	809
16	0.487	809
18	0.45	809
20	0.413	809
22	0.386	809
24	0.349	809
26	0.31	809
28	0.279	809
30	0.234	809
32	0.208	809
34	0.177	809
36	0.158	809
38	0.129	809
40	0.086	809

Table A17. Congo Red A against Ionic Liquid Nanocomposite Hybrid D Data

Congo Red (A) Time (Min)	Product D 491 nm	Control
0	0.815	0.815
2	0.774	0.815
4	0.732	0.815
6	0.687	0.815
8	0.645	0.815
10	0.613	0.815
12	0.582	0.815
14	0.556	0.815
16	0.528	0.815
18	0.51	0.815
20	0.474	0.815
22	0.468	0.815
24	0.429	0.815
26	0.379	0.815
28	0.325	0.815
30	0.281	0.815
32	0.231	0.815
34	0.212	0.815
36	0.194	0.815
38	0.176	0.815
40	0.132	0.815

Table A18. Congo Red B against Ionic Liquid Nanocomposite Hybrid A Data

Congo Red (B)	Product A	Absorbance Peak (nm)	Control
Time (Min)			
0	1.546	490	1.546
2	1.498	490	1.546
4	1.451	490	1.546
6	1.39	490	1.546
8	1.347	490	1.546
10	1.306	490	1.546
12	1.242	490	1.546
14	1.212	490	1.546
16	1.175	490	1.546
18	1.128	490	1.546
20	1.086	490	1.546
22	1.035	490	1.546
24	0.99	490	1.546
26	0.945	490	1.546
28	0.899	490	1.546
30	0.824	490	1.546
32	0.778	490	1.546
34	0.73	490	1.546
36	0.692	490	1.546
38	0.638	490	1.546
40	0.593	490	1.546

Table A 19. Congo Red B against Ionic Liquid Nanocomposite Hybrid B Data

Congo Red (B)	Product B	Control
Time (Min)	491 nm	
0	1.549	1.549
2	1.518	1.549
4	1.503	1.549
6	1.496	1.549
8	1.468	1.549
10	1.449	1.549
12	1.431	1.549
14	1.412	1.549
16	1.39	1.549
18	1.374	1.549
20	1.345	1.549
22	1.318	1.549
24	1.281	1.549
26	1.245	1.549
28	1.21	1.549
30	1.163	1.549
32	1.135	1.549
34	1.094	1.549
36	1.048	1.549
38	1.012	1.549
40	0.973	1.549

Table A20. Congo Red B against Ionic Liquid Nanocomposite Hybrid C Data

Congo Red (A) Time (Min)	Product C 491 nm	Control
0	1.542	1.542
2	1.505	1.542
4	1.468	1.542
6	1.424	1.542
8	1.371	1.542
10	1.328	1.542
12	1.265	1.542
14	1.219	1.542
16	1.166	1.542
18	1.11	1.542
20	0.975	1.542
22	0.938	1.542
24	0.88	1.542
26	0.837	1.542
28	0.782	1.542
30	0.726	1.542
32	0.671	1.542
34	0.638	1.542
36	0.581	1.542
38	0.538	1.542
40	0.482	1.542

Table A21. Congo Red B against Ionic Liquid Nanocomposite Hybrid D Data

Congo Red (B)	Product D	Control
Time (Min)	490 nm	
0	1.551	1.551
2	1.495	1.551
4	1.446	1.551
6	1.383	1.551
8	1.329	1.551
10	1.287	1.551
12	1.265	1.551
14	1.21	1.551
16	1.172	1.551
18	1.146	1.551
20	1.103	1.551
22	0.971	1.551
24	0.928	1.551
26	0.869	1.551
28	0.822	1.551
30	0.774	1.551
32	0.74	1.551
34	0.711	1.551
36	0.679	1.551
38	0.638	1.551
40	0.599	1.551

Table A22. Allura Red AC (A) against Ionic Liquid Nanocomposite Hybrid A Data

Allura Red AC (A)	Product A	Control
Time (Min)	504 nm	
0	0.509	0.509
2	0.428	0.509
4	0.335	0.509
6	0.285	0.509
8	0.243	0.509
10	0.211	0.509
12	0.159	0.509
14	0.13	0.509
16	0.103	0.509
18	0.092	0.509
20	0.088	0.509

Table A23. Allura Red AC (A) against Ionic Liquid Nanocomposite Hybrid B Data

Allura Red (A)	Product B	Control
Time (Min)	504 nm	
0	0.512	0.512
2	0.449	0.512
4	0.402	0.512
6	0.353	0.512
8	0.289	0.512
10	0.247	0.512
12	0.201	0.512
14	0.172	0.512
16	0.134	0.512
18	0.131	0.512
20	0.124	0.512

Table A24. Allura Red AC (A) against Ionic Liquid Nanocomposite Hybrid C Data

Allura Red (A)	Product C	Control
Time (Min)	504 nm	
0	0.508	0.508
2	0.301	0.508
4	0.172	0.508
6	0.118	0.508
8	0.082	0.508
10	0.034	0.508

Table A25. Allura Red AC (A) against Ionic Liquid Nanocomposite Hybrid D Graph

Allura Red (A)	Product D	Control
Time (Min)	504 nm	
0	0.506	0.506
2	0.431	0.506
4	0.349	0.506
6	0.289	0.506
8	0.214	0.506
10	0.201	0.506
12	0.172	0.506
14	0.134	0.506
16	0.131	0.506
18	0.099	0.506
20	0.092	0.506

Table A26. Allura Red AC (A) against Ionic Liquid Nanocomposite Hybrid D Graph

Allura Red (B)	Product A	Control
Time (Min)	504 nm	
0	1.548	1.548
2	1.25	1.548
4	0.987	1.548
6	0.845	1.548
8	0.69	1.548
10	0.572	1.548
12	0.51	1.548
14	0.422	1.548
16	0.335	1.548
18	0.284	1.548
20	0.258	1.548
22	0.209	1.548
24	0.161	1.548
26	0.133	1.548
28	0.108	1.548
30	0.094	1.548
32	0.088	1.548
34	0.084	1.548
36	0.077	1.548
38	0.073	1.548
40	0.069	1.548

Table A27. Allura Red AC (B) against Ionic Liquid Nanocomposite Hybrid B Data

Allura Red (B)	Product B	Control
Time (Min)	504 nm	
0	1.552	1.552
2	1.465	1.552
4	1.268	1.552
6	1.147	1.552
8	1.099	1.552
10	0.92	1.552
12	0.878	1.552
14	0.713	1.552
16	0.653	1.552
18	0.536	1.552
20	0.501	1.552
22	0.469	1.552
24	0.422	1.552
26	0.376	1.552
28	0.291	1.552
30	0.257	1.552
32	0.207	1.552
34	0.17	1.552
36	0.148	1.552
38	0.139	1.552
40	0.128	1.552

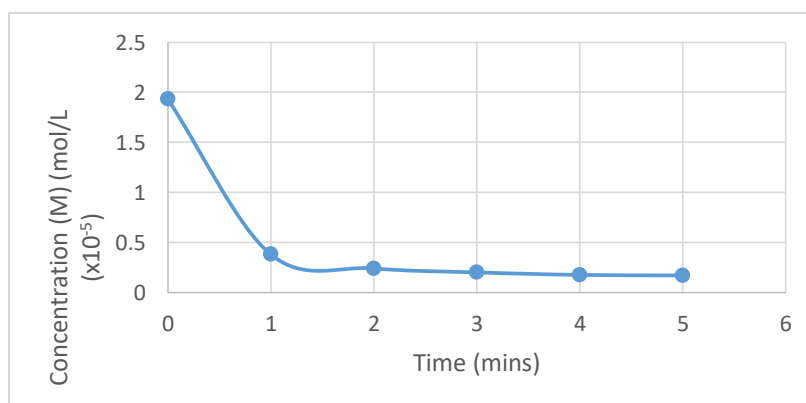
Table A28. Allura Red AC (B) against Ionic Liquid Nanocomposite Hybrid D Data

Allura Red (B)	Product D	Control
Time (Min)	504 nm	
0	1.546	1.546
2	1.471	1.546
4	1.299	1.546
6	1.162	1.546
8	1.003	1.546
10	0.962	1.546
12	0.873	1.546
14	0.74	1.546
16	0.622	1.546
18	0.566	1.546
20	0.501	1.546
22	0.42	1.546
24	0.35	1.546
26	0.265	1.546
28	0.228	1.546
30	0.211	1.546
32	0.175	1.546
34	0.158	1.546
36	0.129	1.546
38	0.109	1.546
40	0.091	1.546

## Concentration against Time Graphs for Carbon + Iron Oxide Nanocomposites

Table A29. Iron Oxide + Activated Charcoal against Methylene Blue A Data

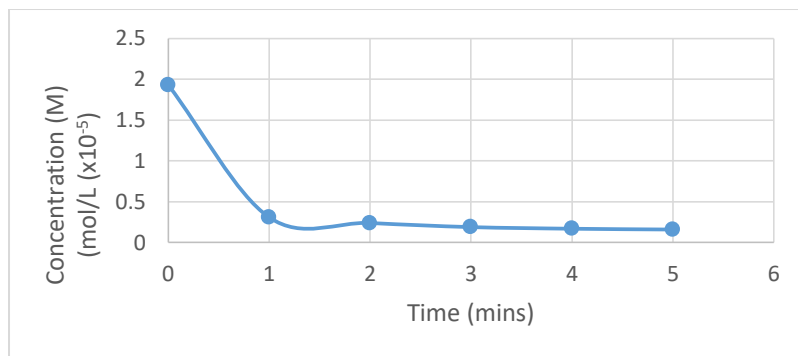
Methylene Blue A Solution	Standard Dilutions of MB
Time (Mins)	Concentration (M) (mol/L ( $\times 10^{-5}$ ))
0	1.93
1	0.38
2	0.24
3	0.2
4	0.175
5	0.17



Iron Oxide + Activated Charcoal against Methylene Blue A Graph

Table A30. Iron Oxide + Activated Charcoal +  $\text{TiO}_2$  against Methylene Blue A Data

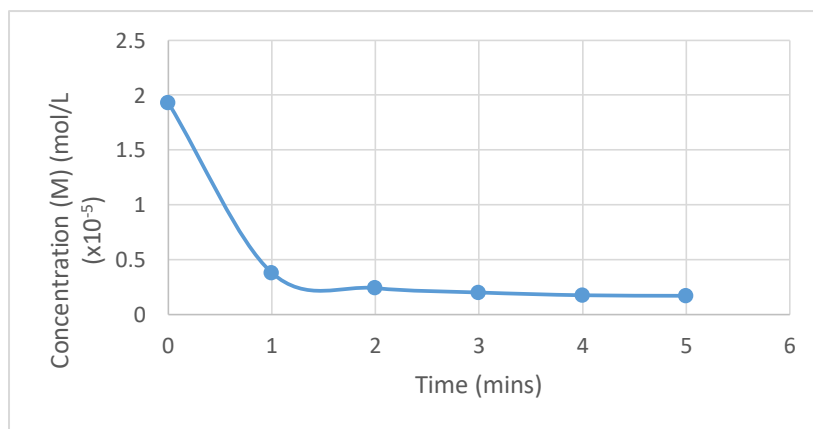
Methylene Blue A Solution	Standard Dilutions of MB
Time (Mins)	Concentration (M) (mol/L ( $\times 10^{-5}$ ))
0	1.93
1	0.31
2	0.24
3	0.19
4	0.17
5	0.16



Iron Oxide + Activated Charcoal + TiO<sub>2</sub> against Methylene Blue A Graph

Table A31. Iron Oxide + Multi-Walled Carbon Nanotube against Methylene Blue A Data

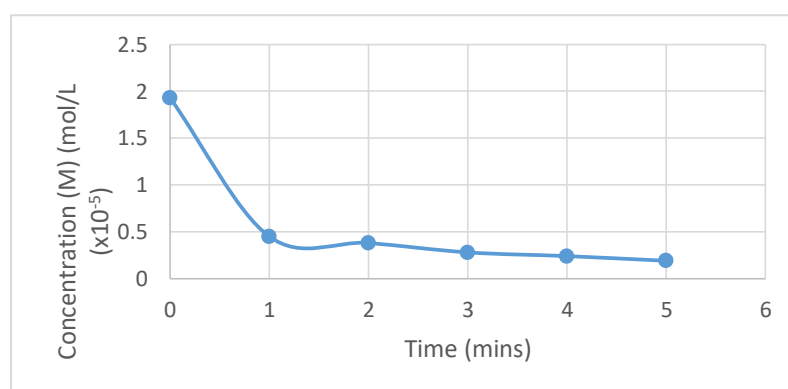
Methylene Blue A Solution	Standard Dilutions of MB
Time (Mins)	Concentration (M) (mol/L (x10 <sup>-5</sup> ))
0	1.93
1	0.38
2	0.24
3	0.2
4	0.175
5	0.17



Iron Oxide + Multi-Walled Carbon Nanotube against Methylene Blue A Graph

Table A32. Iron Oxide + Multi-Walled Carbon Nanotube + TiO<sub>2</sub> against Methylene Blue A Data

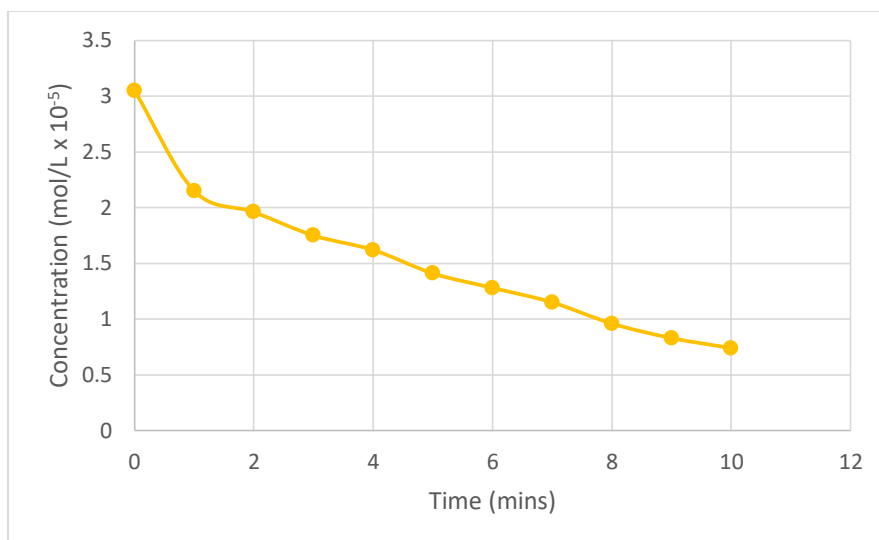
Methylene Blue A Solution	Standard Dilutions of MB
Time (Mins)	Concentration (M) (mol/L ( $\times 10^{-5}$ ))
0	1.93
1	0.45
2	0.38
3	0.28
4	0.24
5	0.19



Iron Oxide + Multi-Walled Carbon Nanotube + TiO<sub>2</sub> against Methylene Blue A

Table A33. Iron Oxide + Activated Charcoal against Congo Red A

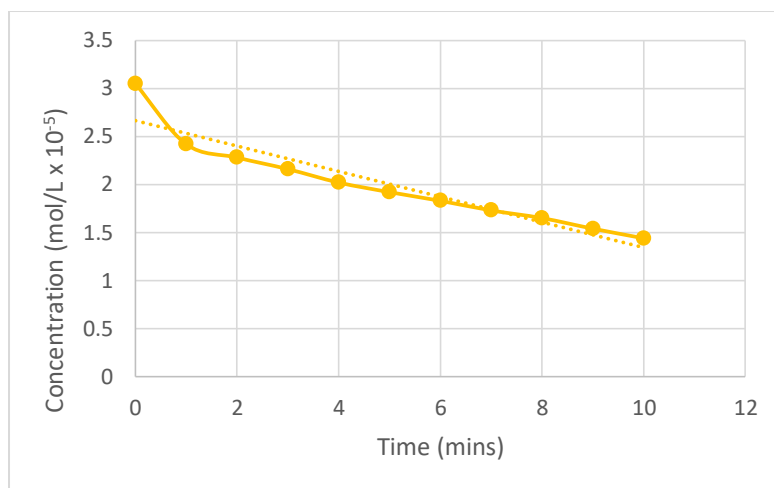
Congo Red A Solution	Standard Dilution Of CR
Time (Mins)	Concentration (M) (mol/L ( $\times 10^{-5}$ ))
0	3.05
1	2.15
2	1.96
3	1.75
4	1.62
5	1.41
6	1.28
7	1.15
8	0.96
9	0.83
10	0.74



Iron Oxide + Activated Charcoal against Congo Red A

Table A34. Iron Oxide + Activated Charcoal + TiO<sub>2</sub> against Congo Red A

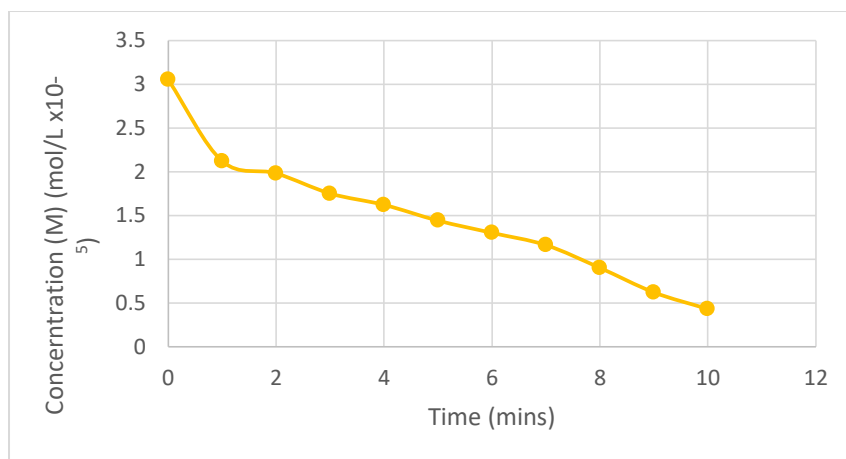
Congo Red A Solution	Standard Dilution Of CR
Time (Mins)	Concentration (M) (mol/L (x10 <sup>-5</sup> ))
0	3.05
1	2.42
2	2.28
3	2.16
4	2.02
5	1.92
6	1.83
7	1.73
8	1.65
9	1.54
10	1.44



Iron Oxide + Activated Charcoal + TiO<sub>2</sub> against Congo Red A

Table A35. Iron Oxide + Multi-Walled Carbon Nanotube against Congo Red A

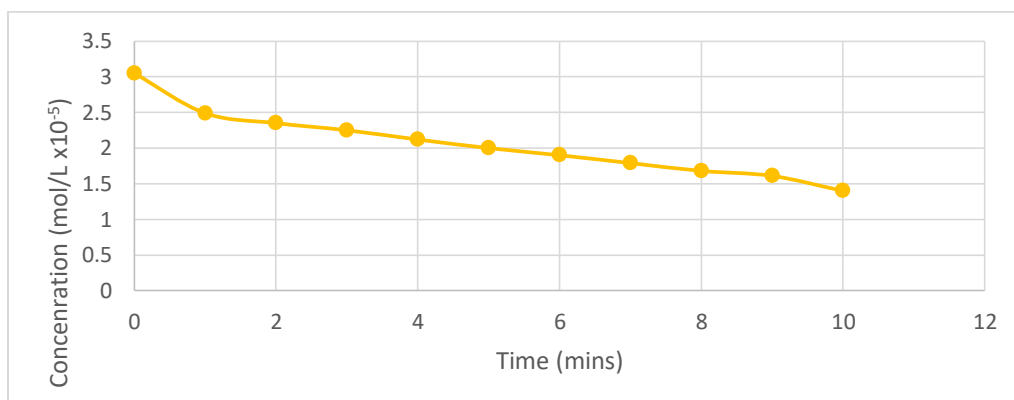
Congo Red A Solution	Standard Dilution Of CR
Time (Mins)	Concentration (M) (mol/L (x10 <sup>-5</sup> ))
0	3.05
1	2.12
2	1.98
3	1.75
4	1.62
5	1.44
6	1.3
7	1.16
8	0.9
9	0.62
10	0.43



Iron Oxide + Multi-Walled Carbon Nanotube against Congo Red A Graph

Table 36. Iron Oxide + Multi-Walled Carbon Nanotube + TiO<sub>2</sub> against Congo Red A Data

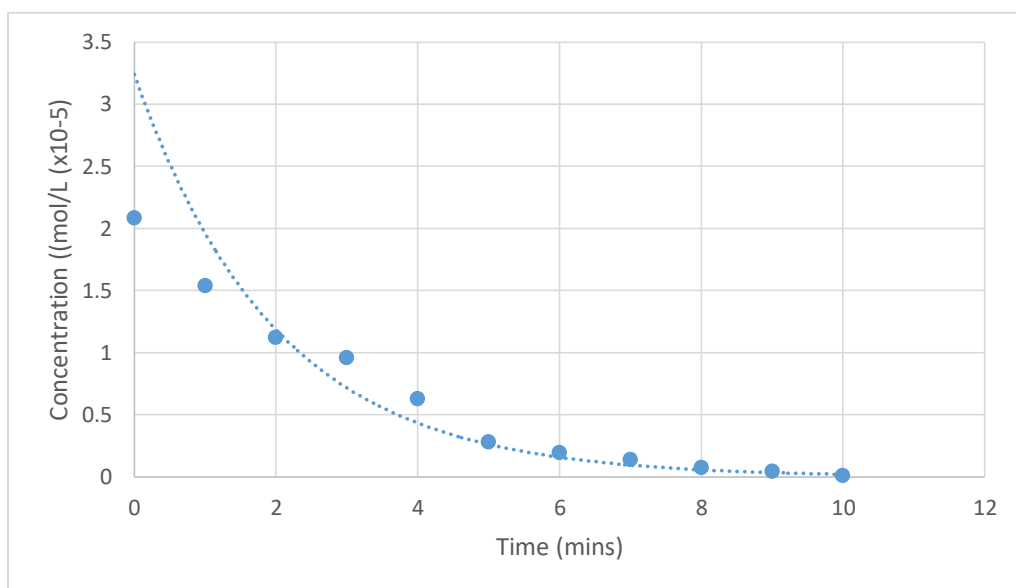
Congo Red A Solution	Standard Dilution Of CR
Time (Mins)	Concentration (M) (mol/L (x10 <sup>-5</sup> ))
0	3.05
1	2.49
2	2.35
3	2.25
4	2.12
5	2
6	1.9
7	1.79
8	1.68
9	1.61
10	1.4



Iron Oxide + Multi-Walled Carbon Nanotube + TiO<sub>2</sub> against Congo Red A Graph

Table A37. Methylene Blue Solution A against Hybrid A

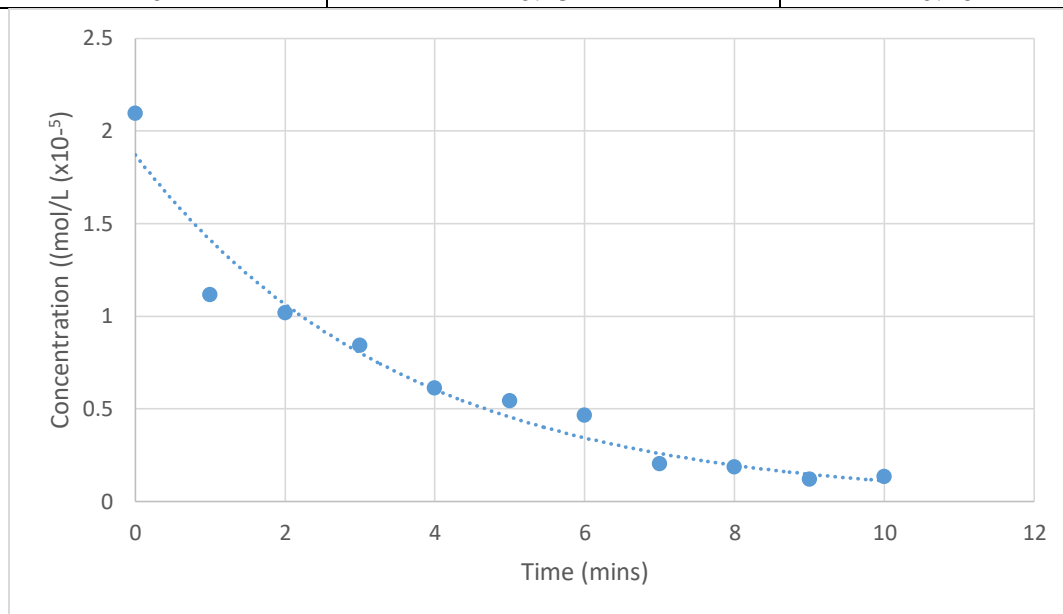
Methylene Blue A Solution	Concentration (M) (mol/L ( $\times 10^{-5}$ ))	Hybrid A (Absorbance)
Time (Mins)		
0	2.08	0.873
1	1.536	0.674
2	1.12	0.522
3	0.957	0.462
4	0.626	0.341
5	0.281	0.215
6	0.191	0.182
7	0.139	0.163
8	0.074	0.139
9	0.043	0.128
10	0.008	0.115



Concentration Vs Time Graph Methylene Blue Solution A against Hybrid A

Table A38. Methylene Blue Solution A against Hybrid B

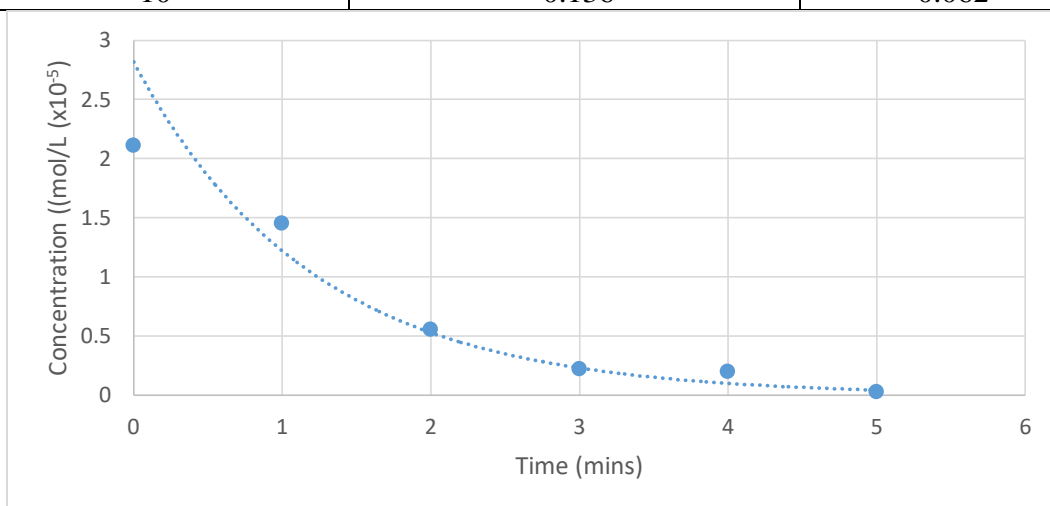
Methylene Blue A Solution	Concentration (M) (mol/L ( $\times 10^{-5}$ ))	Hybrid B (Absorbance)
Time (Mins)		
0	2.093	0.878
1	1.115	0.52
2	1.017	0.484
3	0.8417	0.42
4	0.61	0.335
5	0.541	0.31
6	0.464	0.282
7	0.202	0.186
8	0.185	0.18
9	0.118	0.155
10	0.131	0.16



Concentration Vs Time Graph Methylene Blue Solution A against Hybrid B

Table A39. Methylene Blue Solution A against Hybrid C

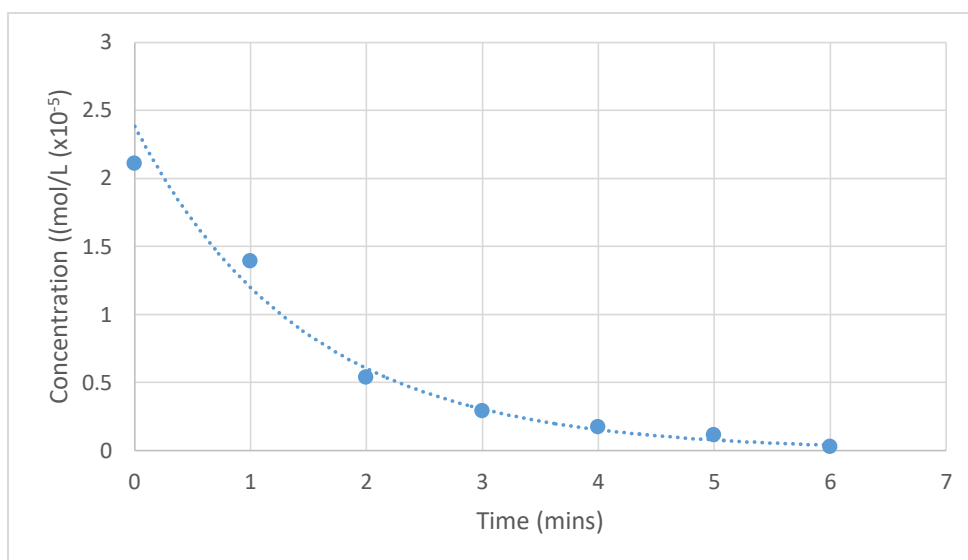
Methylene Blue A Solution Time (Mins)	Concentration (M) (mol/L ( $\times 10^{-5}$ ))	Hybrid C (Absorbance)
0	2.11	0.884
1	1.45	0.645
2	0.555	0.315
3	0.219	0.192
4	0.199	0.185
5	0.024	0.121
6	-0.088	0.08
7	-0.082	0.082
8	-0.128	0.065
9	-0.134	0.063
10	-0.136	0.062



Concentration Vs Time Graph Methylene Blue Solution A against Hybrid C

Table A40. Methylene Blue Solution A against Hybrid D

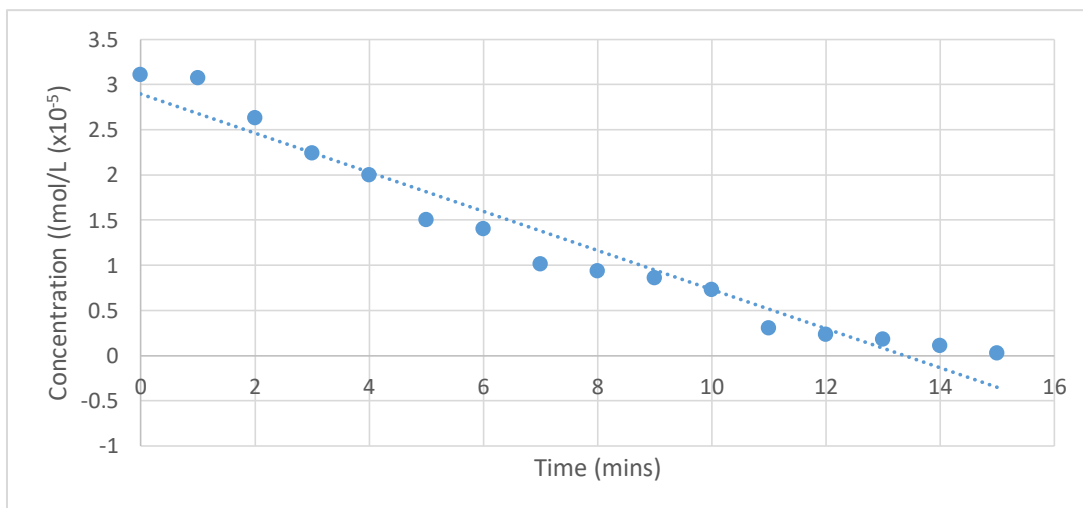
Methylene Blue A Solution	Concentration (M) (mol/L ( $\times 10^{-5}$ ))	Hybrid D (Absorbance)
Time (Mins)		
0	2.107	0.883
1	1.389	0.62
2	0.535	0.308
3	0.289	0.218
4	0.172	0.175
5	0.112	0.153
6	0.027	0.122
7	-0.019	0.105
8	-0.03	0.101
9	-0.033	0.1
10	-0.038	0.098



Concentration Vs Time Graph Methylene Blue Solution B against Hybrid A

Table A41. Methylene Blue Solution B against Hybrid A

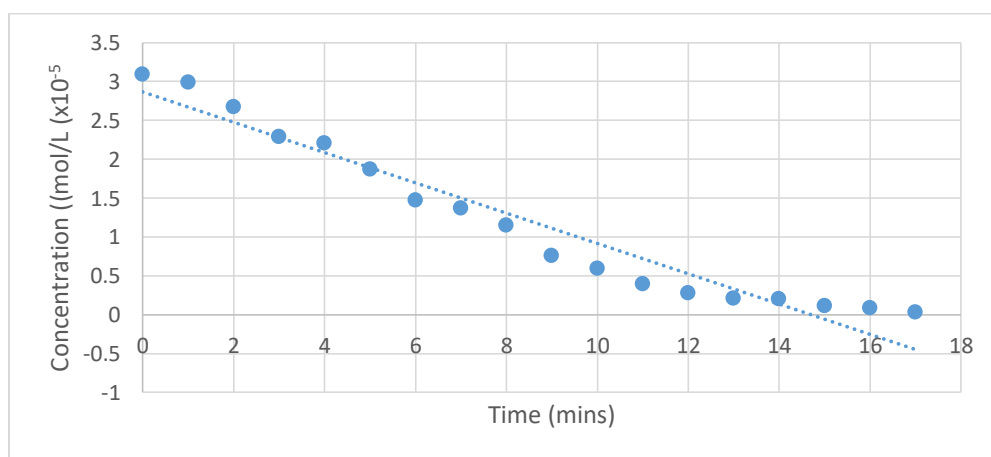
Methylene Blue B Solution	Concentration (M) (mol/L (x10 <sup>-5</sup> ))	Hybrid A (Absorbance)
Time (Mins)		
0	3.11	1.252
1	3.07	1.235
2	2.63	1.077
3	2.24	0.93
4	2	0.845
5	1.503	0.662
6	1.402	0.625
7	1.01	0.485
8	0.937	0.455
9	0.858	0.426
10	0.732	0.38
11	0.306	0.224
12	0.235	0.198
13	0.18	0.178
14	0.112	0.153
15	0.0246	0.121



Concentration Vs Time Graph Methylene Blue Solution B against Hybrid A

Table A42. Methylene Blue Solution B against Hybrid B

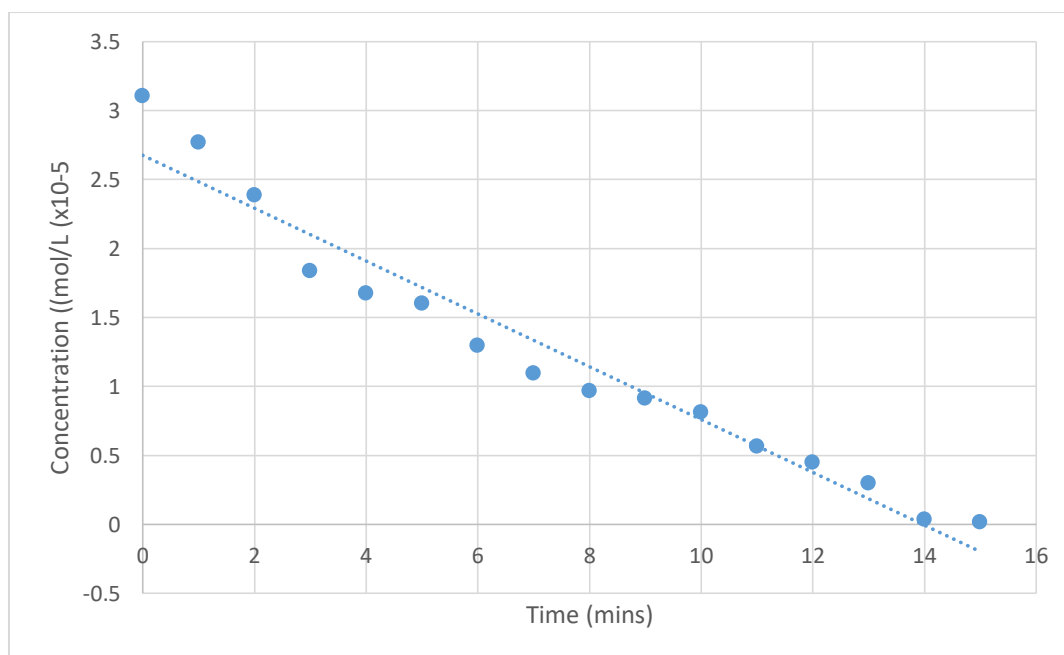
Methylene Blue B Solution	Concentration (M) (mol/L) ( $\times 10^{-5}$ )	Hybrid B (Absorbance)
Time (Mins)		
0	3.09	1.243
1	2.99	1.206
2	2.67	1.098
3	2.29	0.951
4	2.21	0.92
5	1.87	0.796
6	1.47	0.65
7	1.37	0.613
8	1.15	0.52
9	0.757	0.389
10	0.596	0.33
11	0.394	0.256
12	0.279	0.214
13	0.213	0.19
14	0.203	0.186
15	0.117	0.155
16	0.0847	0.143
17	0.03	0.123



Concentration Vs Time Graph Methylene Blue Solution B against Hybrid B

Table A43 Methylene Blue Solution B against Hybrid C

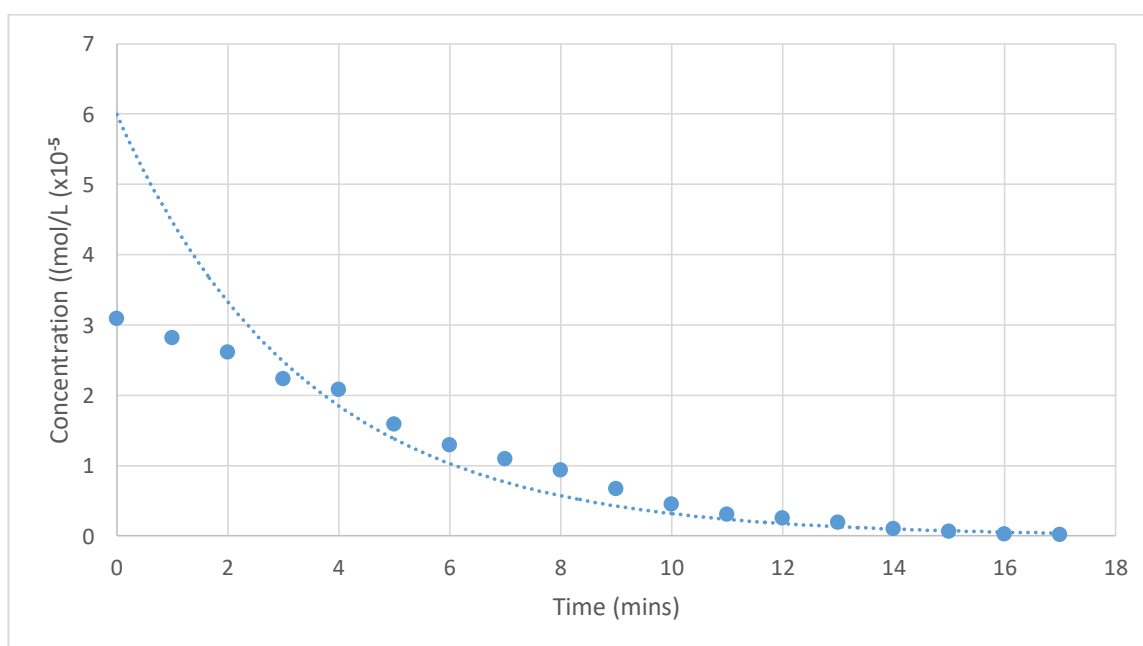
Methylene Blue B Solution Time (Mins)	Concentration (M) (mol/L ( $\times 10^{-5}$ )	Hybrid C (Absorbance)
0	3.105	1.248
1	2.768	1.125
2	2.386	0.985
3	1.836	0.784
4	1.672	0.724
5	1.601	0.698
6	1.293	0.585
7	1.093	0.512
8	0.967	0.466
9	0.91	0.445
10	0.811	0.409
11	0.563	0.318
12	0.4482	0.276
13	0.298	0.221
14	0.0355	0.125
15	0.0164	0.118
16	-0.163	0.106
17	-0.0136	0.107
18	N/A	0.099
19	N/A	0.096
20	N/A	0.095



Concentration Vs Time Graph Methylene Blue Solution B against Hybrid C

Table A44. Methylene Blue Solution B against Hybrid D

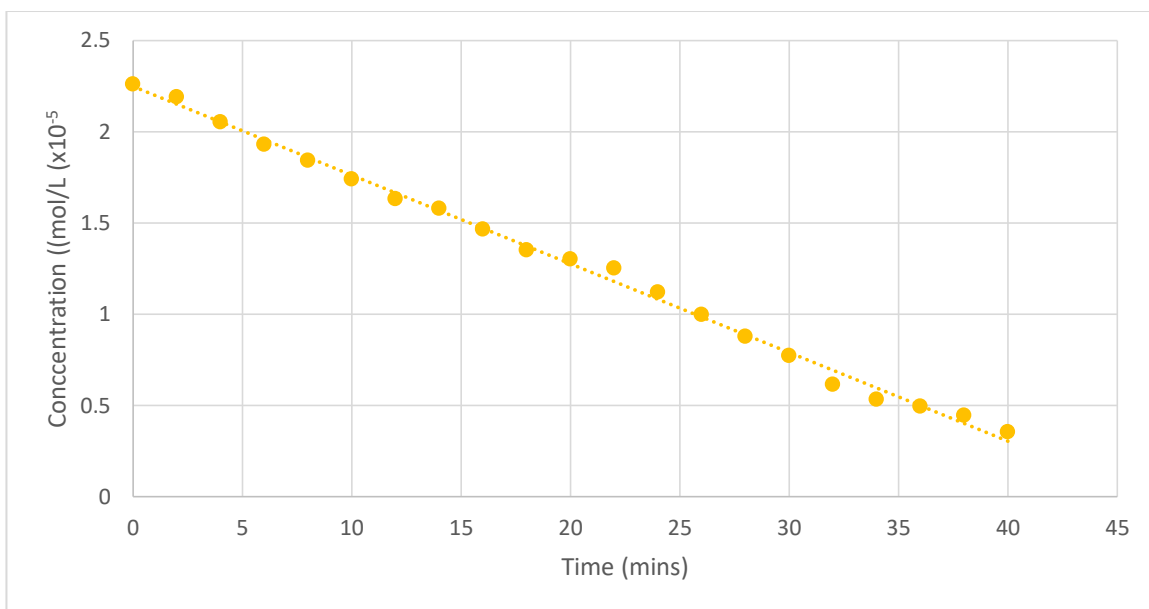
Methylene Blue B Solution	Concentration (M) (mol/L (x10 <sup>-5</sup> ))	Hybrid D (Absorbance)
Time (Mins)		
0	3.094	1.244
1	2.818	1.143
2	2.616	1.069
3	2.235	0.93
4	2.085	0.875
5	1.59	0.694
6	1.295	0.586
7	1.093	0.512
8	0.937	0.455
9	0.668	0.356
10	0.453	0.278
11	0.306	0.224
12	0.251	0.204
13	0.191	0.182
14	0.101	0.149
15	0.0628	0.135
16	0.0246	0.121
17	0.0192	0.119
18	-0.0546	0.092
19	N/A	0.087
20	N/A	0.086



Concentration Vs Time Graph Methylene Blue Solution B against Hybrid D

Table 45. Congo Red Solution A against Hybrid A

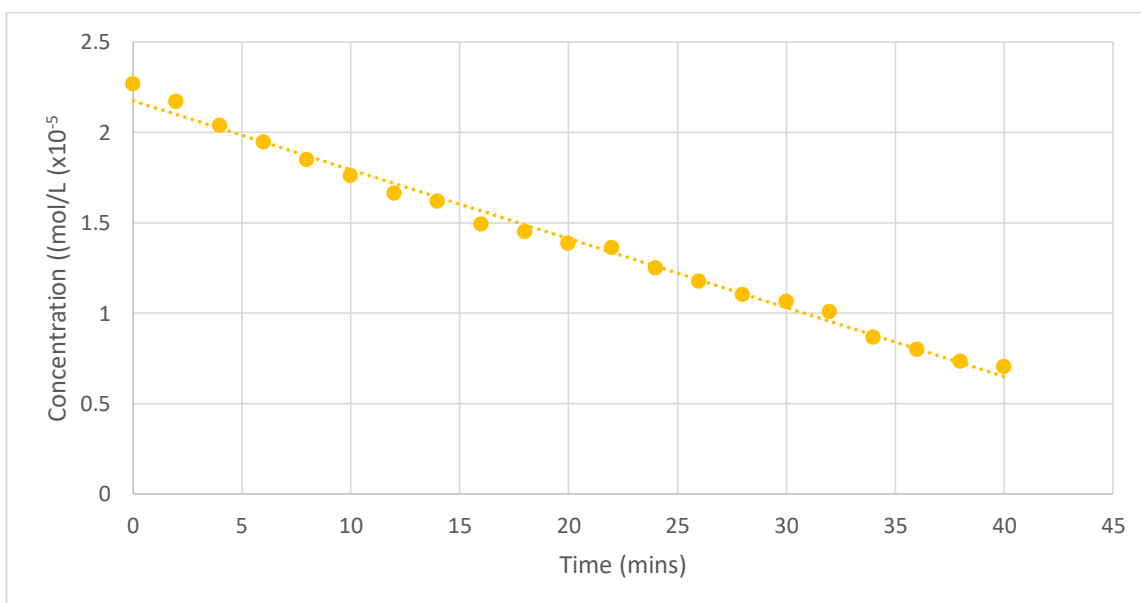
Congo Red (A) Time (Mins)	Concentration (M) (mol/L ( $\times 10^{-5}$ )	Hybrid A (Absorbance)
0	2.26	0.811
2	2.188	0.788
4	2.05	0.745
6	1.93	0.709
8	1.84	0.682
10	1.74	0.651
12	1.632	0.615
14	1.577	0.598
16	1.464	0.563
18	1.35	0.53
20	1.299	0.512
22	1.251	0.497
24	1.119	0.456
26	0.997	0.418
28	0.878	0.381
30	0.772	0.348
32	0.613	0.299
34	0.533	0.274
36	0.494	0.262
38	0.443	0.246
40	0.353	0.218



Concentration Vs Time Graph Congo Red Solution A against Hybrid A

Table A46. Congo Red Solution A against Hybrid B

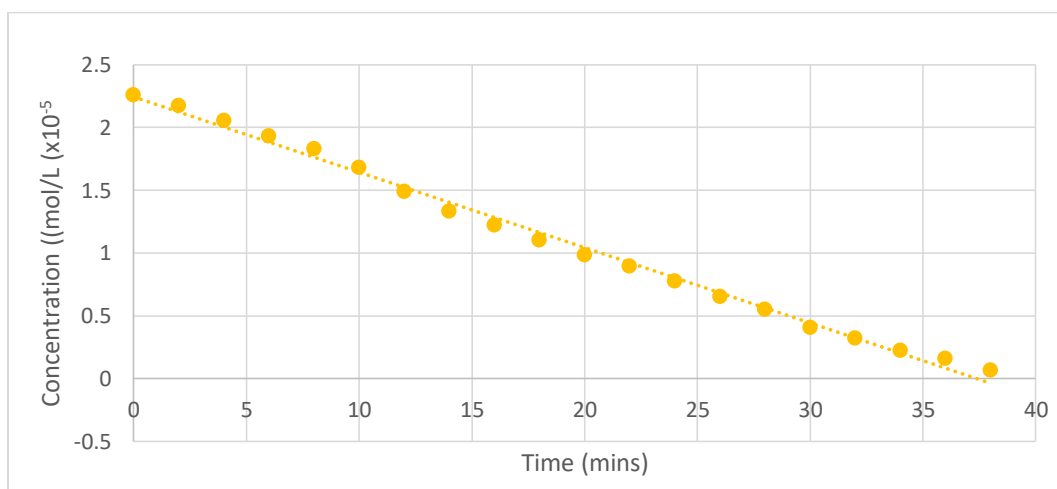
Congo Red (A) Time (Mins)	Concentration (M) (mol/L ( $\times 10^{-5}$ )	Hybrid B (Absorbance)
0	2.266	0.812
2	2.169	0.782
4	2.037	0.741
6	1.944	0.712
8	1.847	0.682
10	1.76	0.655
12	1.66	0.624
14	1.618	0.611
16	1.489	0.571
18	1.448	0.557
20	1.383	0.538
22	1.361	0.531
24	1.248	0.496
26	1.174	0.473
28	1.1	0.45
30	1.064	0.439
32	1.007	0.421
34	0.865	0.377
36	0.797	0.356
38	0.733	0.336
40	0.704	0.327



Concentration Vs Time Graph Congo Red Solution A against Hybrid B

Table A47. Congo Red Solution A against Hybrid C

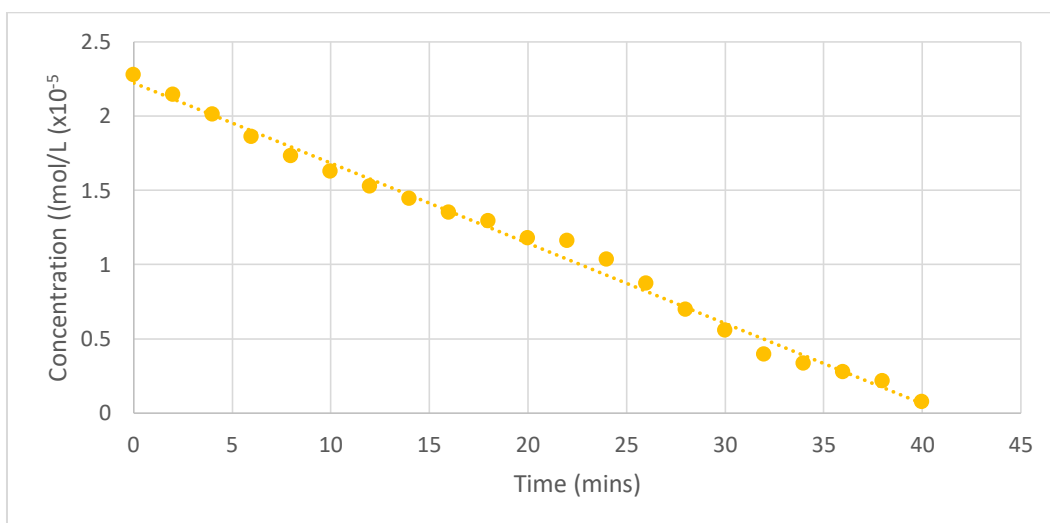
Congo Red (A) Time (Mins)	Concentration (M) (mol/L ( $\times 10^{-5}$ ))	Hybrid C (Absorbance)
0	2.256	0.809
2	2.172	0.783
4	2.054	0.746
6	1.928	0.707
8	1.825	0.675
10	1.677	0.629
12	1.487	0.57
14	1.332	0.522
16	1.22	0.487
18	1.1	0.45
20	0.981	0.413
22	0.894	0.386
24	0.775	0.349
26	0.65	0.31
28	0.549	0.279
30	0.404	0.234
32	0.32	0.208
34	0.22	0.177
36	0.159	0.158
38	0.066	0.129
40	-0.0723	0.086



Concentration Vs Time Graph Congo Red Solution A against Hybrid C

Table A48. Congo Red Solution A against Hybrid D

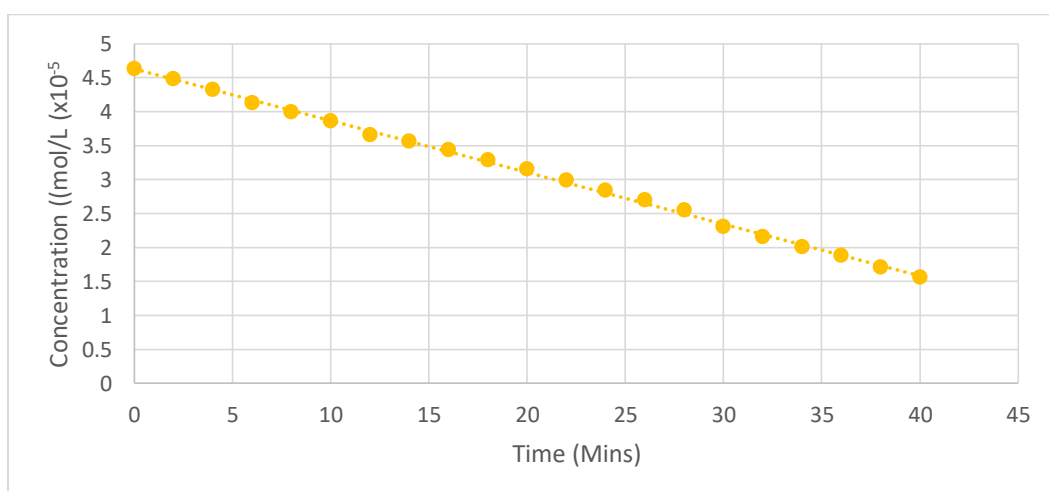
Congo Red (A)	Concentration (M) (mol/L (x10 <sup>-5</sup> ))	Hybrid D (Absorbance)
Time (Mins)		
0	2.275	0.815
2	2.144	0.774
4	2.009	0.732
6	1.86	0.687
8	1.729	0.645
10	1.625	0.613
12	1.525	0.582
14	1.442	0.556
16	1.35	0.528
18	1.293	0.51
20	1.177	0.474
22	1.158	0.468
24	1.032	0.429
26	0.871	0.379
28	0.697	0.325
30	0.555	0.281
32	0.395	0.231
34	0.333	0.212
36	0.275	0.194
38	0.217	0.176
40	0.075	0.132



Concentration Vs Time Graph Congo Red Solution A against Hybrid D

Table A49. Congo Red Solution B against Hybrid A

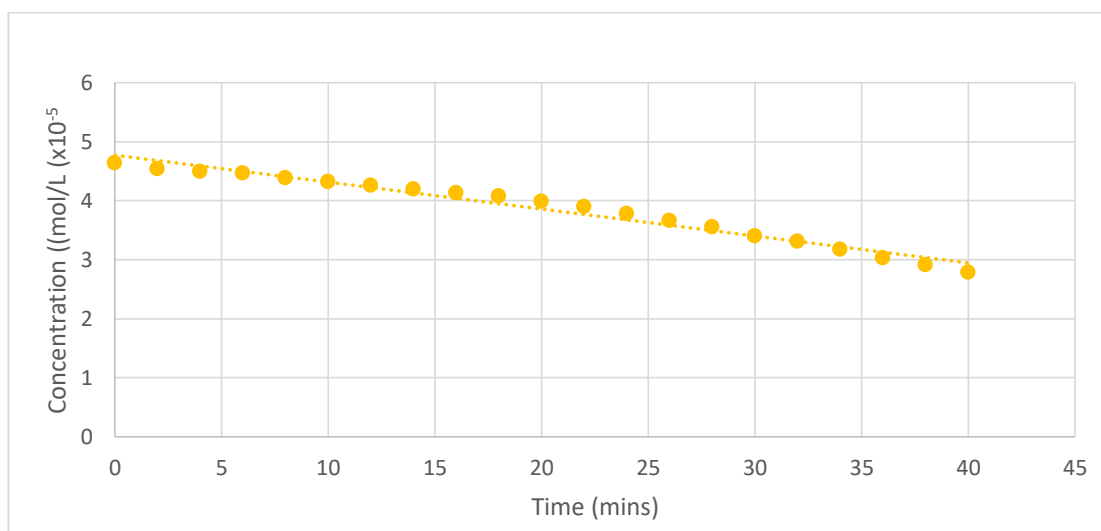
Congo Red (B) Time (Mins)	Concentration (M) (mol/L ( $\times 10^{-5}$ )	Hybrid A (Absorbance)
0	4.63	1.546
2	4.475	1.498
4	4.324	1.451
6	4.128	1.39
8	3.989	1.347
10	3.857	1.306
12	3.651	1.242
14	3.556	1.212
16	3.435	1.175
18	3.284	1.128
20	3.148	1.086
22	2.985	1.035
24	2.839	0.99
26	2.695	0.945
28	2.546	0.899
30	2.304	0.824
32	2.156	0.778
34	2.002	0.73
36	1.879	0.692
38	1.705	0.638
40	1.56	0.593



Concentration Vs Time Graph Congo Red Solution B against Hybrid A

Table A50. Congo Red Solution B against Hybrid B

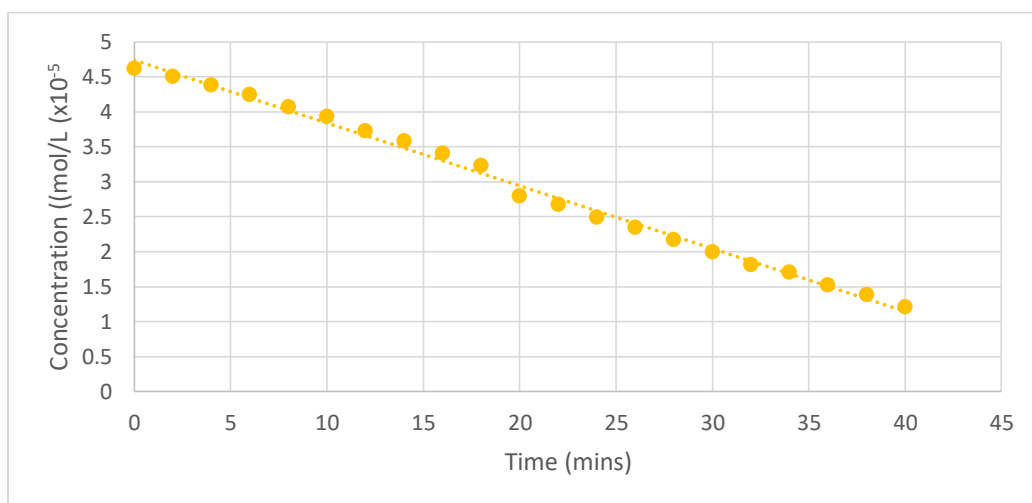
Congo Red (B) Time (Mins)	Concentration (M) (mol/L ( $\times 10^{-5}$ ))	Hybrid B (Absorbance)
0	4.64	1.549
2	4.54	1.518
4	4.49	1.503
6	4.469	1.496
8	4.379	1.468
10	4.318	1.449
12	4.26	1.431
14	4.198	1.412
16	4.128	1.39
18	4.076	1.374
20	3.983	1.345
22	3.896	1.318
24	3.777	1.281
26	3.661	1.245
28	3.548	1.21
30	3.396	1.163
32	3.306	1.135
34	3.174	1.094
36	3.026	1.048
38	2.91	1.012
40	2.784	0.973



Concentration Vs Time Graph Congo Red Solution B against Hybrid B

Table A 51. Congo Red Solution B against Hybrid C

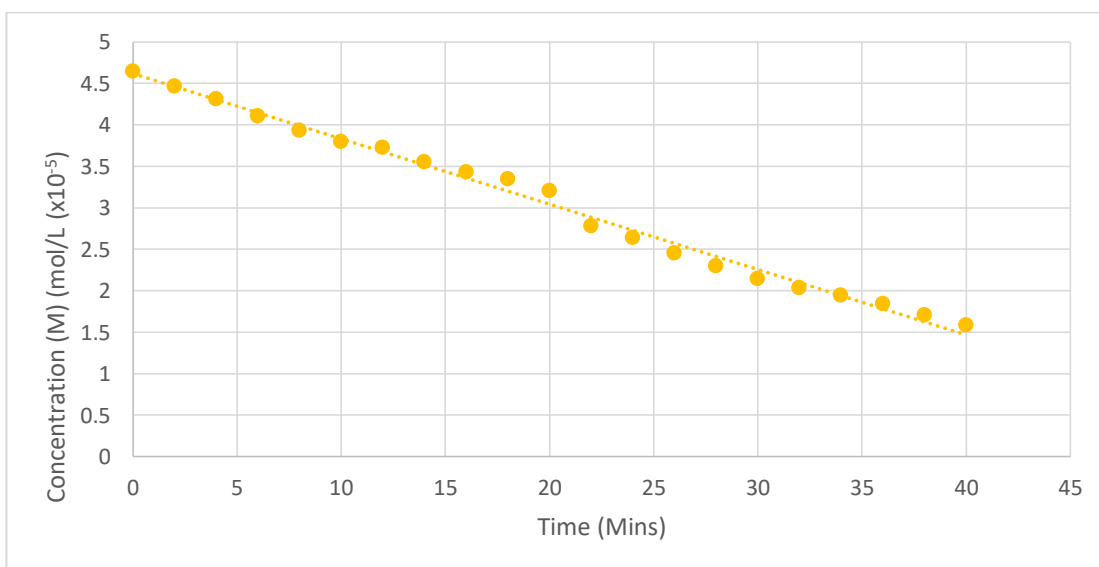
Congo Red (B) Time (Mins)	Concentration (M) (mol/L ( $\times 10^{-5}$ ))	Hybrid C (Absorbance)
0	4.617	1.542
2	4.498	1.505
4	4.379	1.468
6	4.238	1.424
8	4.066	1.371
10	3.928	1.328
12	3.725	1.265
14	3.577	1.219
16	3.406	1.166
18	3.226	1.11
20	2.791	0.975
22	2.672	0.938
24	2.485	0.88
26	2.346	0.837
28	2.169	0.782
30	1.989	0.726
32	1.812	0.671
34	1.705	0.638
36	1.522	0.581
38	1.384	0.538
40	1.203	0.482



Concentration Vs Time Graph Congo Red Solution B against Hybrid C

Table A52. Congo Red Solution B against Hybrid D

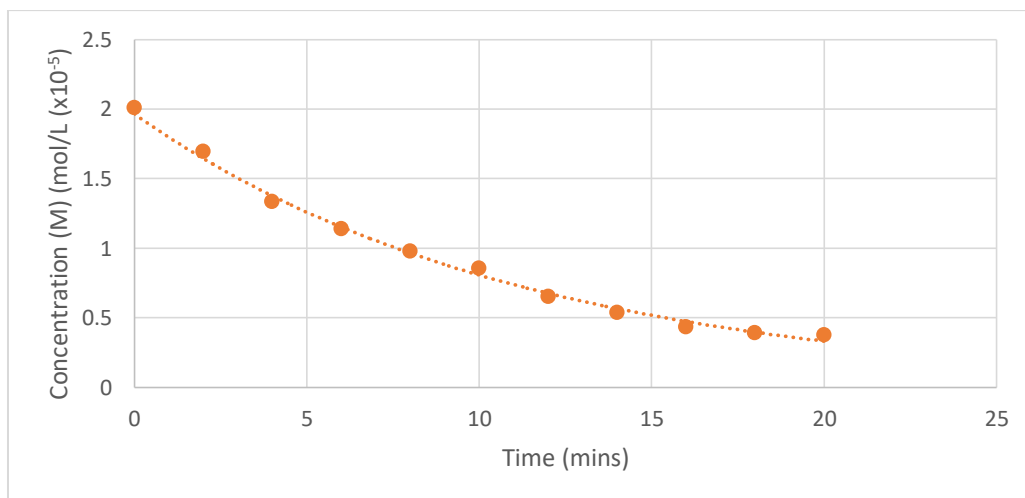
Congo Red (B) Time (Mins)	Concentration (M) (mol/L ( $\times 10^{-5}$ )	Hybrid D (Absorbance)
0	4.646	1.551
2	4.466	1.495
4	4.308	1.446
6	4.105	1.383
8	3.931	1.329
10	3.796	1.287
12	3.725	1.265
14	3.548	1.21
16	3.426	1.172
18	3.342	1.146
20	3.204	1.103
22	2.778	0.971
24	2.639	0.928
26	2.449	0.869
28	2.298	0.822
30	2.143	0.774
32	2.034	0.74
34	1.941	0.711
36	1.837	0.679
38	1.705	0.638
40	1.58	0.599



Concentration Vs Time Graph Congo Red Solution B against Hybrid D

Table A53. Allura Red AC Solution A against Hybrid A

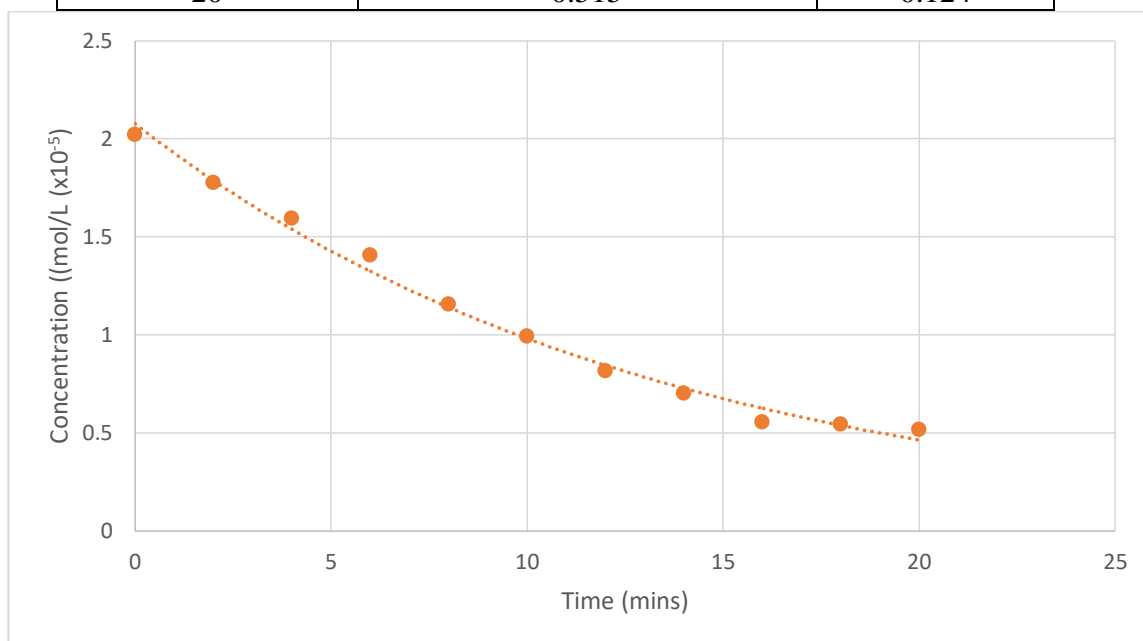
Allura Red AC (A)	Concentration (M) (mol/L ( $\times 10^{-5}$ ))	Hybrid A (Absorbance)
Time (Mins)		
0	2.009	0.509
2	1.695	0.428
4	1.333	0.335
6	1.139	0.285
8	0.977	0.243
10	0.853	0.211
12	0.651	0.159
14	0.538	0.13
16	0.434	0.103
18	0.391	0.092
20	0.375	0.088



Concentration Vs Time Graph Allura Red AC Solution A against Hybrid A

Table A54. Allura Red AC Solution A against Hybrid B

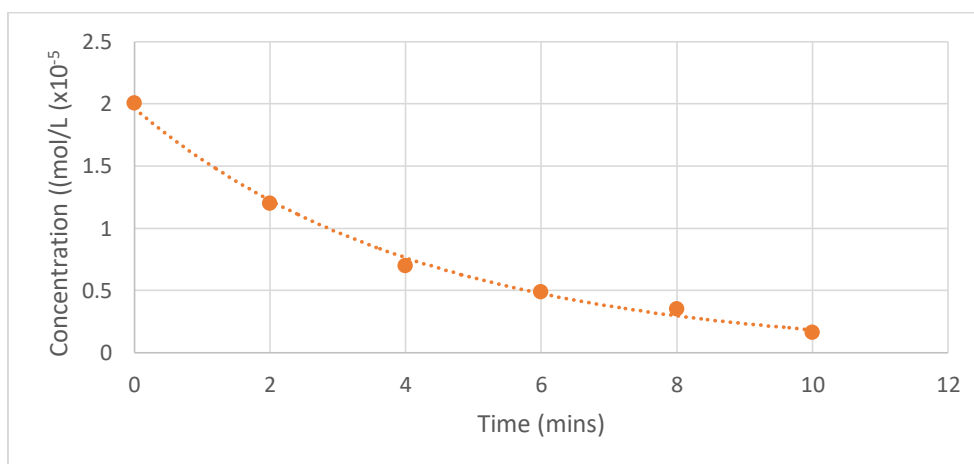
Allura Red AC (A) Time (Mins)	Concentration (M) (mol/L ( $\times 10^{-5}$ ))	Hybrid B (Absorbance)
0	2.02	0.512
2	1.776	0.449
4	1.594	0.402
6	1.404	0.353
8	1.155	0.289
10	0.992	0.247
12	0.814	0.201
14	0.701	0.172
16	0.554	0.134
18	0.542	0.131
20	0.515	0.124



Concentration Vs Time Graph Allura Red AC Solution A against Hybrid B

Table A55. Allura Red AC Solution A against Hybrid C

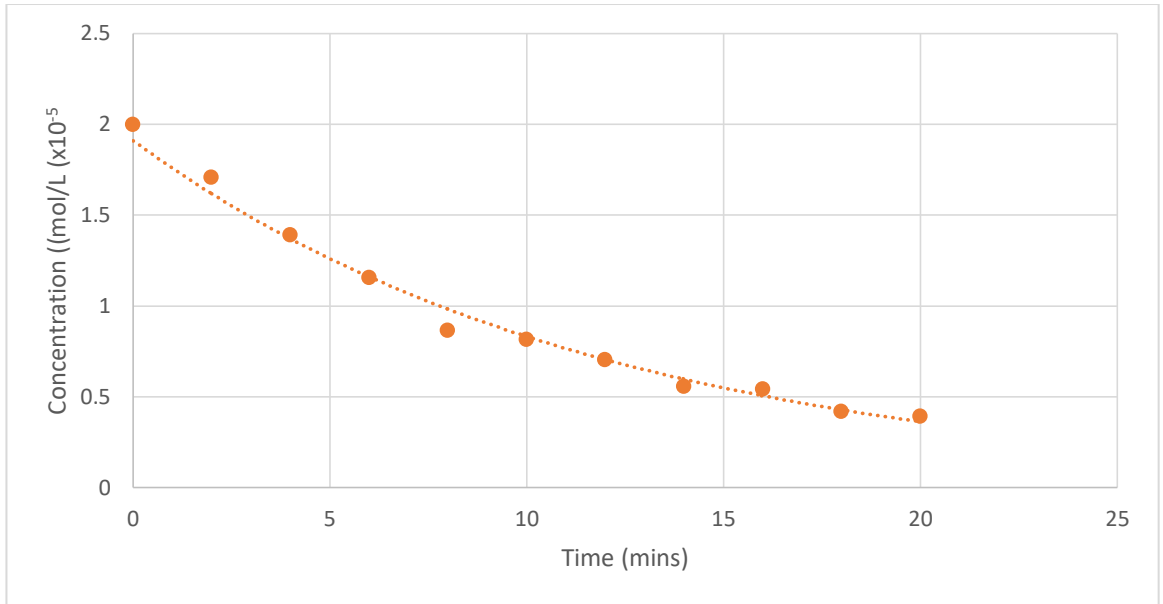
Allura Red AC (A)	Concentration (M) (mol/L ( $\times 10^{-5}$ ))	Hybrid C (Absorbance)
Time (Mins)		
0	2.005	0.508
2	1.201	0.301
4	0.701	0.172
6	0.491	0.118
8	0.352	0.082
10	0.165	0.034



Concentration Vs Time Graph Allura Red AC Solution A against Hybrid C

Table A56. Allura Red AC Solution A against Hybrid D

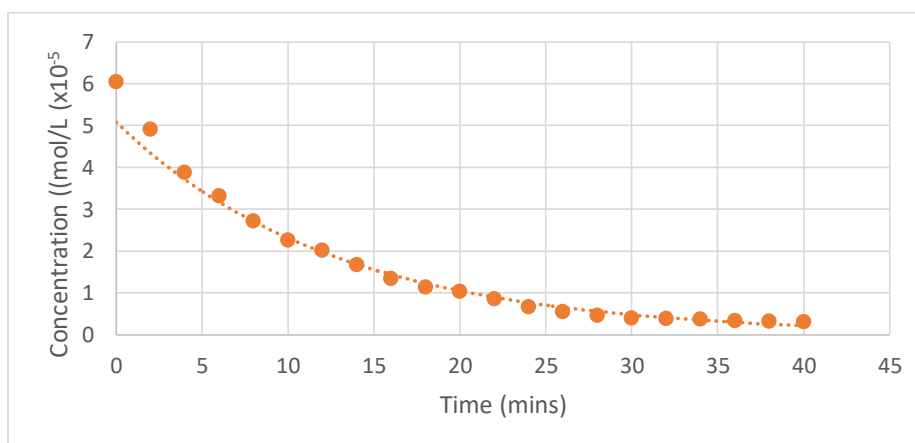
Allura Red AC (A)	Concentration (M) (mol/L ( $\times 10^{-5}$ ))	Hybrid D (Absorbance)
Time (Mins)		
0	1.998	0.506
2	1.706	0.431
4	1.388	0.349
6	1.155	0.289
8	0.864	0.214
10	0.814	0.201
12	0.701	0.172
14	0.554	0.134
16	0.542	0.131
18	0.418	0.099
20	0.391	0.092



Concentration Vs Time Graph Allura Red AC Solution A against Hybrid D

Table A57. Allura Red AC Solution B against Hybrid A

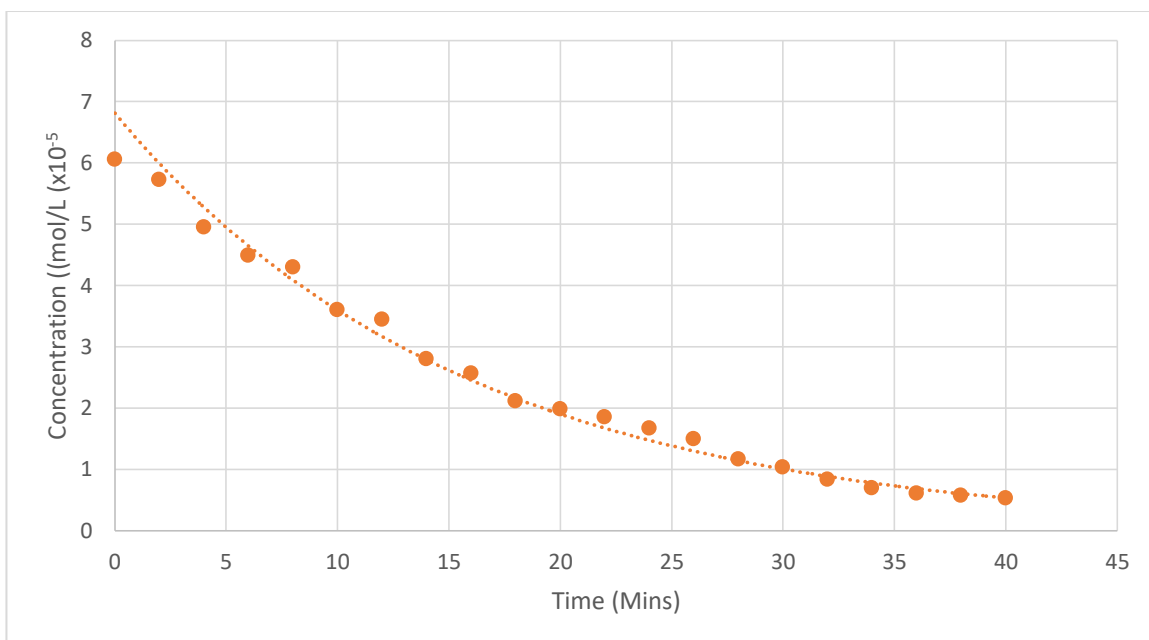
Allura Red AC (B)	Concentration (M) (mol/L ( $\times 10^5$ ))	Hybrid A (Absorbance)
Time (Mins)		
0	6.04	1.548
2	4.899	1.25
4	3.865	0.987
6	3.313	0.845
8	2.711	0.69
10	2.253	0.572
12	2.013	0.51
14	1.671	0.422
16	1.334	0.335
18	1.136	0.284
20	1.035	0.258
22	0.845	0.209
24	0.659	0.161
26	0.55	0.133
28	0.453	0.108
30	0.398	0.094
32	0.375	0.088
34	0.36	0.084
36	0.333	0.077
38	0.317	0.073
40	0.301	0.069



Concentration Vs Time Graph Allura Red AC Solution B against Hybrid A

Table A58. Allura Red AC Solution B against Hybrid B

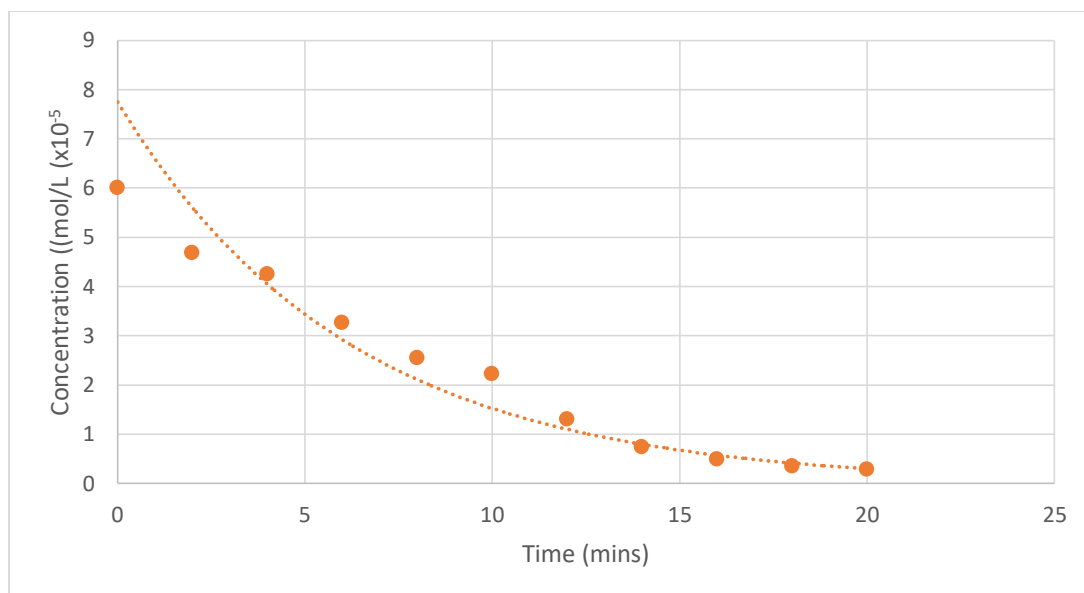
Allura Red AC (B)	Concentration (M) (mol/L ( $\times 10^5$ ))	Hybrid B (Absorbance)
Time (Mins)		
0	6.057	1.552
2	5.72	1.465
4	4.95	1.268
6	4.485	1.147
8	4.298	1.099
10	3.604	0.92
12	3.441	0.878
14	2.8	0.713
16	2.568	0.653
18	2.114	0.536
20	1.978	0.501
22	1.854	0.469
24	1.671	0.422
26	1.493	0.376
28	1.163	0.291
30	1.031	0.257
32	0.837	0.207
34	0.694	0.17
36	0.608	0.148
38	0.573	0.139
40	0.53	0.128



Concentration Vs Time Graph Allura Red AC Solution B against Hybrid B

Table A59. Allura Red AC Solution B against Hybrid C

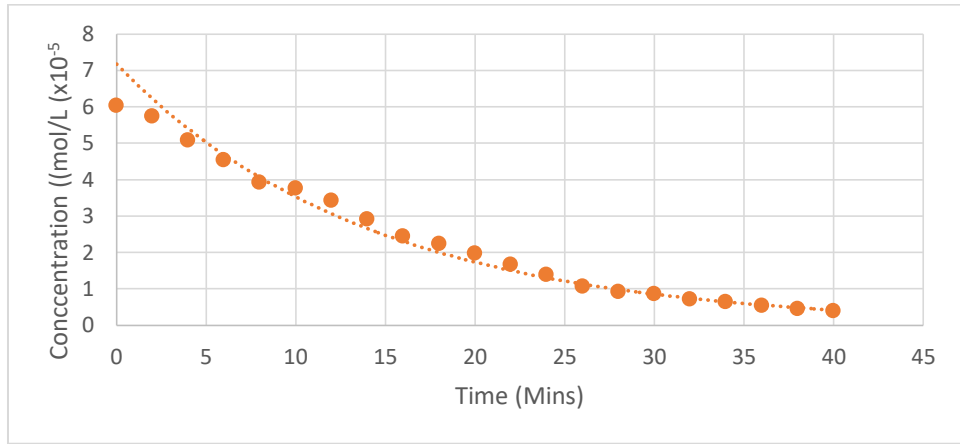
Allura Red AC (B)	Concentration (M) (mol/L (x10 <sup>-5</sup> ))	Hybrid C (Absorbance)
Time (Mins)		
0	6.006	1.539
2	4.679	1.197
4	4.256	1.088
6	3.27	0.834
8	2.548	0.648
10	2.222	0.564
12	1.306	0.328
14	0.744	0.183
16	0.491	0.118
18	0.352	0.082
20	0.2822	0.064



Concentration Vs Time Graph Allura Red AC Solution B against Hybrid C

Table A60. Allura Red AC Solution B against Hybrid D

Allura Red AC (B) Time (Mins)	Concentration (M) (mol/L (x10 <sup>-5</sup> ))	Hybrid D (Absorbance)
0	6.033	1.546
2	5.742	1.471
4	5.075	1.299
6	4.534	1.162
8	3.926	1.003
10	3.767	0.962
12	3.421	0.873
14	2.905	0.74
16	2.447	0.622
18	2.23	0.566
20	1.978	0.501
22	1.663	0.42
24	1.392	0.35
26	1.062	0.265
28	0.918	0.228
30	0.853	0.211
32	0.713	0.175
34	0.647	0.158
36	0.534	0.129
38	0.457	0.109
40	0.386	0.091

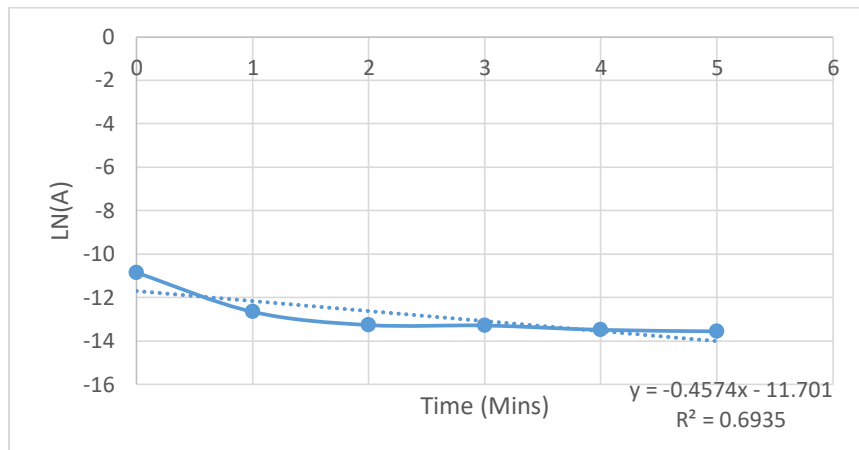


Concentration Vs Time Graph Allura Red AC Solution B against Hybrid D

### Rate constant graphs and equations:

Table A61. Iron Oxide + Activated Charcoal against Methylene Blue Data

Methylene Blue A Solution (Time)	Ln(A)
0	-10.85
1	-12.65
2	-13.26
3	-13.28
4	-13.48
5	-13.55



Iron Oxide + Activated Charcoal against Methylene Blue Ln/(A) Graph

1st Order Due to Straight Ln/(A) Graph - Calculate Rate Constant K,  
 Rate Law =  $[A] = [A]_0 \cdot e^{-(kT)}$   $0.13 \times 10^{-5} = 1.93 \times 10^{-5} e^{-k(300)}$ ,  $6.74 \times 10^{-12} = e^{-k(300)}$

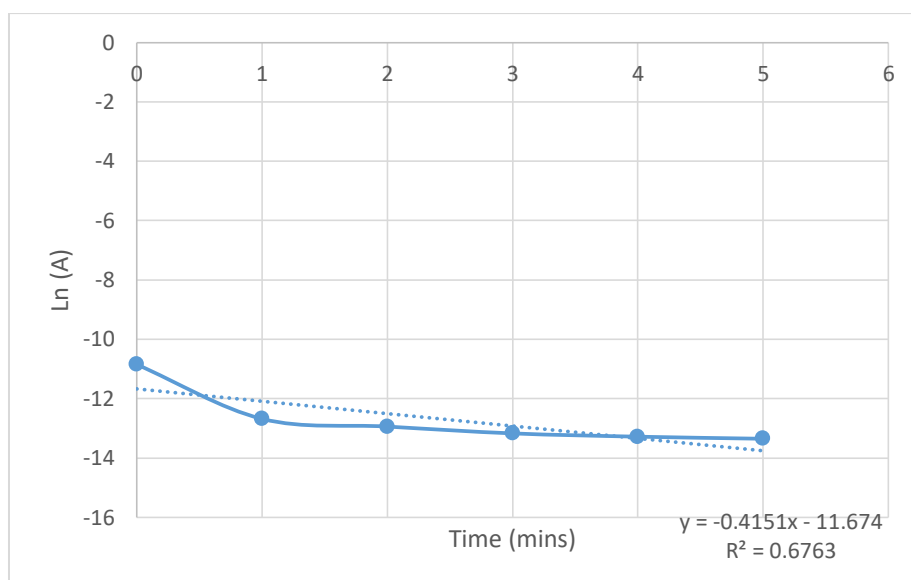
$$\ln 6.74 \times 10^{-12} = -K(300)$$

$$-0.0857k$$

$$k = 0.00857 \text{ s}^{-1}$$

Table A62. Iron Oxide + Activated Charcoal +TiO<sub>2</sub> against Methylene Blue Data

Methylene Blue A Solution (Time)	Ln(A)
0	-10.85
1	-12.68
2	-12.94
3	-13.17
4	-13.28
5	-13.35

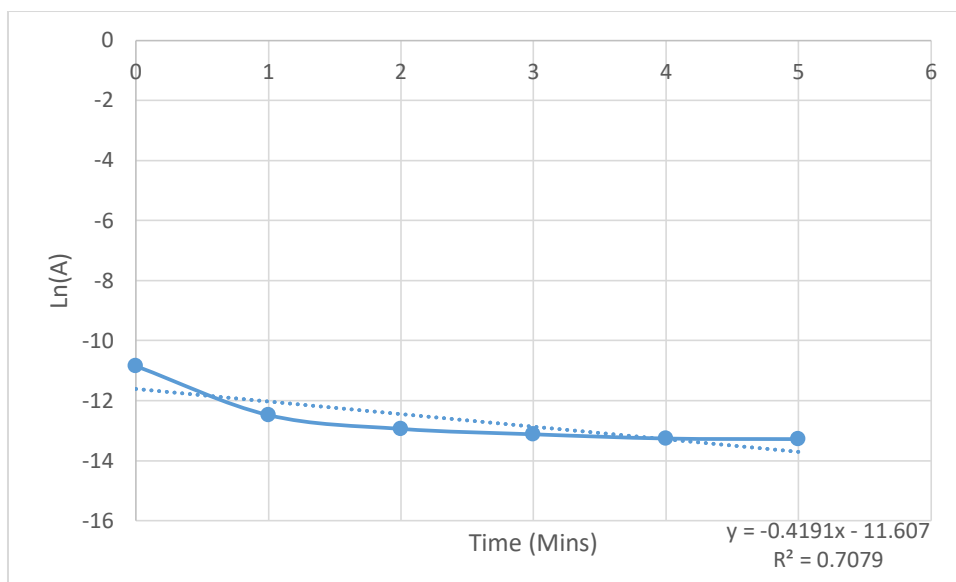


Iron Oxide + Activated Charcoal +TiO<sub>2</sub> against Methylene Blue Ln/A Graph

1st Order Due to Straight Ln/(A) Graph - Calculate Rate Constant K,  
 Rate Law =  $[A] = [A]_0 \cdot e^{-Kt}$   $0.16 \times 10^{-5} = 1.93 \times 10^{-5} \cdot e^{-K(300)}$   
 $8.29 \times 10^{-12} = e^{-K(300)}$   
 $\ln 8.29 \times 10^{-12} = -K(300)$   
 $-0.0851k$   
 $k = 0.00851 \text{ s}^{-1}$

Table A63. Iron Oxide + Multi-Walled Carbon Nanotube against Methylene Blue Data

Methylene Blue A Solution Time	Ln(A)
0	-10.85
1	-12.48
2	-12.94
3	-13.12
4	-13.26
5	-13.28

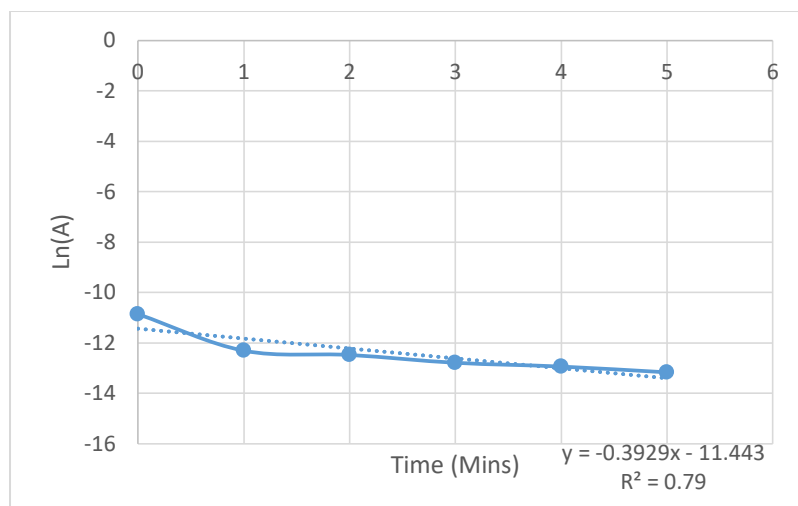


Iron Oxide + Multi-Walled Carbon Nanotube against Methylene Blue Ln/A Graph

1st Order Due to Straight Ln/(A) Graph - Calculate Rate Constant K,  
 Rate Law =  $[A] = [A]_0 e^{-kT}$   $0.17 \times 10^{-5} = 1.93 \times 10^{-5} e^{-k(300)}$   
 $8.80 \times 10^{-12} = e^{-k(300)}$   
 $\ln 8.80 \times 10^{-12} = -k(300)$   
 $-0.0849k$   
 $k = 0.00849 \text{ s}^{-1}$

Table A64. Iron Oxide + Multi-Walled Carbon Nanotube + TiO<sub>2</sub> against Methylene Blue Data

Methylene Blue A Solution (Time)	Ln(A)
0	-10.86
1	-12.31
2	-12.48
3	-12.79
4	-12.94
5	-13.17

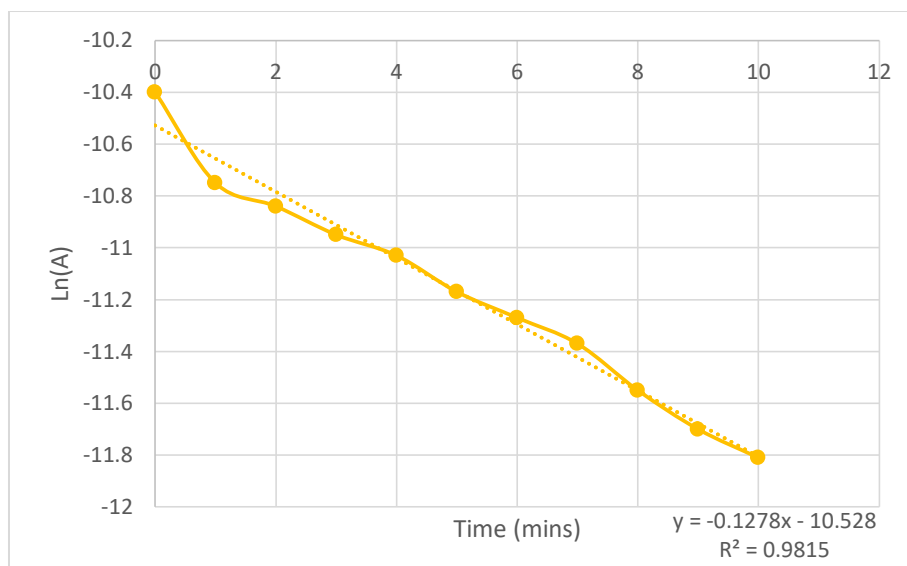


Iron Oxide + Multi-Walled Carbon Nanotube + TiO<sub>2</sub> against Methylene Blue Ln/A Graph

1st Order Due to Straight Ln/(A) Graph - Calculate Rate Constant K,  
 Rate Law =  $[A] = [A]_0 \cdot e^{(power\ of\ -KT)}$   $0.19 \times 10^{-5} = 1.93 \times 10^{-5} e^{-k(300)}$   
 $9.845 \times 10^{-12} = e^{-K(300)}$   
 $\ln 9.845 \times 10^{-12} = -K(300)$   
 $-0.0844k$   
 $k = 0.00844s^{-1}$

Table A65. Iron Oxide + Activated Charcoal against Congo Red Data

Congo Red A Solution (Time)	Ln(A)
0	-10.4
1	-10.75
2	-10.84
3	-10.95
4	-11.03
5	-11.17
6	-11.27
7	-11.37
8	-11.55
9	-11.7
10	-11.81

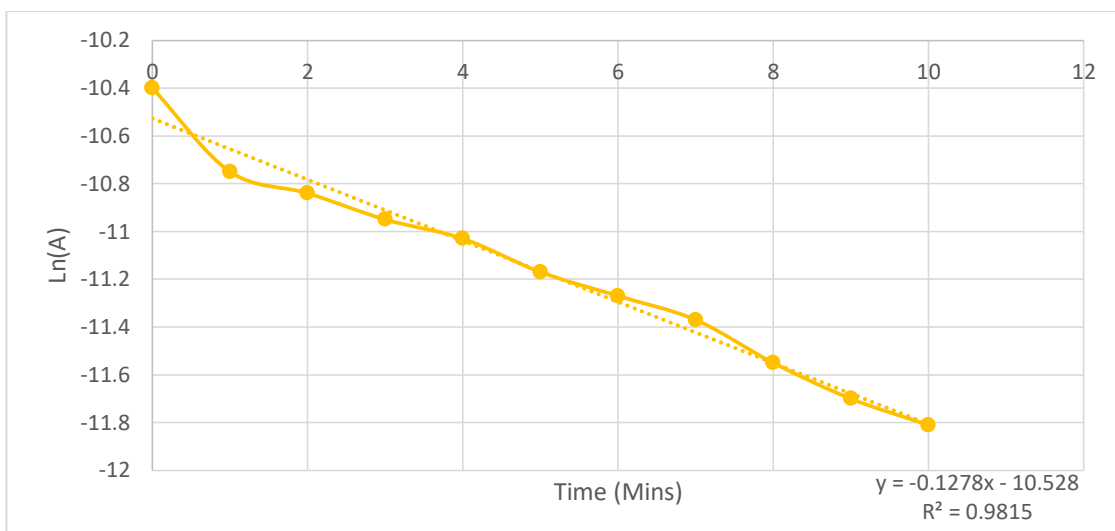


Iron Oxide + Activated Charcoal against Congo Red Ln/A Graph

1st Order Due to Straight Ln/(A) Graph - Calculate Rate Constant K,  
 Rate Law =  $[A] = [A]_0 \cdot e^{(\text{power of } -KT)}$   $0.74 \times 10^{-5} = 3.05 \times 10^{-5} e^{-k(600)}$   
 $2.426 \times 10^{-11} = e^{-K(600)}$   
 $\ln 2.426 \times 10^{-11} = -K(600)$   
 $-0.0407k$   
 $k = 0.00407 \text{ s}^{-1}$

Table A66. Iron Oxide + Activated Charcoal + TiO<sub>2</sub> against Congo Red Data

Congo Red A Solution (Time)	Ln(A)
0	-10.39
1	-10.63
2	-10.69
3	-10.74
4	-10.81
5	-10.86
6	-10.9
7	-10.96
8	-11.01
9	-11.08
10	-11.15



Iron Oxide + Activated Charcoal + TiO<sub>2</sub> against Congo Red Ln/A Graph

1st Order Due to Straight Ln/(A) Graph - Calculate Rate Constant K,

$$\text{Rate Law} = [A] = [A]_0 e^{(\text{power of } -KT)} \quad 1.44 \times 10^{-5} = 3.05 \times 10^{-5} e^{-k(600)}$$

$$4.721 \times 10^{-11} = e^{-K(600)}$$

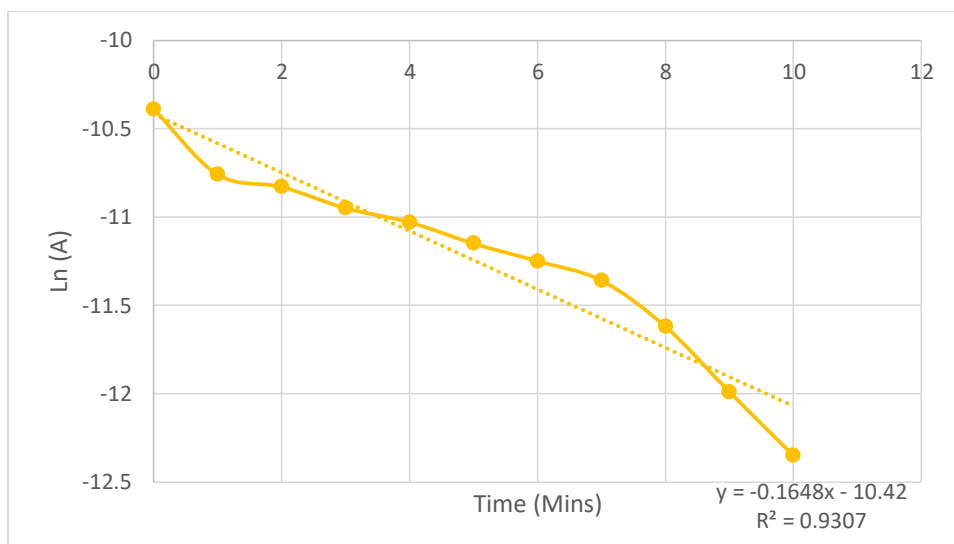
$$\text{Ln} 4.721 \times 10^{-11} = -K(600)$$

$$-0.0396k$$

$$k = 0.00396 \text{ s}^{-1}$$

Table A67. Iron Oxide + Multi-Walled Carbon Nanotube against Congo Red Data

Congo Red A Solution (Time)	Ln(A)
0	-10.39
1	-10.76
2	-10.83
3	-10.95
4	-11.03
5	-11.15
6	-11.25
7	-11.36
8	-11.62
9	-11.99
10	-12.35



Iron Oxide + Multi-Walled Carbon Nanotube against Congo Red Ln/A Graph

1st Order Due to Straight Ln/(A) Graph - Calculate Rate Constant K,

$$\text{Rate Law} = [A] = [A]_0 e^{-(kT)} \quad 0.43 \times 10^{-5} = 3.05 \times 10^{-5} e^{-k(600)}$$

$$1.41 \times 10^{-11} = e^{-k(600)}$$

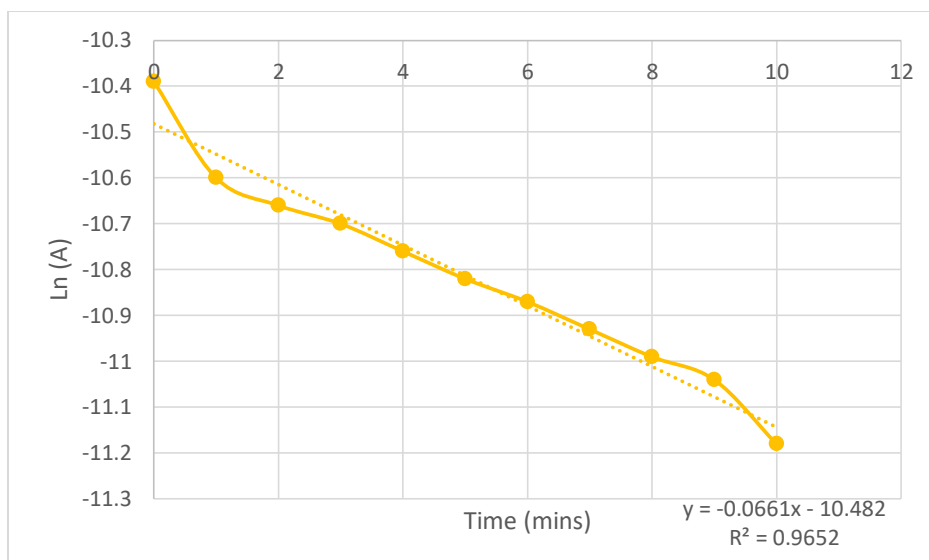
$$\ln 1.41 \times 10^{-11} = -k(600)$$

$$-0.0416k$$

$$k = 0.00416 \text{ s}^{-1}$$

Table A68. Iron Oxide + Multi-Walled Carbon Nanotube + TiO<sub>2</sub> against Congo Red Data

Congo Red A Solution (Time)	Ln(A)
0	-10.39
1	-10.6
2	-10.66
3	-10.7
4	-10.76
5	-10.82
6	-10.87
7	-10.93
8	-10.99
9	-11.04
10	-11.18

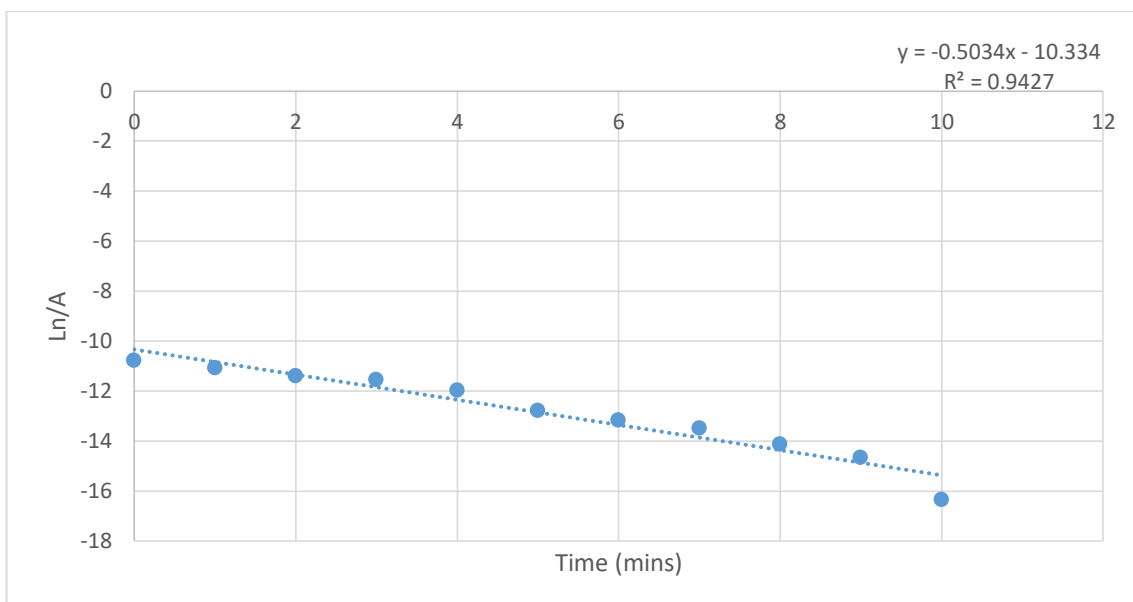


Iron Oxide + Multi-Walled Carbon Nanotube + TiO<sub>2</sub> against Congo Red Ln/A Graph

1st Order Due to Straight Ln/(A) Graph - Calculate Rate Constant K,  
 Rate Law =  $[A] = [A]_0 e^{-kT}$   $1.40 \times 10^{-5} = 3.05 \times 10^{-5} e^{-k(600)}$   
 $4.59 \times 10^{-11} = e^{-k(600)}$   
 $\ln 4.59 \times 10^{-11} = -k(600)$   
 $-0.0397k$   
 $k = 0.00397 s^{-1}$

Table A69. Methylene Blue Solution A against Ionic Liquid Hybrid A Data

Methylene Blue A Solution	Hybrid Product A Ln/A
Time	
0	-10.78
1	-11.08
2	-11.4
3	-11.55
4	-11.98
5	-12.78
6	-13.17
7	-13.5
8	-14.12
9	-14.66
10	-16.34

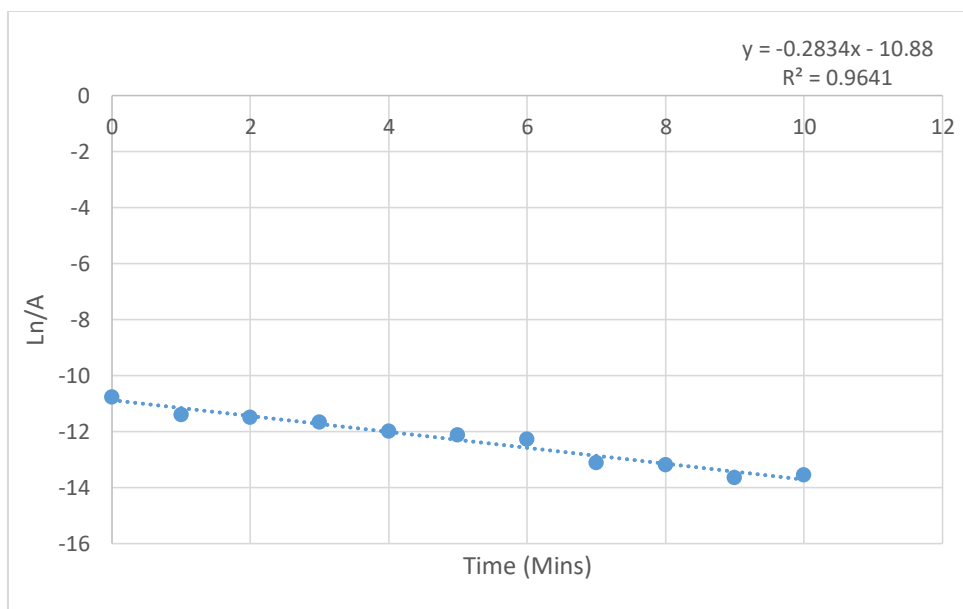


Methylene Blue Solution A against Ionic Liquid Hybrid A Ln/A Graph

1st Order Due to Straight Ln/(A) Graph - Calculate Rate Constant K,  
 Rate Law =  $[A] = [A]_0 \cdot e^{-Kt}$   $0.008 \times 10^{-5} = 2.08 \times 10^{-5} \cdot e^{-k(600)}$   
 $3.846 \times 10^{-13} = e^{-K(600)}$   
 $\ln 3.846 \times 10^{-13} = -K(600)$   
 $-0.0476k$   
 $k = 0.00476 \text{ s}^{-1}$

Table A70. Methylene Blue Solution A against Ionic Liquid Hybrid A Data

Methylene Blue A Solution	Ln/A
Time	
0	-10.77
1	-11.4
2	-11.49
3	-11.68
4	-12
5	-12.13
6	-12.28
7	-13.11
8	-13.2
9	-13.65
10	-13.55

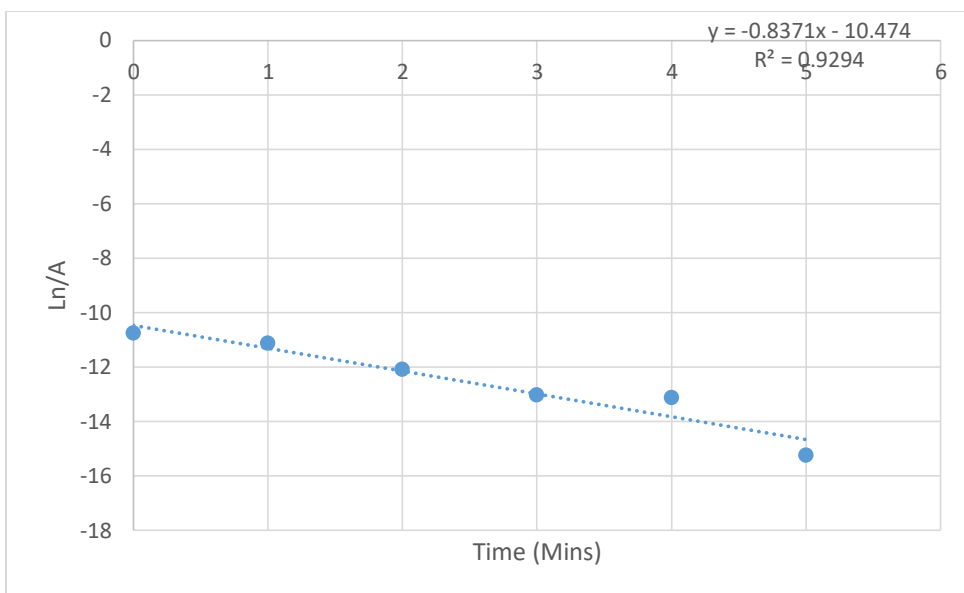


Appendix Figure 42. Methylene Blue Solution A against Ionic Liquid Hybrid B Ln/A Graph

1st Order Due to Straight Ln/(A) Graph - Calculate Rate Constant K,  
 Rate Law =  $[A] = [A]_0 e^{(power\ of\ -KT)}$   $0.131 \times 10^{-5} = 2.093 \times 10^{-5} e^{-k(600)}$   
 $2.742 \times 10^{-11} = e^{-K(600)}$   
 $\ln 2.742 \times 10^{-11} = -K(600)$   
 $-0.0405k$   
 $k = 0.00405 s^{-1}$

Table A71. Methylene Blue Solution A against Ionic Liquid Hybrid C Data

Methylene Blue A Solution Time	Ln/A Hybrid C (MB A)
0	-10.76
1	-11.14
2	-12.1
3	-13.03
4	-13.13
5	-15.24
6	N/A
7	N/A
8	N/A
9	N/A
10	N/A



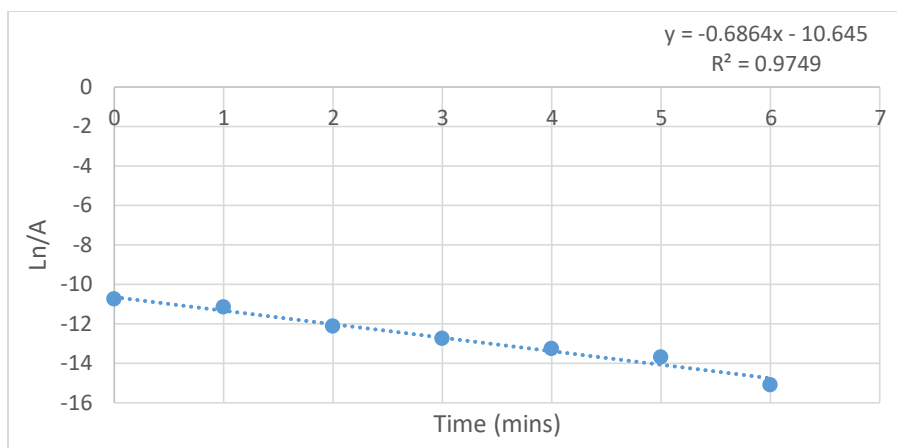
Appendix Figure 43. Methylene Blue Solution A against Ionic Liquid Hybrid C  
Ln/A Graph

1st Order Due to Straight Ln/(A) Graph - Calculate Rate Constant K,  
 Rate Law =  $[A] = [A]_0 \cdot e^{-kT}$   $0.024 \times 10^{-5} = 2.11 \times 10^{-5} \cdot e^{-k(300)}$   
 $1.137 \times 10^{-12} = e^{-K(300)}$   
 $\ln 1.137 \times 10^{-12} = -K(300)$   
 $-0.0916k$   
 $k = 0.00916 \text{ s}^{-1}$

Note: This result was completed in 10 minutes, however results after 5 minutes produced a negative concentration on the calibration graph. Therefore was impossible to plot onto the graph.

Table A72. Methylene Blue Solution A against Ionic Liquid Hybrid D Data

Methylene Blue B Solution	Ln/A Hybrid D (MB A)
Time	
0	-10.77
1	-11.18
2	-12.14
3	-12.75
4	-13.27
5	-13.7
6	-15.12



Methylene Blue Solution A against Ionic Liquid Hybrid D Ln/A Graph

1st Order Due to Straight Ln/(A) Graph - Calculate Rate Constant K,

$$\text{Rate Law} = [A] = [A]_0 e^{(power of -KT)} \quad 0.027 \times 10^{-5} = 2.107 \times 10^{-5} e^{-k(360)}$$

$$1.28 \times 10^{-12} = e^{-K(360)}$$

$$\text{Ln} 1.28 \times 10^{-12} = -K(360)$$

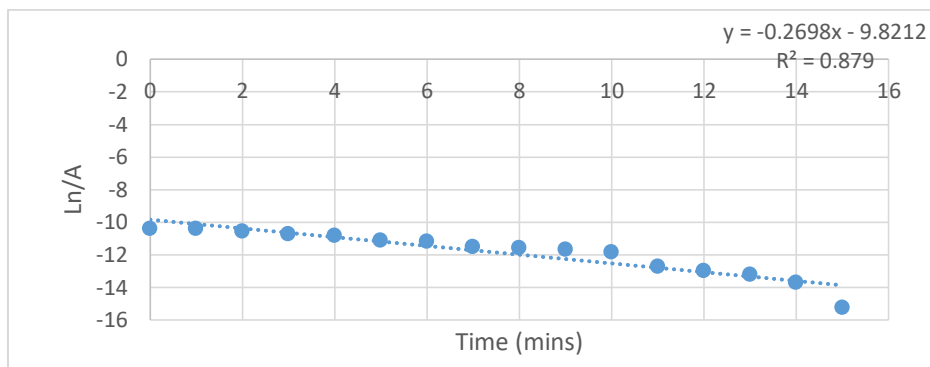
$$-0.076k$$

$$k = 0.00760 \text{ s}^{-1}$$

Note: This result was completed in 10 minutes, however results after 7 minutes produced a negative concentration on the calibration graph. Therefore was impossible to plot onto the graph.

Table A73. Methylene Blue Solution B against Ionic Liquid Hybrid A

Methylene Blue B Solution	Ln/A Hybrid A (MB B)
Time	
0	-10.38
1	-10.4
2	-10.55
3	-10.71
4	-10.82
5	-11.101
6	-11.18
7	-11.5
8	-11.58
9	-11.66
10	-11.84
11	-12.7
12	-12.96
13	-13.22
14	-13.7
15	-15.22

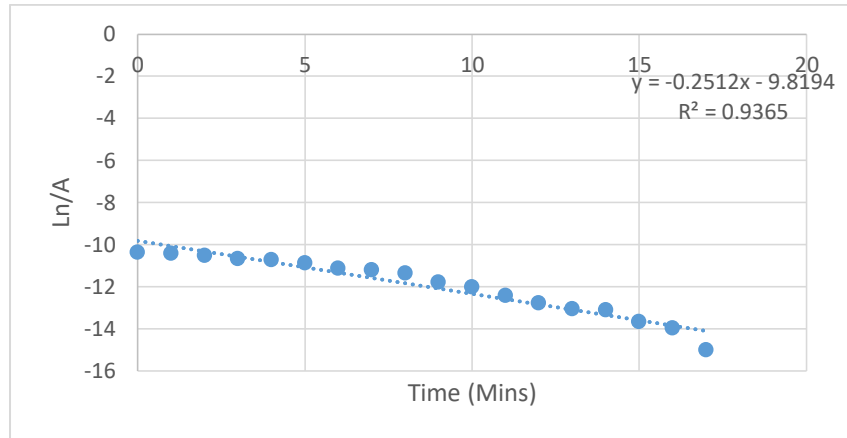


Methylene Blue Solution B against Ionic Liquid Hybrid A Ln/A Graph

1st Order Due to Straight Ln/(A) Graph - Calculate Rate Constant K,  
 Rate Law =  $[A] = [A]_0 e^{-kT}$   
 $0.0246 \times 10^{-5} = 3.11 \times 10^{-5} e^{-k(900)}$   
 $7.909 \times 10^{-13} = e^{-k(900)}$   
 $\ln 7.909 \times 10^{-13} = -k(900)$   
 $-0.03096k$   
 $k = 0.003096 \text{ s}^{-1}$

Table A74. Methylene Blue Solution B against Ionic Liquid Hybrid B Data

Methylene Blue B Solution	Ln/A Hybrid B (MB B)
Time	
0	-10.38
1	-10.42
2	-10.53
3	-10.68
4	-10.72
5	-10.88
6	-11.13
7	-11.2
8	-11.37
9	-11.8
10	-12.03
11	-12.44
12	-12.79
13	-13.05
14	-13.1
15	-13.66
16	-13.98
17	-15.02
18	N/A
19	N/A
20	N/A



Methylene Blue Solution B against Ionic Liquid Hybrid B Ln/A Graph

1st Order Due to Straight Ln/(A) Graph - Calculated Rate Constant K,

$$\text{Rate Law} = [A] = [A]_0 e^{(\text{power of } -KT)} \quad 0.03 \times 10^{-5} = 3.09 \times 10^{-5} e^{-k(1020)}$$

$$9.708 \times 10^{-13} = e^{-K(1020)}$$

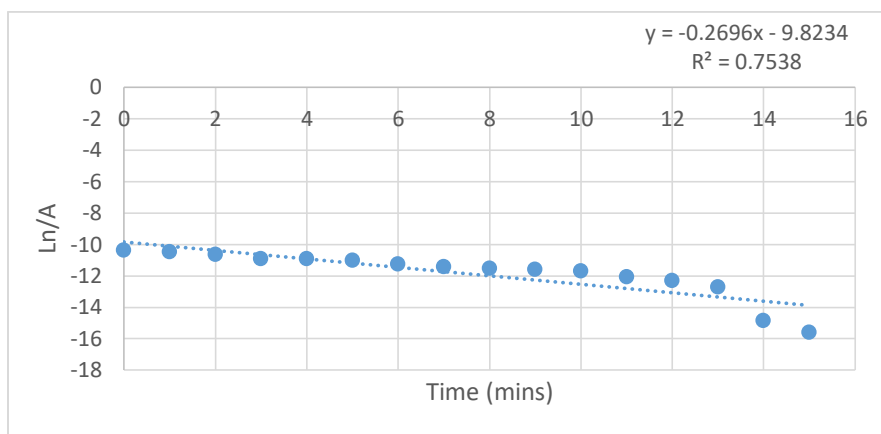
$$\text{Ln} 9.708 \times 10^{-13} = -K(1020)$$

$$-0.0271k$$

$$k = 0.00271 \text{ s}^{-1}$$

Table A75. Methylene Blue Solution B against Ionic Liquid Hybrid C Data

Methylene Blue B Solution	Ln/A Hybrid C (MB B)
Time	
0	-10.38
1	-10.5
2	-10.64
3	-10.91
4	-10.93
5	-11.04
6	-11.25
7	-11.42
8	-11.55
9	-11.6
10	-11.72
11	-12.08
12	-12.32
13	-12.72
14	-14.85
15	-15.62
16	N/A
17	N/A
18	N/A
19	N/A
20	N/A

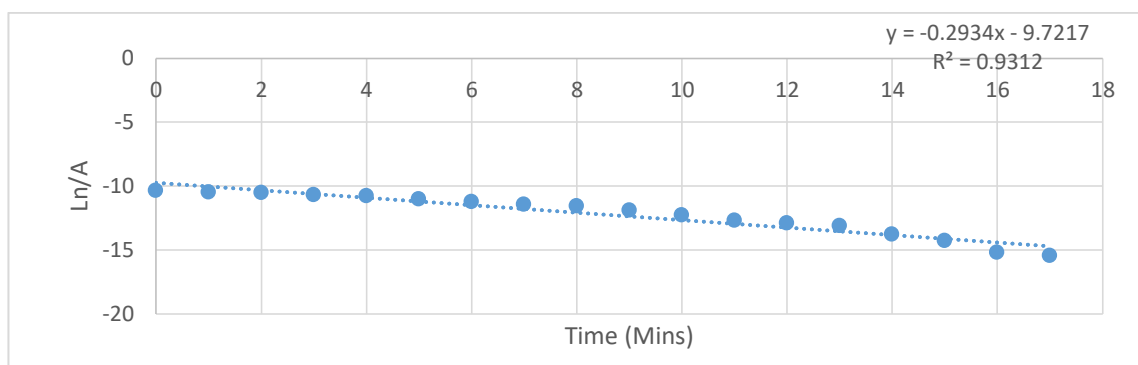


Methylene Blue Solution B against Ionic Liquid Hybrid C Ln/A Graph

1st Order Due to Straight Ln/(A) Graph - Calculate Rate Constant K,  
 Rate Law =  $[A] = [A]_0 \cdot e^{-kT}$   $0.0164 \times 10^{-5} = 3.105 \times 10^{-5} \cdot e^{-k(1080)}$   
 $5.281 \times 10^{-13} = e^{-k(1080)}$   
 $\ln 5.281 \times 10^{-13} = -k(1080)$   
 $-0.0262$   
 $k = 0.00262 \text{ s}^{-1}$

Table A76. Methylene Blue Solution B against Ionic Liquid Hybrid D Data

Methylene Blue B Solution	Ln/A Hybrid D (MB B)
Time	
0	-10.38
1	-10.48
2	-10.55
3	-10.7
4	-10.77
5	-11.05
6	-11.25
7	-11.43
8	-11.58
9	-11.92
10	-12.3
11	-12.69
12	-12.9
13	-13.12
14	-13.8
15	-14.28
16	-15.22
17	-15.46
18	N/A
19	N/A
20	N/A

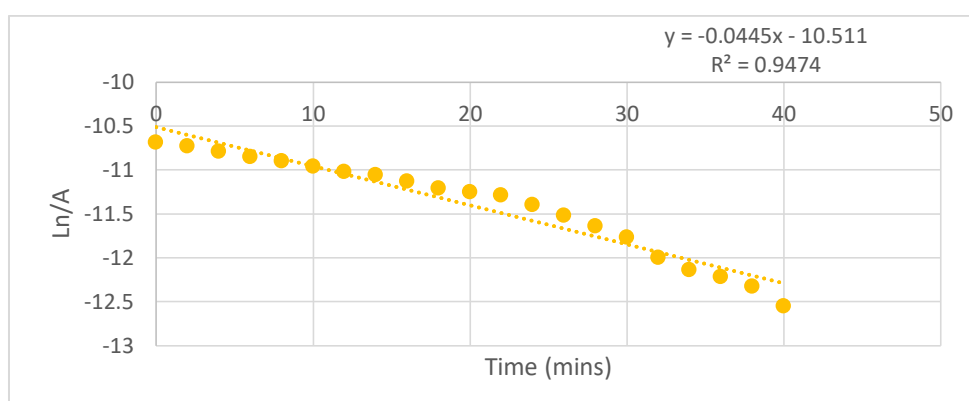


Methylene Blue Solution B against Ionic Liquid Hybrid D Ln/A Graph

1st Order Due to Straight Ln/(A) Graph - Calculate Rate Constant K,  
 Rate Law =  $[A] = [A]_0 e^{(power\ of\ -KT)}$   $0.0192 \times 10^{-5} = 3.094 \times 10^{-5} e^{-k(1020)}$   
 $6.205 \times 10^{-13} = e^{-K(1020)}$   
 $\ln 4.59 \times 10^{-11} = -K(1020)$   
 $-0.0275k$   
 $k = 0.00275 s^{-1}$

Table A77. Congo Red Solution A against Ionic Liquid Hybrid A Data

Congo Red (A)	Ln/A Hybrid A (CR A)
Time (Min)	
0	-10.69
2	-10.73
4	-10.79
6	-10.85
8	-10.9
10	-10.96
12	-11.02
14	-11.06
16	-11.13
18	-11.21
20	-11.25
22	-11.29
24	-11.4
26	-11.52
28	-11.64
30	-11.77
32	-12
34	-12.14
36	-12.22
38	-12.33
40	-12.55

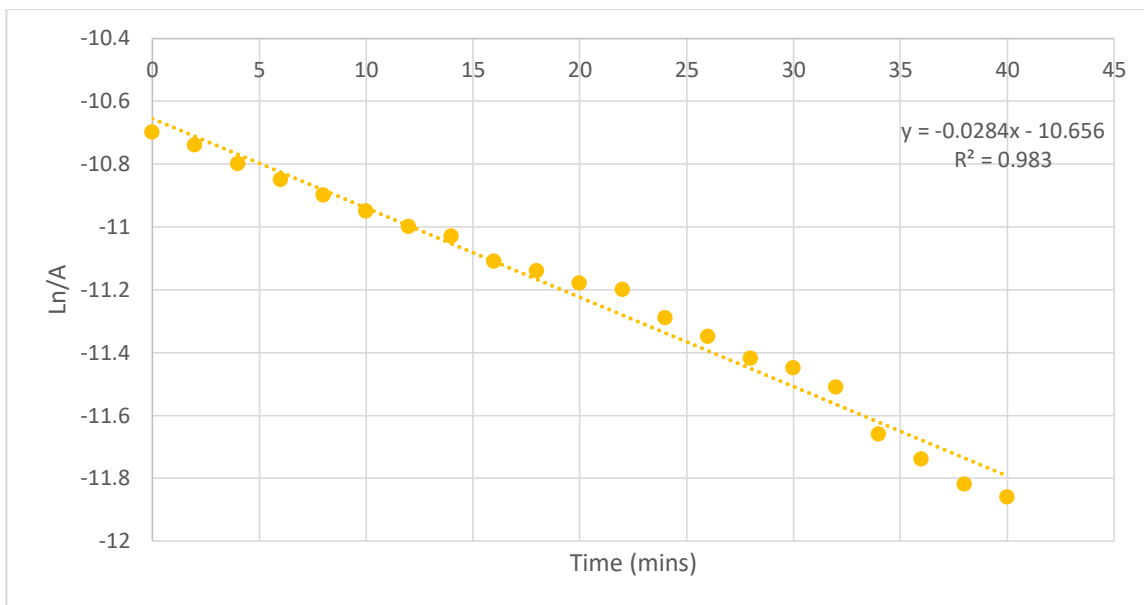


Congo Red Solution A against Ionic Liquid Hybrid Product A Ln/A Graph

1st Order Due to Straight Ln/(A) Graph - Calculate Rate Constant K,  
 Rate Law =  $[A] = [A]_0 \cdot e^{(power\ of\ -KT)}$   $0.353 \times 10^{-5} = 2.26 \times 10^{-5} \cdot e^{-k(2400)}$   
 $1.562 \times 10^{-11} = e^{-K(2400)}$   
 $\ln 1.562 \times 10^{-11} = -K(2400)$   
 $-0.01036k$   
 $k = 0.001036s^{-1}$

Table A78. Congo Red Solution A against Ionic Liquid Hybrid B Graph

Congo Red (A) Time (Min)	Ln/A Hybrid B (CR A)
0	-10.7
2	-10.74
4	-10.8
6	-10.85
8	-10.9
10	-10.95
12	-11
14	-11.03
16	-11.11
18	-11.14
20	-11.18
22	-11.2
24	-11.29
26	-11.35
28	-11.42
30	-11.45
32	-11.51
34	-11.66
36	-11.74
38	-11.82
40	-11.86

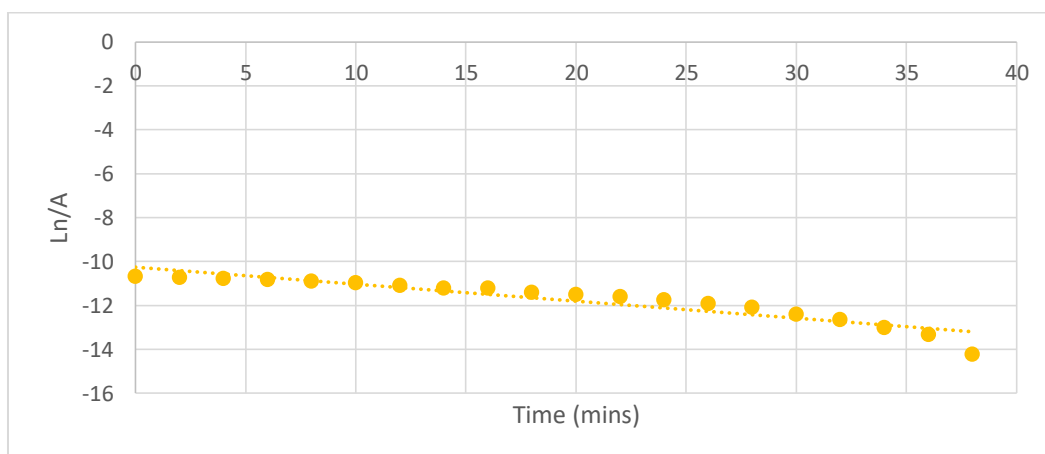


Congo Red Solution A against Ionic Liquid Hybrid Product B Ln/A Graph

1st Order Due to Straight Ln/(A) Graph - Calculate Rate Constant K,  
 Rate Law =  $[A] = [A]_0 e^{-kT}$   $0.704 \times 10^{-5} = 2.266 \times 10^{-5} e^{-k(2400)}$   
 $3.107 \times 10^{-11} = e^{-k(2400)}$   
 $\ln 3.107 \times 10^{-11} = -k(2280)$   
 $-0.01061k$   
 $k = 0.00106 s^{-1}$

Table A79. Congo Red Solution A against Ionic Liquid Hybrid C Data

Congo Red (A)	Ln/A Hybrid C (CR A)
Time (Min)	
0	-10.7
2	-10.74
4	-10.8
6	-10.85
8	-10.91
10	-10.99
12	-11.12
14	-11.22
16	-11.23
18	-11.42
20	-11.53
22	-11.62
24	-11.77
26	-11.94
28	-12.11
30	-12.42
32	-12.65
34	-13.03
36	-13.35
38	-14.23
40	N/A



Congo Red Solution A against Ionic Liquid Hybrid C Ln/A Graph

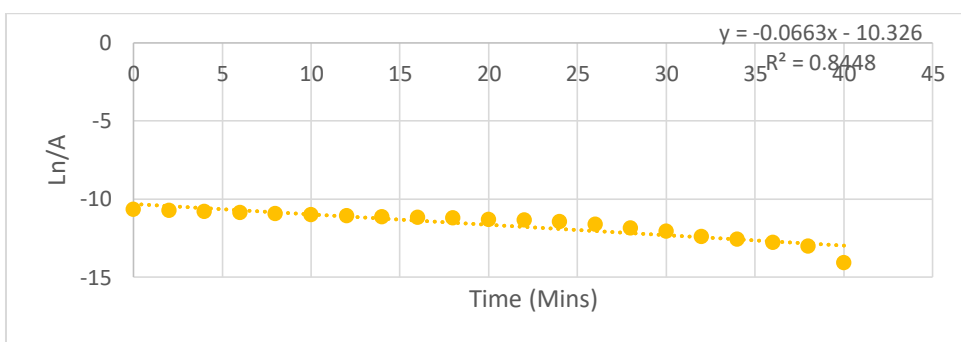
1st Order Due to Straight Ln/(A) Graph - Calculate Rate Constant K,  
 Rate Law =  $[A] = [A]_0 e^{-kT}$   
 $0.066 \times 10^{-5} = 2.256 \times 10^{-5} e^{-k(2280)}$   
 $2.925 \times 10^{-12} = e^{-k(2280)}$

$$\ln 2.925 \times 10^{-12} = -k(2280) - 0.0116k$$

$$k = 0.00116 \text{ s}^{-1}$$

Table A80. Congo Red Solution A against Ionic Liquid Hybrid D Data

Congo Red (A)	Ln/A Hybrid D (CR A)
Time (Min)	
0	-10.69
2	-10.75
4	-10.82
6	-10.89
8	-10.97
10	-11.03
12	-11.1
14	-11.15
16	-11.21
18	-11.25
20	-11.35
22	-11.37
24	-11.48
26	-11.65
28	-11.88
30	-12.1
32	-12.44
34	-12.61
36	-12.8
38	-13.04
40	-14.1

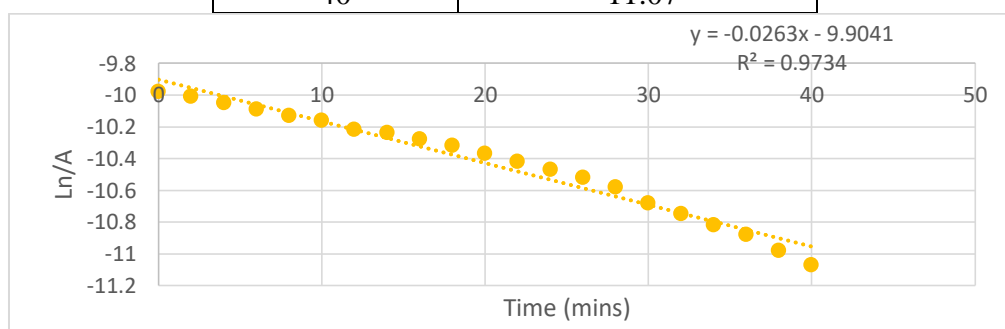


Congo Red Solution A against Ionic Liquid Hybrid D Ln/A Graph

1st Order Due to Straight Ln/(A) Graph - Calculate Rate Constant K,  
Rate Law =  $[A]=[A]_0 \cdot e^{-kT}$   $0.075 \times 10^{-5} = 2.275 \times 10^{-5} e^{-k(2400)}$   
 $3.29 \times 10^{-12} = e^{-k(2400)}$   
 $\ln 3.29 \times 10^{-12} = -k(2400)$   
 $-0.011k$   
 $k=0.0011s^{-1}$

Table A81. Congo Red Solution B against Ionic Liquid Hybrid Product A Data

Congo Red (B) Time (Min)	Ln/A Hybrid A (CR B)
0	-9.98
2	-10.01
4	-10.05
6	-10.09
8	-10.13
10	-10.16
12	-10.22
14	-10.24
16	-10.28
18	-10.32
20	-10.37
22	-10.42
24	-10.47
26	-10.52
28	-10.58
30	-10.68
32	-10.75
34	-10.82
36	-10.88
38	-10.98
40	-11.07

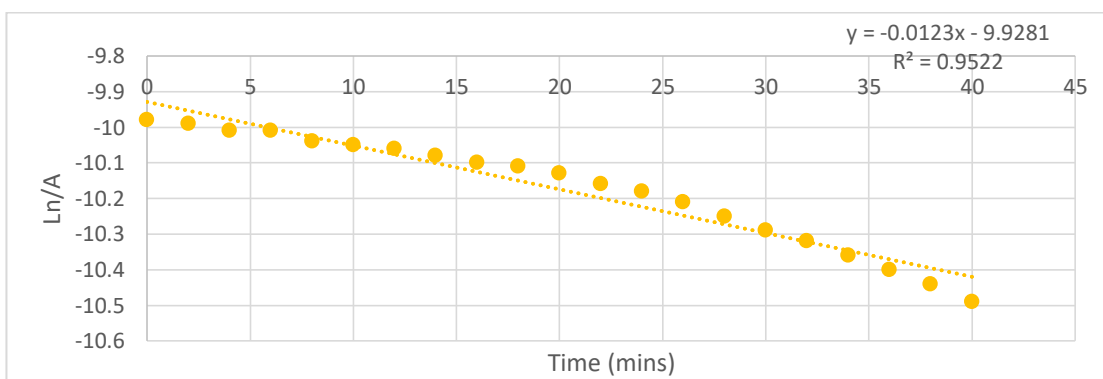


Congo Red Solution B against Ionic Liquid Hybrid Product A Ln/A Graph.

1st Order Due to Straight Ln/(A) Graph - Calculate Rate Constant K,  
 Rate Law =  $[A]=[A]_0 \cdot e^{-kT}$   $1.56 \times 10^{-5} = 4.63 \times 10^{-5} e^{-k(2400)}$   
 $3.37 \times 10^{-11} = e^{-K(2400)}$   
 $\ln 3.37 \times 10^{-11} = -K(2400)$   
 $-0.01k$   
 $k=0.001s^{-1}$

Table A82. Congo Red Solution B against Ionic Liquid Hybrid B Data

Congo Red (B) Time (Min)	Ln/A Hybrid B (CR B)
0	-9.98
2	-9.99
4	-10.01
6	-10.01
8	-10.04
10	-10.05
12	-10.06
14	-10.08
16	-10.1
18	-10.11
20	-10.13
22	-10.16
24	-10.18
26	-10.21
28	-10.25
30	-10.29
32	-10.32
34	-10.36
36	-10.4
38	-10.44
40	-10.49

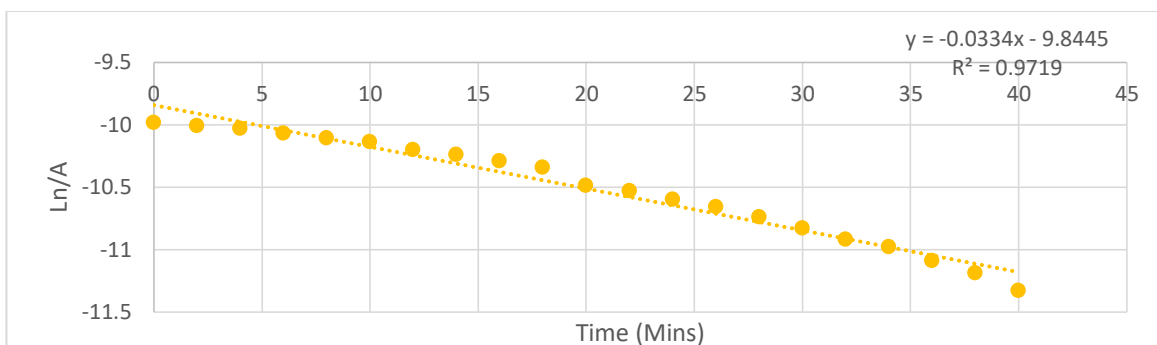


Congo Red Solution B against Ionic Liquid Hybrid B Ln/A Graph

1st Order Due to Straight Ln/(A) Graph - Calculate Rate Constant K,  
 Rate Law =  $[A]=[A].e(\text{power of } -KT)$   $2.784 \times 10^{-5} = 4.64 \times 10^{-5} e^{-k(2400)}$   
 $6 \times 10^{-11} = e^{-K(2400)}$   
 $\ln 6 \times 10^{-11} = -K(2400)$   
 $-0.0098k$   
 $k=0.00098s^{-1}$

Table A83. Congo Red Solution B against Ionic Liquid Hybrid C Data

Congo Red (B) Time (Min)	Ln/A Hybrid C (CR B)
0	-9.983
2	-10.01
4	-10.03
6	-10.07
8	-10.11
10	-10.14
12	-10.2
14	-10.24
16	-10.29
18	-10.341
20	-10.49
22	-10.53
24	-10.6
26	-10.66
28	-10.74
30	-10.83
32	-10.92
34	-10.98
36	-11.09
38	-11.19
40	-11.33

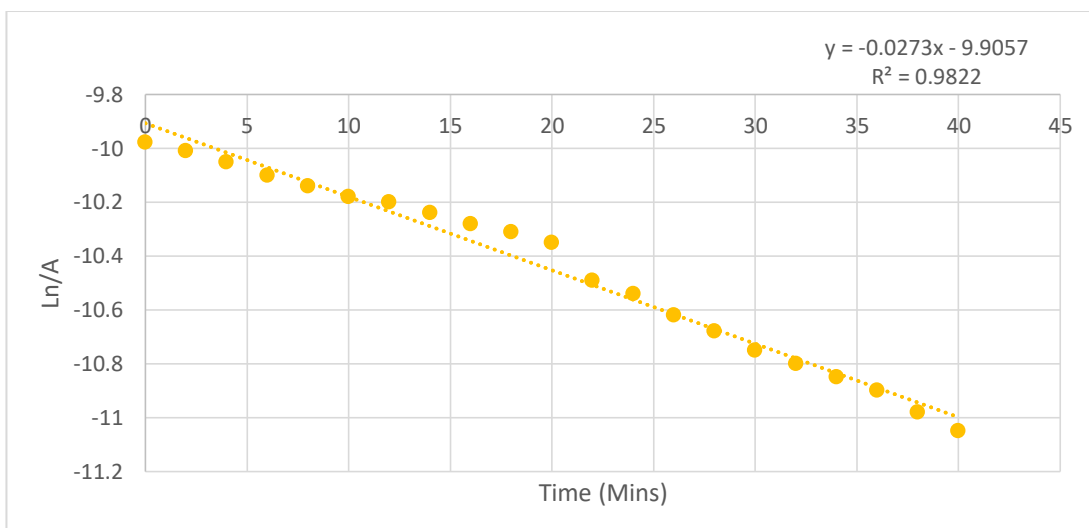


Congo Red Solution B against Ionic Liquid Hybrid C Ln/A Graph

1st Order Due to Straight Ln/(A) Graph - Calculate Rate Constant K,  
 Rate Law =  $[A] = [A]_0 e^{-kT}$   $1.203 \times 10^{-5} = 4.617 \times 10^{-5} e^{-k(2400)}$   
 $5.55 \times 10^{-10} = e^{-k(2400)}$   
 $\ln 5.55 \times 10^{-10} = -K(2400)$   
 $-0.00888k$   
 $k = 0.000888 s^{-1}$

Table A84. Congo Red Solution B against Ionic Liquid Hybrid D Data

Congo Red (B) Time (Min)	Ln/A Hybrid D (CR B)
0	-9.977
2	-10.01
4	-10.05
6	-10.1
8	-10.14
10	-10.18
12	-10.2
14	-10.24
16	-10.28
18	-10.31
20	-10.35
22	-10.49
24	-10.54
26	-10.62
28	-10.68
30	-10.75
32	-10.8
34	-10.85
36	-10.9
38	-10.98
40	-11.05

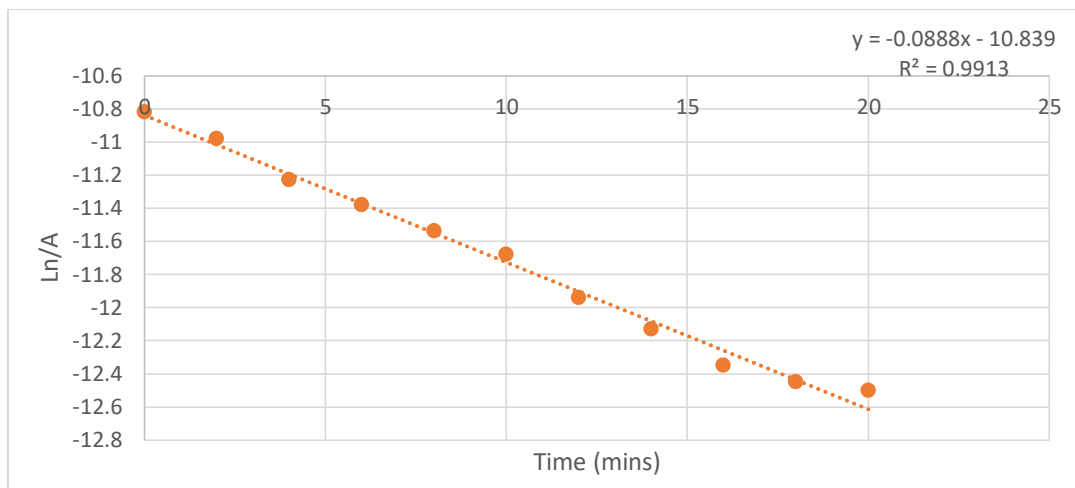


Congo Red Solution B against Ionic Liquid Hybrid D Ln/A Graph

1st Order Due to Straight Ln/(A) Graph - Calculate Rate Constant K,  
 Rate Law =  $[A]=[A]_0 \cdot e^{(power\ of\ -KT)}$   $1.58 \times 10^{-5} = 4.646 \times 10^{-5} \cdot e^{-k(2400)}$   
 $3.4 \times 10^{-11} = e^{-K(2400)}$   
 $\ln 3.4 \times 10^{-11} = -K(2400)$   
 $-0.0100$   
 $k=0.001s^{-1}$

Table A85. Allura Red AC Solution A against Ionic Liquid Hybrid A Data

Allura Red AC (A)	Ln/A Hybrid A (ARAC A)
Time (Min)	
0	-10.82
2	-10.98
4	-11.23
6	-11.38
8	-11.54
10	-11.68
12	-11.94
14	-12.13
16	-12.35
18	-12.45
20	-12.5

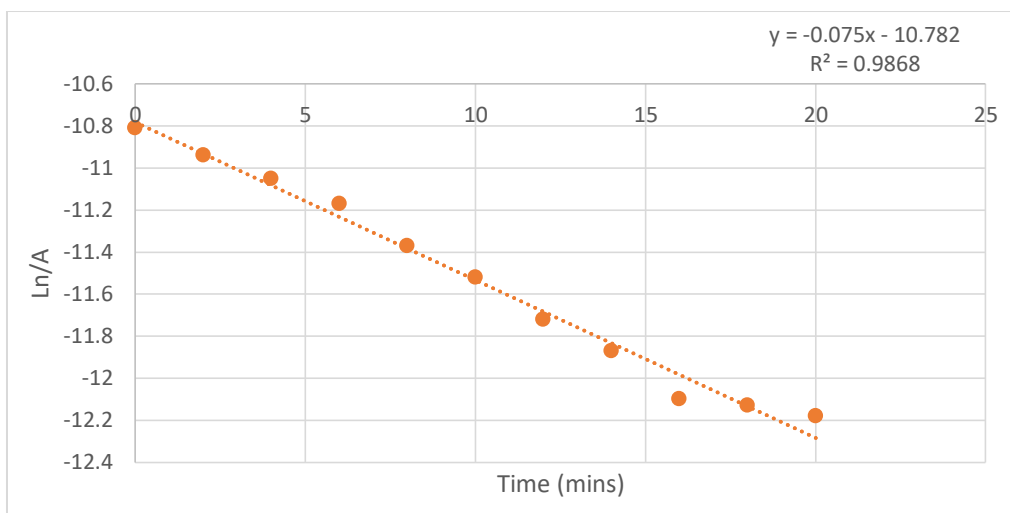


Allura Red AC Solution A against Ionic Liquid Hybrid A Ln/A Graph

1st Order Due to Straight Ln/(A) Graph - Calculate Rate Constant K,  
 Rate Law =  $[A] = [A]_0 e^{-kT}$   $0.375 \times 10^{-5} = 2.009 \times 10^{-5} e^{-k(1200)}$   
 $1.86 \times 10^{-11} = e^{-K(1200)}$   
 $\ln 1.86 \times 10^{-11} = -K(1200)$   
 $-0.02059k$   
 $k = 0.002059 \text{ s}^{-1}$

Table A86. Allura Red AC Solution A against Ionic Liquid Hybrid B Data

Allura Red AC (A)	Ln/A Hybrid B (ARAC A)
Time (Min)	
0	-10.81
2	-10.94
4	-11.05
6	-11.17
8	-11.37
10	-11.52
12	-11.72
14	-11.87
16	-12.1
18	-12.13
20	-12.18

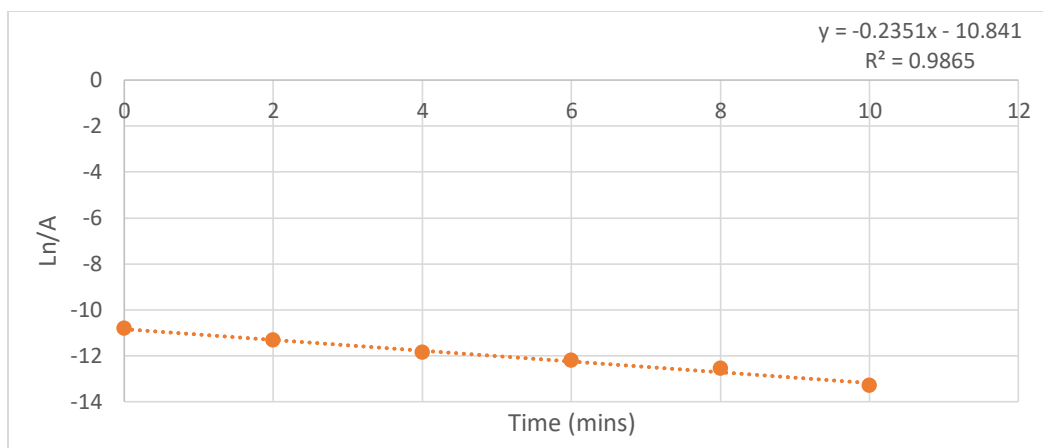


Allura Red AC Solution A against Ionic Liquid Hybrid B Ln/A Graph

1st Order Due to Straight Ln/(A) Graph - Calculate Rate Constant K,  
 Rate Law =  $[A] = [A]_0 \cdot e^{(power\ of\ -KT)}$   $0.515 \times 10^{-5} = 2.02 \times 10^{-5} e^{-k(1200)}$   
 $2.55 \times 10^{-11} = e^{-K(1200)}$   
 $\ln 2.55 \times 10^{-11} = -K(1200)$   
 $-0.02032k$   
 $k = 0.002032 s^{-1}$

Table A87. Allura Red AC Solution A against Ionic Liquid Hybrid C Data

Allura Red AC (A)	Ln/A Hybrid C (ARAC A)
Time (Min)	
0	-10.82
2	-11.33
4	-11.87
6	-12.22
8	-12.55
10	-13.31

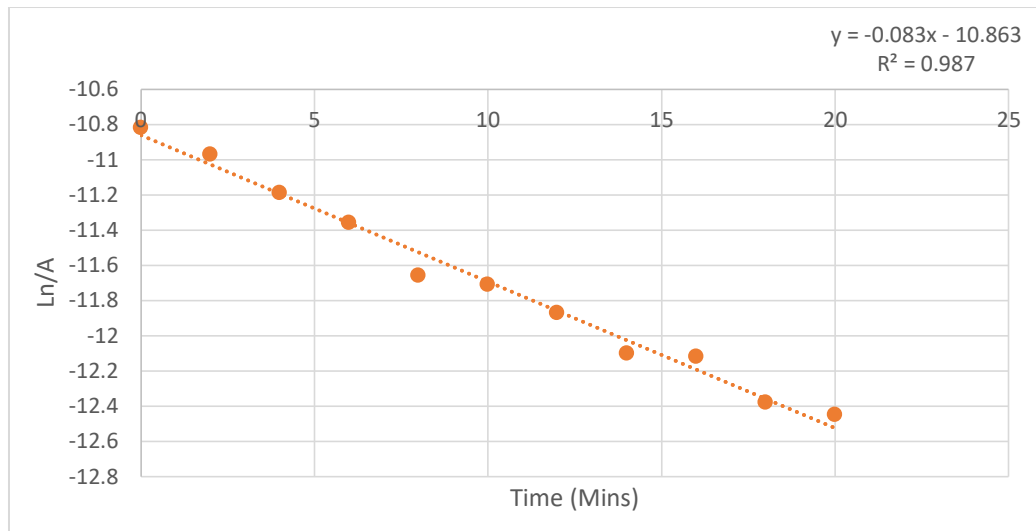


Allura Red AC Solution A against Ionic Liquid Hybrid C Ln/A Graph

1st Order Due to Straight Ln/(A) Graph - Calculate Rate Constant K,  
 Rate Law =  $[A] = [A]_0 e^{-kT}$   
 $0.165 \times 10^{-5} = 2.005 \times 10^{-5} e^{-k(1200)}$   
 $8.23 \times 10^{-12} = e^{-K(1200)}$   
 $\ln 8.23 \times 10^{-12} = -K(1200)$   
 $-0.02127k$   
 $k = 0.002127 s^{-1}$

Table A88. Allura Red AC Solution A against Ionic Liquid Hybrid D Data

Allura Red AC (A)	Ln/A Hybrid D (ARAC A)
Time (Min)	
0	-10.82
2	-10.97
4	-11.19
6	-11.36
8	-11.66
10	-11.71
12	-11.87
14	-12.1
16	-12.12
18	-12.38
20	-12.45

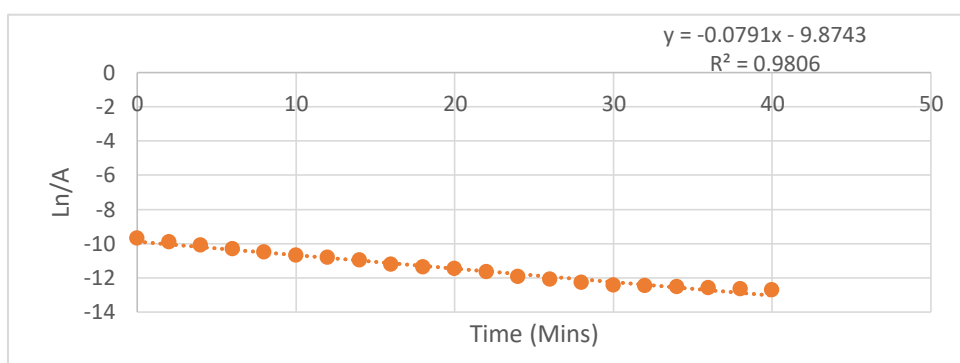


Allura Red AC Solution A against Ionic Liquid Hybrid D Ln/A Graph

1st Order Due to Straight Ln/(A) Graph - Calculate Rate Constant K,  
 Rate Law =  $[A] = [A]_0 \cdot e^{-kT}$   $0.391 \times 10^{-5} = 1.998 \times 10^{-5} \cdot e^{-k(1200)}$   
 $1.957 \times 10^{-11} = e^{-k(1200)}$   
 $\ln 1.957 \times 10^{-11} = -k(1200)$   
 $-0.02055k$   
 $k = 0.002055 \text{ s}^{-1}$

Table A89. Allura Red AC Solution B against Ionic Liquid Hybrid A Data

Allura Red AC (B)	Ln/A Hybrid A (ARAC B)
Time (Min)	
0	-9.71
2	-9.92
4	-10.1
6	-10.31
8	-10.51
10	-10.7
12	-10.81
14	-10.99
16	-11.22
18	-11.39
20	-11.48
22	-11.68
24	-11.93
26	-12.11
28	-12.3
30	-12.43
32	-12.49
34	-12.53
36	-12.61
38	-12.661
40	-12.71



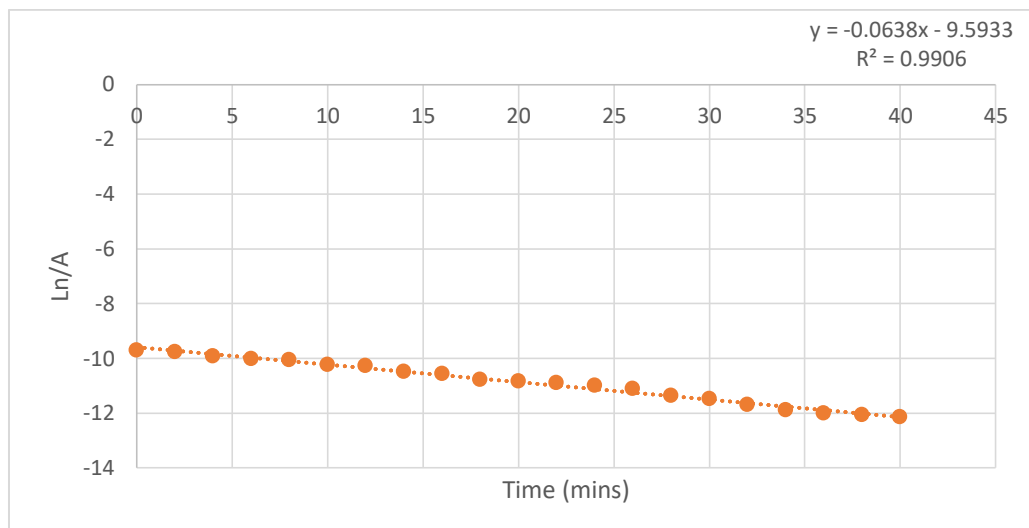
Allura Red AC Solution B against Ionic Liquid Hybrid A Ln/A Graph

1st Order Due to Straight Ln/(A) Graph - Calculate Rate Constant K,  
 Rate Law =  $[A] = [A]_0 \cdot e^{-kT}$   $0.301 \times 10^{-5} = 6.04 \times 10^{-5} \cdot e^{-k(2400)}$   
 $4.983 \times 10^{-12} = e^{-K(2400)}$   
 $\ln 4.983 \times 10^{-12} = -K(2400)$   
 $-0.01084k$

$$k=0.001084s^{-1}$$

Table A90. Allura Red AC Solution B against Ionic Liquid Hybrid B

Allura Red AC (B)	Ln/A Hybrid B (ARAC B)
Time (Min)	
0	-9.711
2	-9.77
4	-9.914
6	-10.01
8	-10.05
10	-10.23
12	-10.277
14	-10.48
16	-10.57
18	-10.77
20	-10.83
22	-10.895
24	-10.99
26	-11.11
28	-11.36
30	-11.48
32	-11.69
34	-11.88
36	-12.01
38	-12.07
40	-12.15

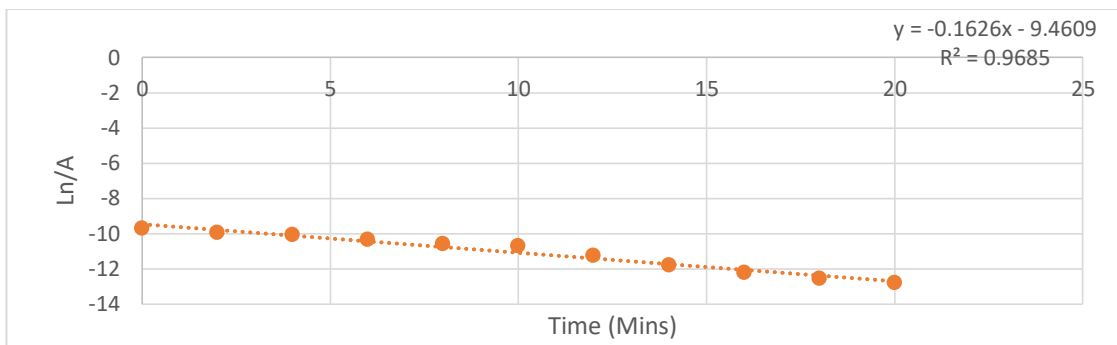


Allura Red AC Solution B against Ionic Liquid Hybrid B Graph

1st Order Due to Straight Ln/(A) Graph - Calculate Rate Constant K,  
 Rate Law =  $[A] = [A]_0 e^{-kT}$   
 $0.530 \times 10^{-5} = 6.057 \times 10^{-5} e^{-k(2400)}$   
 $8.75 \times 10^{-12} = e^{-K(2400)}$   
 $\ln 8.75 \times 10^{-12} = -K(2400)$   
 $-0.01061k$   
 $k = 0.001061 s^{-1}$

Table A91. Allura Red AC Solution B against Ionic Liquid Hybrid C Data

Allura Red AC (B)	Ln/A Hybrid C (ARAC B)
Time (Min)	
0	-9.72
2	-9.96
4	-10.06
6	-10.33
8	-10.58
10	-10.71
12	-11.24
14	-11.8
16	-12.22
18	-12.56
20	-12.78

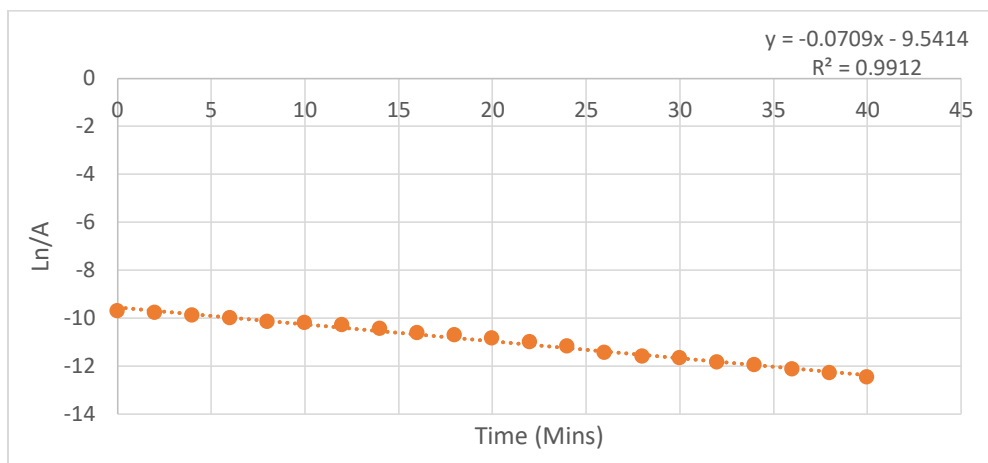


Allura Red AC Solution B against Ionic Liquid Hybrid Product C Ln/A Graph

1st Order Due to Straight Ln/(A) Graph - Calculate Rate Constant K,  
 Rate Law =  $[A] = [A]_0 e^{-kT}$   
 $0.282 \times 10^{-5} = 6.006 \times 10^{-5} e^{-k(2400)}$   
 $4.695 \times 10^{-12} = e^{-K(2400)}$   
 $\ln 4.695 \times 10^{-12} = -K(2400)$   
 $-0.01086k$   
 $k = 0.001086 s^{-1}$

Table A92. Allura Red AC Solution B against Ionic Liquid Hybrid D Data

Allura Red AC (B) Time (Min)	Ln/A Hybrid D (ARAC B)
0	-9.715
2	-9.765
4	-9.889
6	-10
8	-10.14
10	-10.19
12	-10.28
14	-10.44
16	-10.61
18	-10.71
20	-10.83
22	-11
24	-11.18
26	-11.45
28	-11.59
30	-11.67
32	-11.85
34	-11.95
36	-12.14
38	-12.29
40	-12.46



Allura Red AC Solution B against Ionic Liquid Hybrid D Ln/A Graph

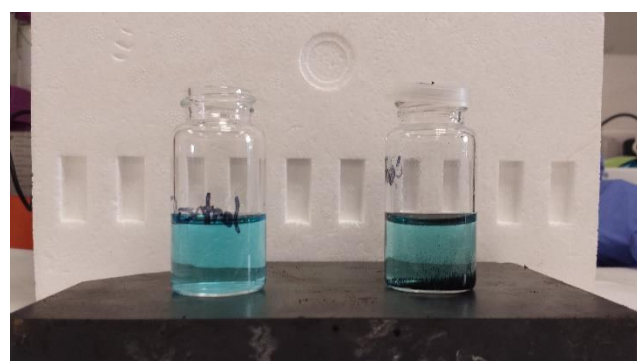
### Degradation Photos:



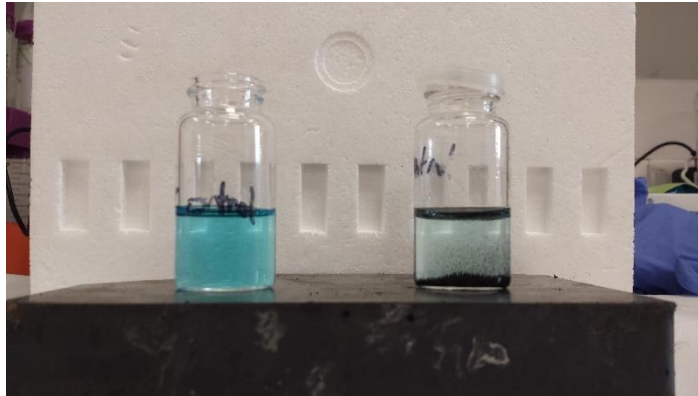
Methylene Blue Solution A against Product A (Start)



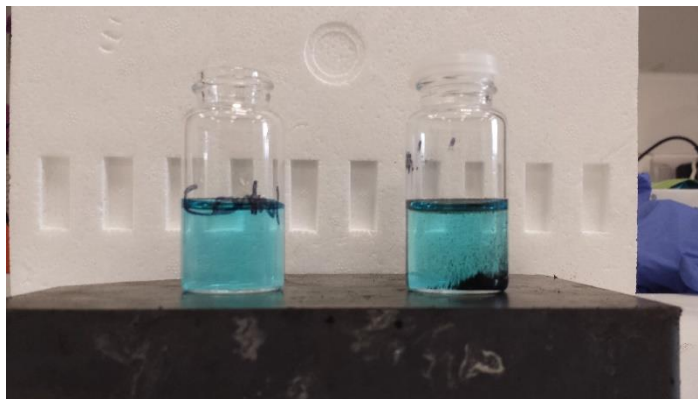
Methylene Blue Solution A against Product A (End)



Methylene Blue Solution A against Product B (Start)



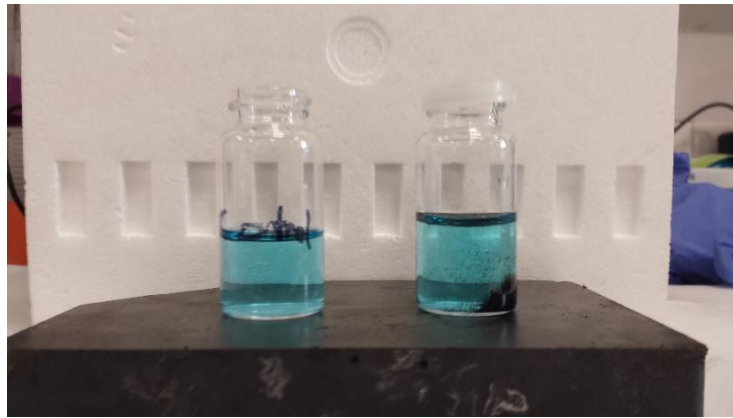
Methylene Blue Solution A against Product B (End)



Methylene Blue Solution A against Product C (Start)



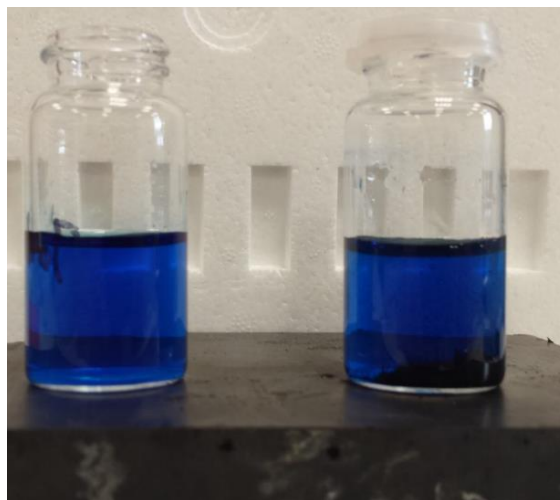
Methylene Blue Solution A against Product C (End)



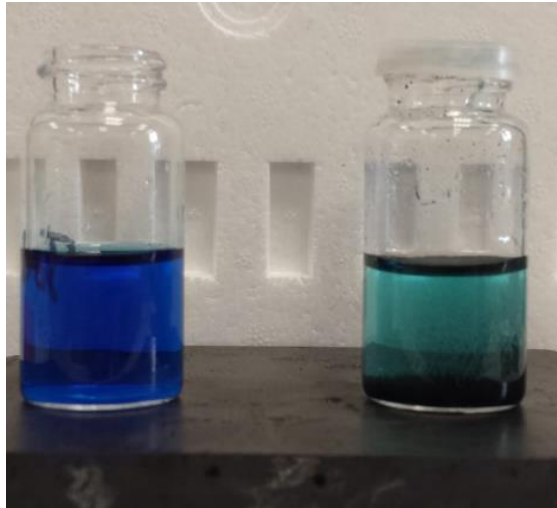
Methylene Blue Solution A against Product D (Start)



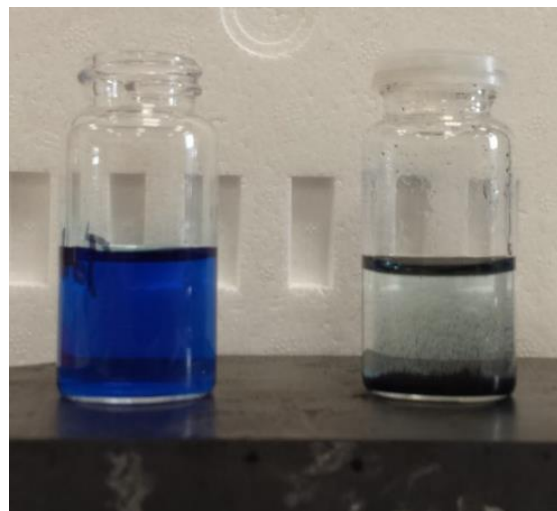
Methylene Blue Solution A against Product D (End)



Methylene Blue Solution B against Product A (Start)



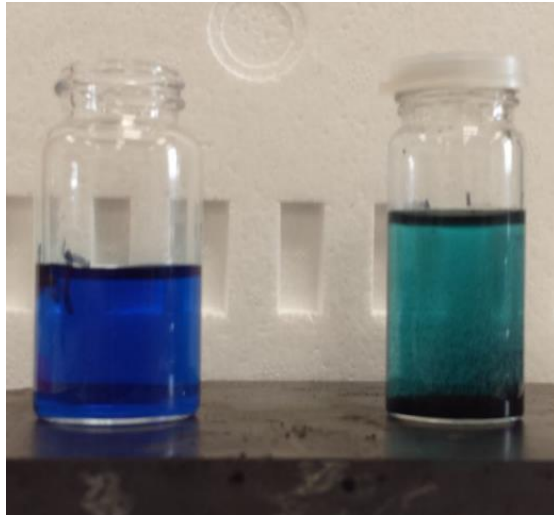
Methylene Blue Solution B against Product A (10 Minute Mark Transition):



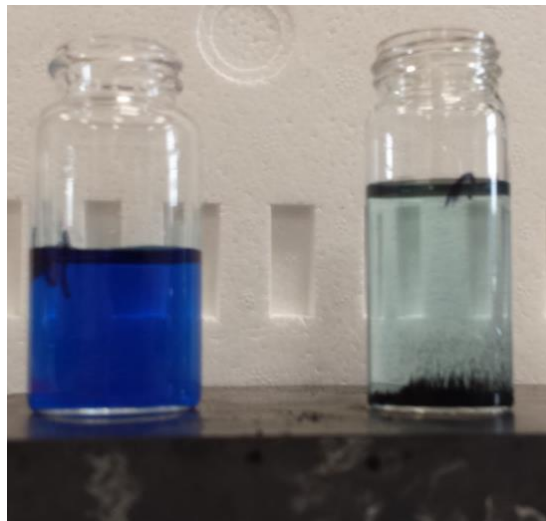
Methylene Blue Solution B against Product A (End):



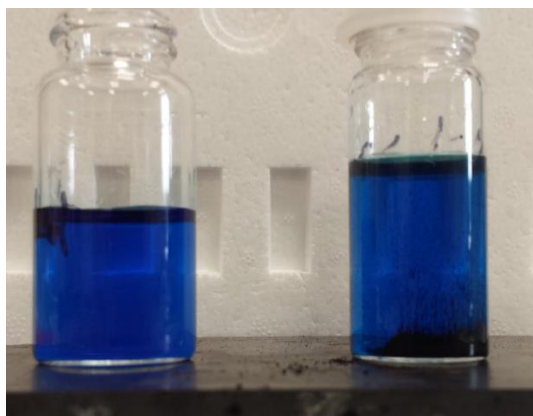
Methylene Blue Solution B against Product B (Start)



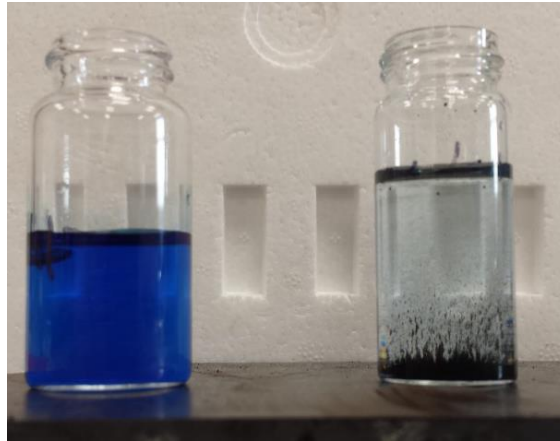
Methylene Blue Solution B against Product B (10 Minute Mark Transition)



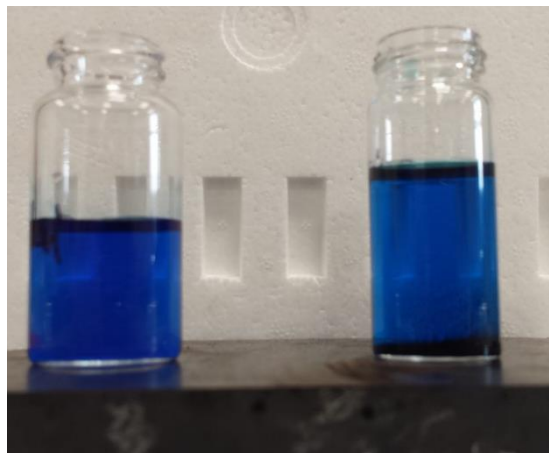
Methylene Blue Solution B against Product B (End)



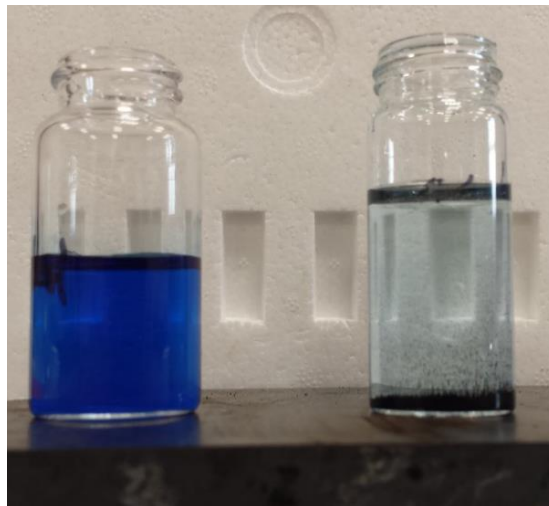
Methylene Blue Solution B against Product C (Start)



Methylene Blue Solution B against Product C (End)



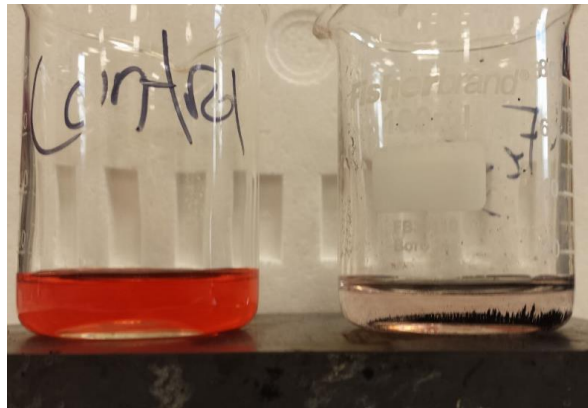
Methylene Blue Solution B against Product D (Start)



Methylene Blue Solution B against Product D (End)



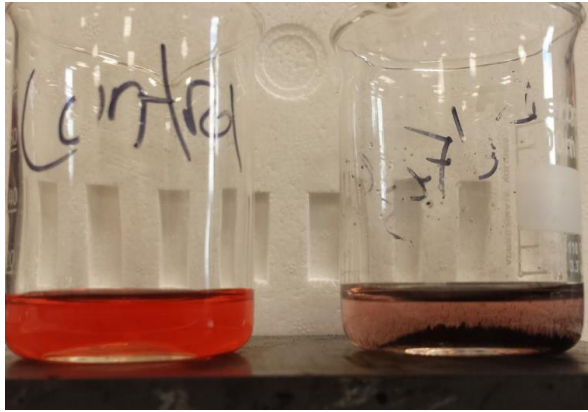
Congo Red Solution A against Product A (Start)



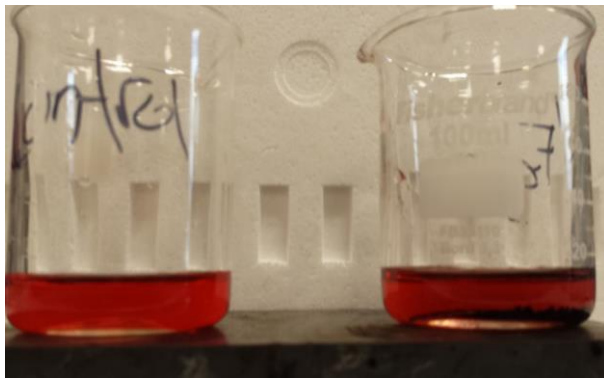
Congo Red Solution A against Product A (End)



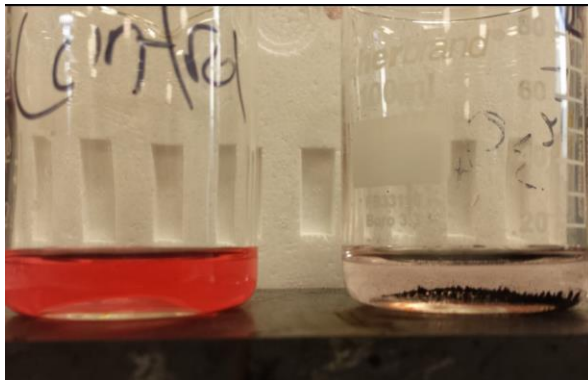
Congo Red Solution A against Product B (Start)



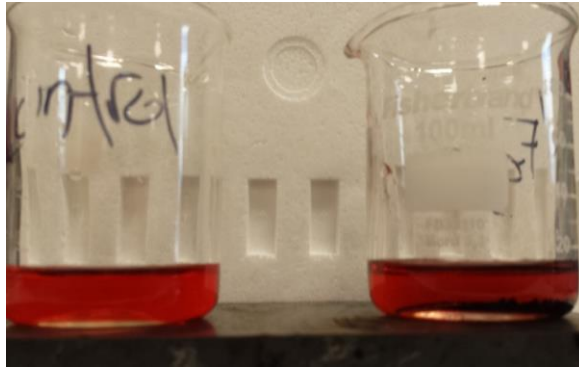
Congo Red Solution A against Product B (End)



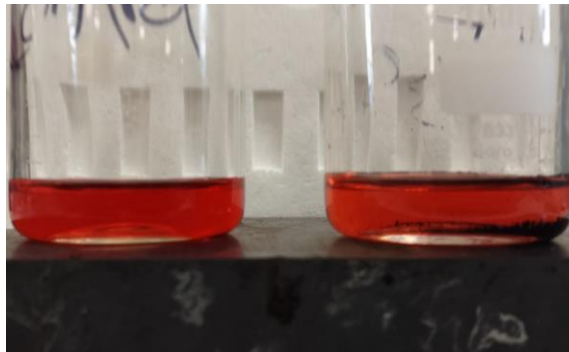
Congo Red Solution A against Product C (Start)



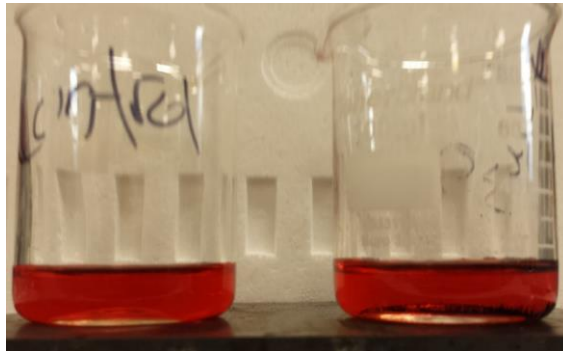
Congo Red Solution A against Product C (End)



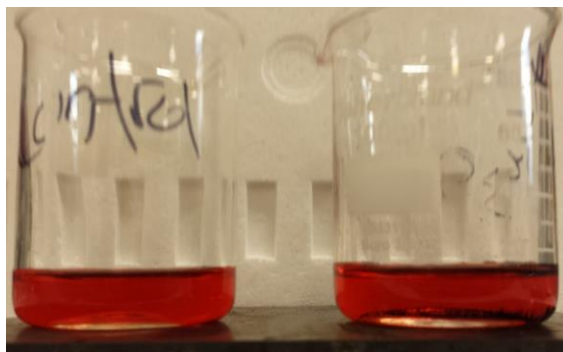
Congo Red Solution B against Product A (Start)



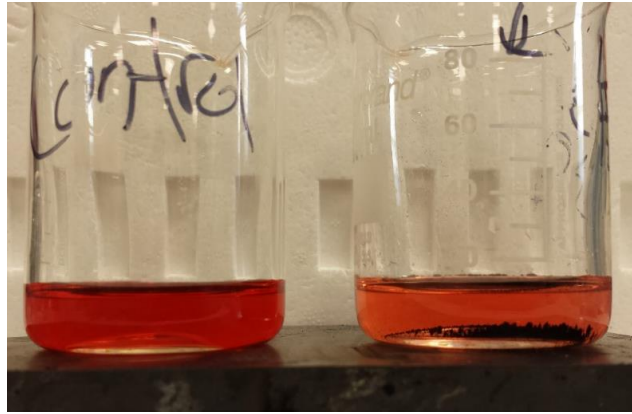
Congo Red Solution B against Product A (End)



Congo Red Solution B against Product B (Start)



Congo Red Solution B against Product C (Start)



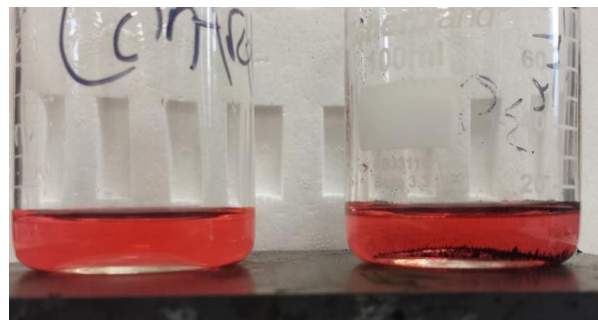
Congo Red Solution B against Product C (End)



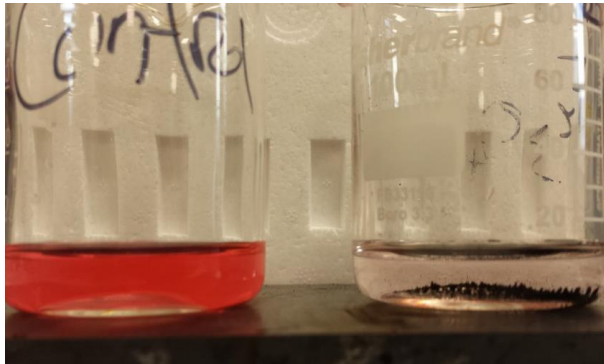
Congo Red Solution B against Product D (Start)



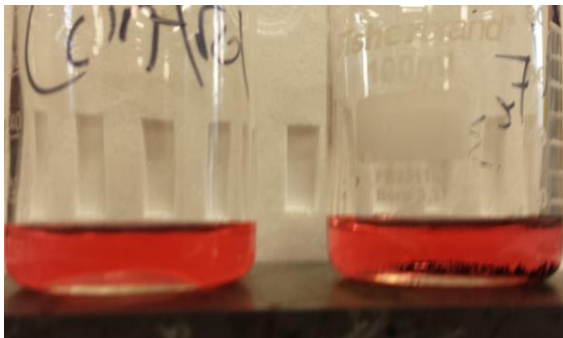
Congo Red Solution B against Product D (End)



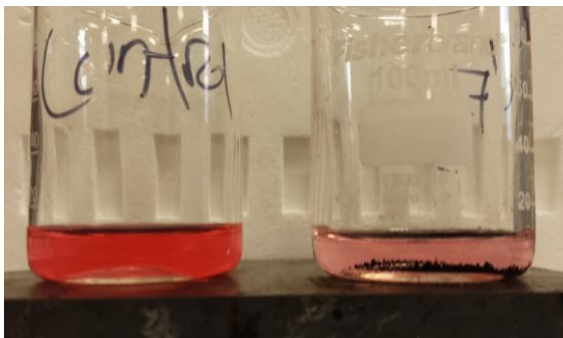
Allura Red AC Solution A against Product A (Start):



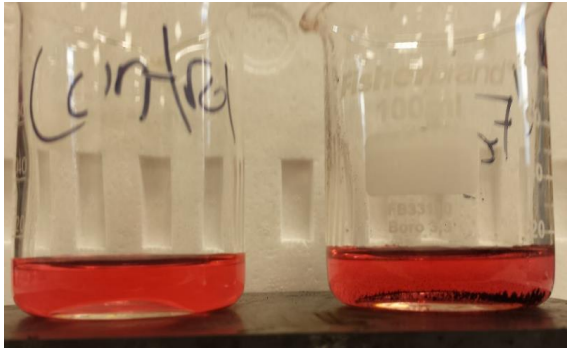
Allura Red AC Solution A against Product A (End)



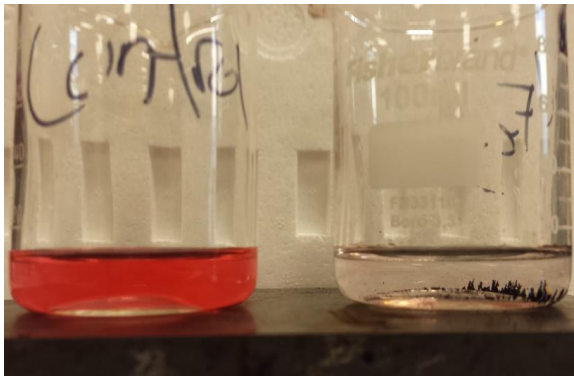
Allura Red AC Solution A against Product B (Start)



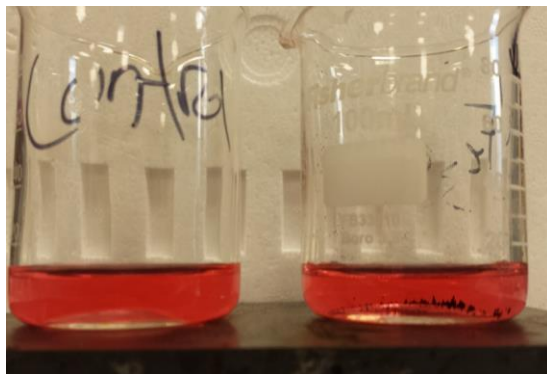
Allura Red AC Solution A against Product B (End)



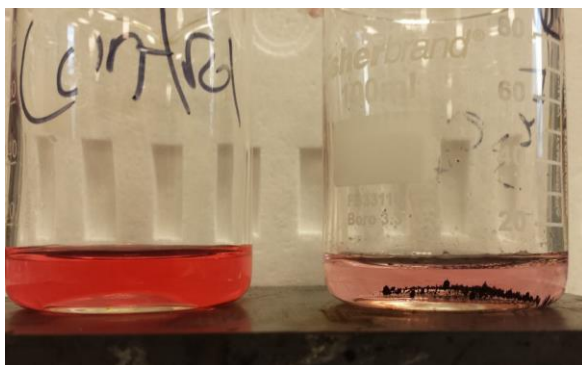
Allura Red AC Solution A against Product C (Start)



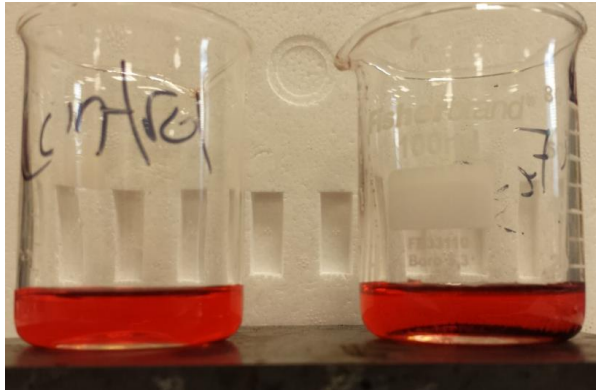
Allura Red AC Solution A against Product C (End)



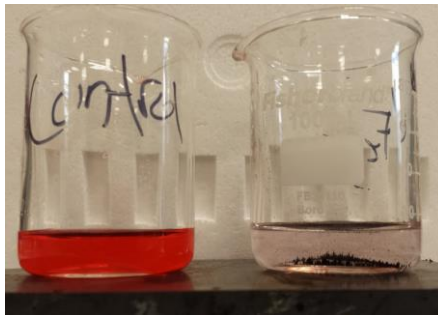
Allura Red AC Solution A against Product D (Start)



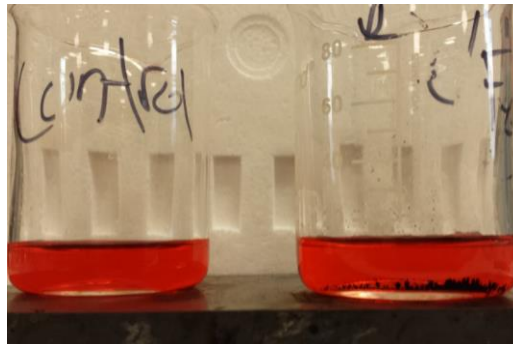
Allura Red AC Solution A against Product D (End)



Allura Red AC Solution B against Product A (Start)



Allura Red AC Solution B against Product A (End)



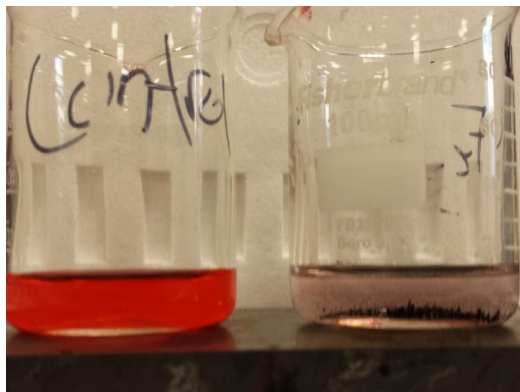
Allura Red AC Solution B against Product B (Start)



Allura Red AC Solution B against Product B (End)



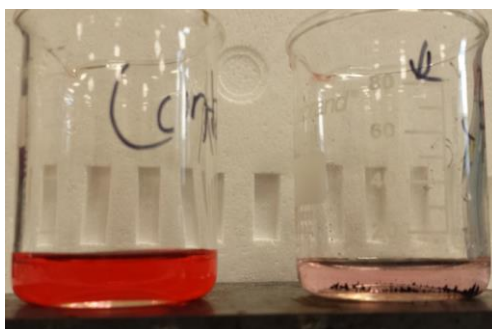
Allura Red AC Solution B against Product C (Start)



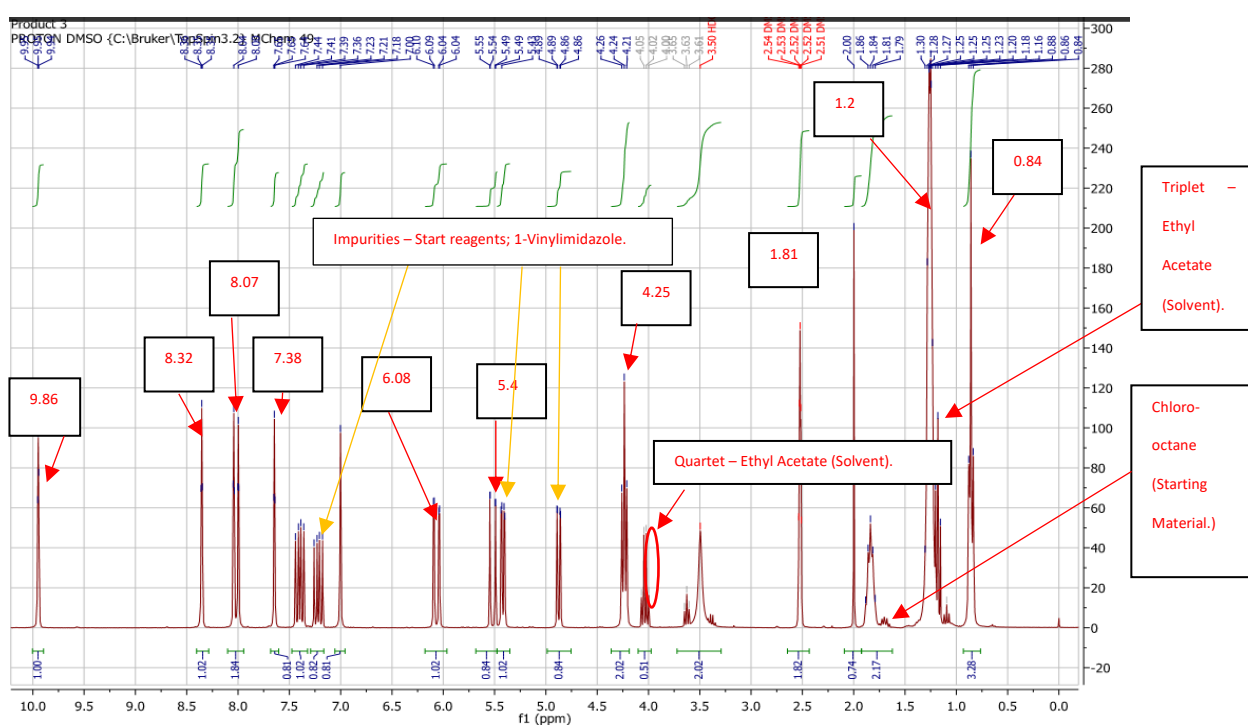
Allura Red AC Solution B against Product C (End)



Allura red AC Solution B against Product D (Start)



Allura Red AC Solution D against Product D (End):

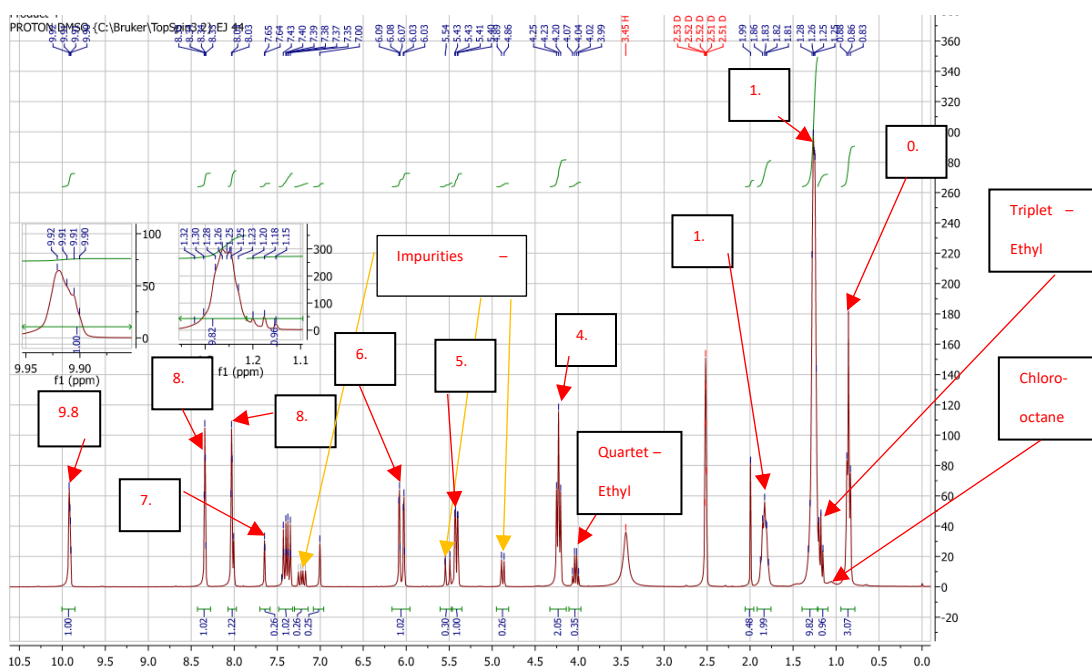


### <sup>1</sup>H NMR Of Ionic Liquid - 1-Vinyl-3-octylimidazole

Literary 1-Vinyl-octylimidazole H-NMR (DMSO-d<sub>6</sub>, d ppm): 9.86 (1H), 8.32 (1H), 8.07 (1H), 7.38 (1H), 6.08 (1H), 5.40 (1H), 4.25 (2H), 1.81 (2H), 1.20 (10H), 0.84 (3H).

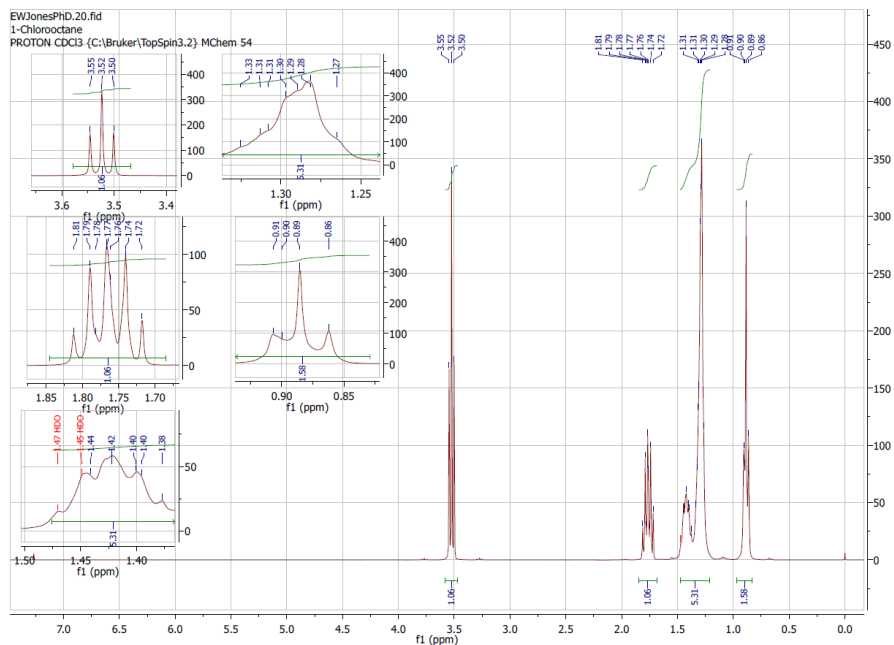
Actual Values: 9.95 (1H), 8.35(1H), 7.65 (1H), 6.06 (2H), 5.5 (2H), 4.25 (3H), 1.9 (3H), 1.25 (10H), 0.86 (3H).

# <sup>1</sup>H NMR Of Ionic Liquid - 1-Vinyl-octylimidazole

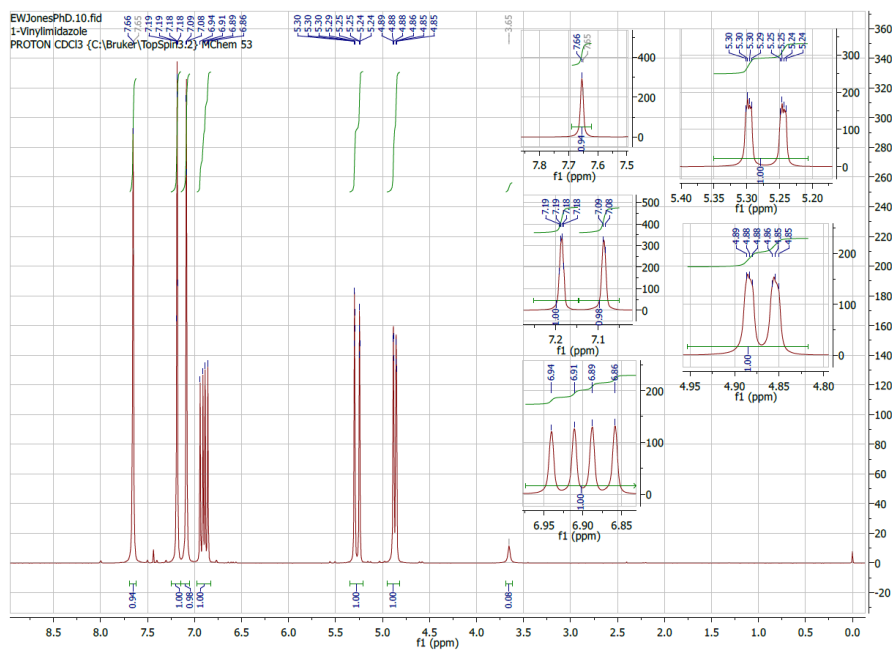


Literary 1-Vinyl-octylimidazole H-NMR (DMSO-d<sub>6</sub>, d ppm): 9.86 (1H), 8.32 (1H), 8.07 (1H), 7.38 (1H), 6.08 (1H), 5.40 (1H), 4.25 (2H), 1.81 (2H), 1.20 (10H), 0.84 (3H).

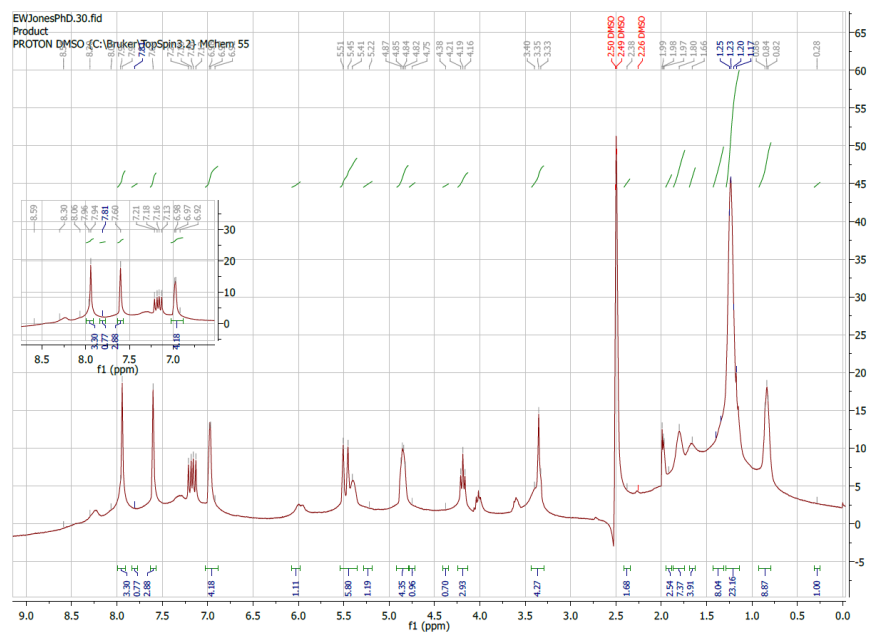
Actual Values: 9.95 (1H), 8.35(1H), 7.65 (1H), **6.06 (2H)**, **5.5 (2H)**, **4.25 (3H)**, **1.9 (3H)**, 1.25 (10H), 0.86 (3H).



$^1\text{H}$ NMR 1-Chloro-octane

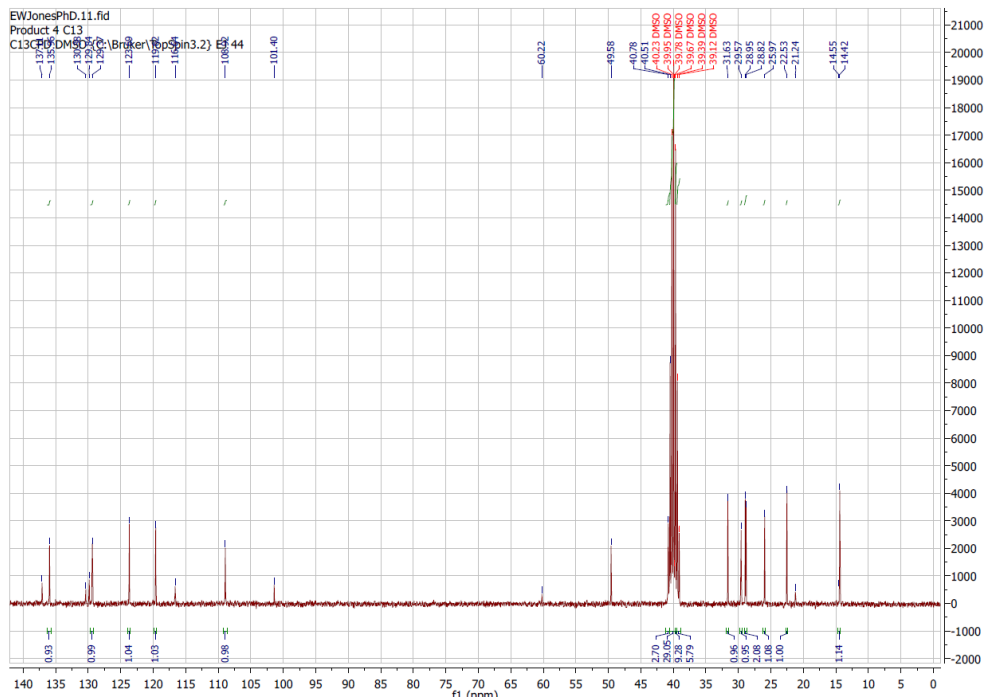


$^1\text{H}$ NMR 1-Vinylimidazole

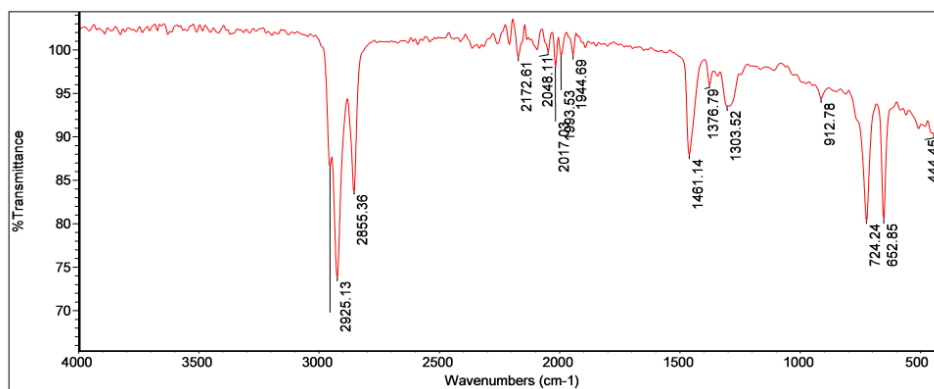


<sup>1</sup>H NMR Ionic Liquid (1-Vinyl-3-octylimidazole) Failed Product

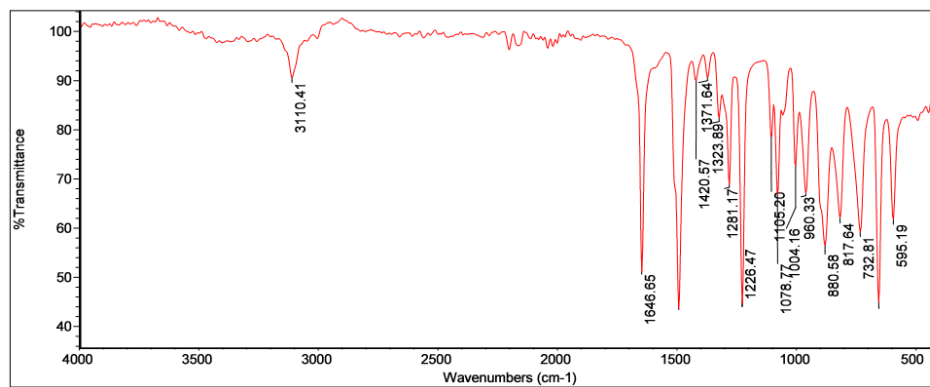




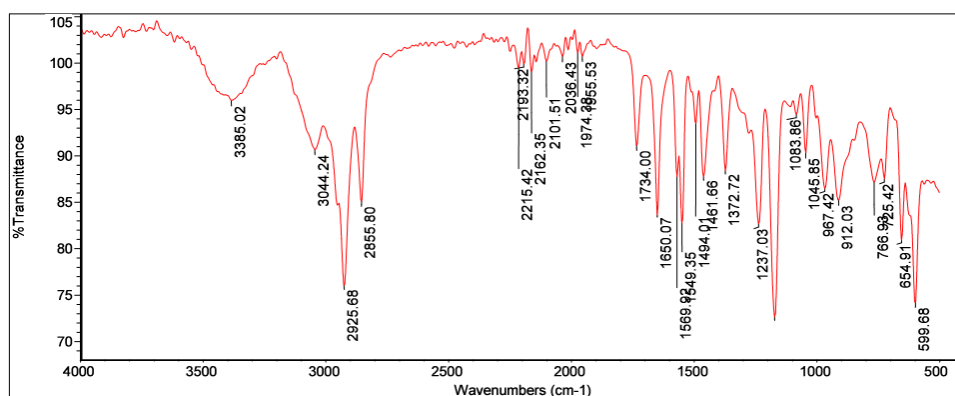
<sup>13</sup>C NMR Ionic Liquid (1-Vinyl-3-octylimidazole).



FT-IR of 1-Chlorooctane.



FT-IR 1-Vinylimidazole.



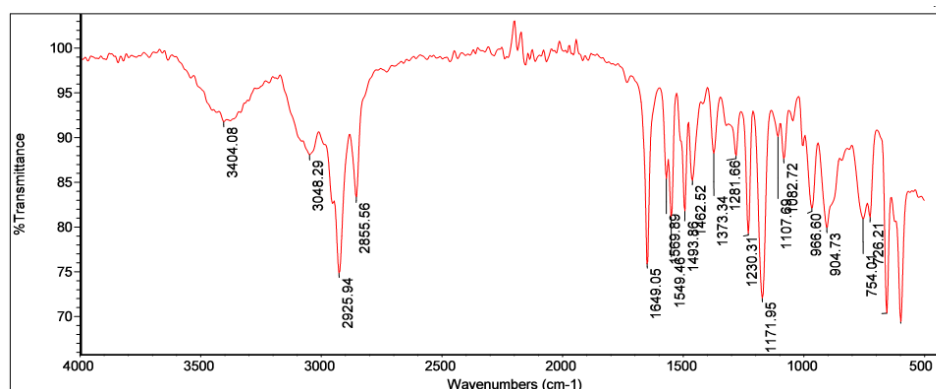
FT-IR 1-Vinyl-octilimidazole.

The bands at  $2925.68\text{ cm}^{-1}$  are assignable to saturated and unsaturated C–H stretching vibrations of  $\text{CH}_2$  (From the octyl chain.)

The band at  $3044.24\text{ cm}^{-1}$  is assignable to an H attached to a Nitrogen (N-H) of the imidazole ring.

The band at  $3385.02$  is assignable to an H attached to a Nitrogen (N-H) of the imidazole ring.

For the imidazolium-IL the bands at  $2865\text{ cm}^{-1}$  is for the aliphatic C–H bending vibration, and  $1549$  and  $1464\text{ cm}^{-1}$  are indicative of the imidazole ring skeleton. In addition, the  $1083\text{ cm}^{-1}$  peak is the imidazole ring C–H bond plane bending vibration.



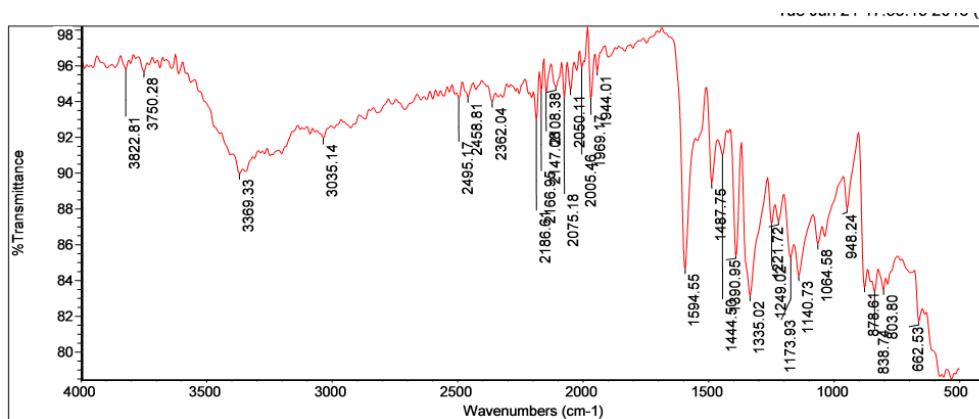
FT-IR 1-Vinyl-octilimidazole

The bands at  $2925.94\text{ cm}^{-1}$  are assignable to saturated and unsaturated C–H stretching vibrations of  $\text{CH}_2$  (From the octyl chain.)

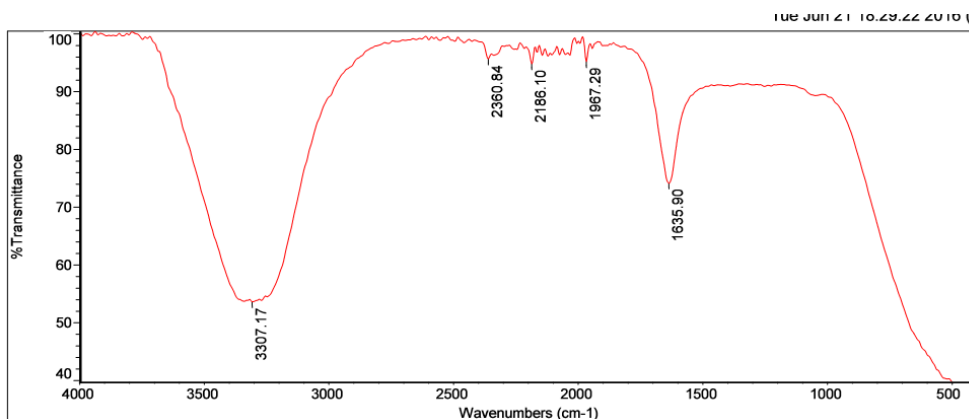
The band at  $3048.29\text{ cm}^{-1}$  is assignable to an H attached to a Nitrogen (N-H) of the imidazole ring.

The band at 3385.02 is assignable to an H attached to a Nitrogen (N-H) of the imidazole ring.

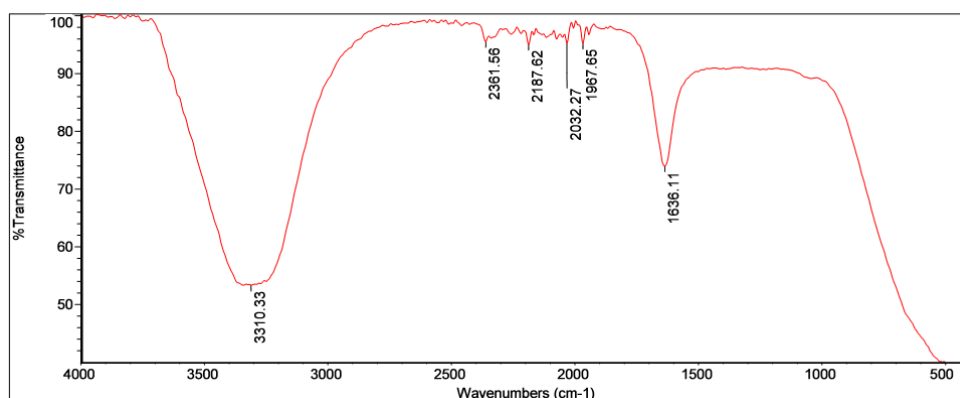
For the imidazolium-IL the bands at 2865  $\text{cm}^{-1}$  is for the aliphatic C-H bending vibration, and 1649.05 and 1493  $\text{cm}^{-1}$  are indicative of the imidazole ring skeleton. In addition, the 1083  $\text{cm}^{-1}$  peak is the imidazole ring C-H bond plane bending vibration.



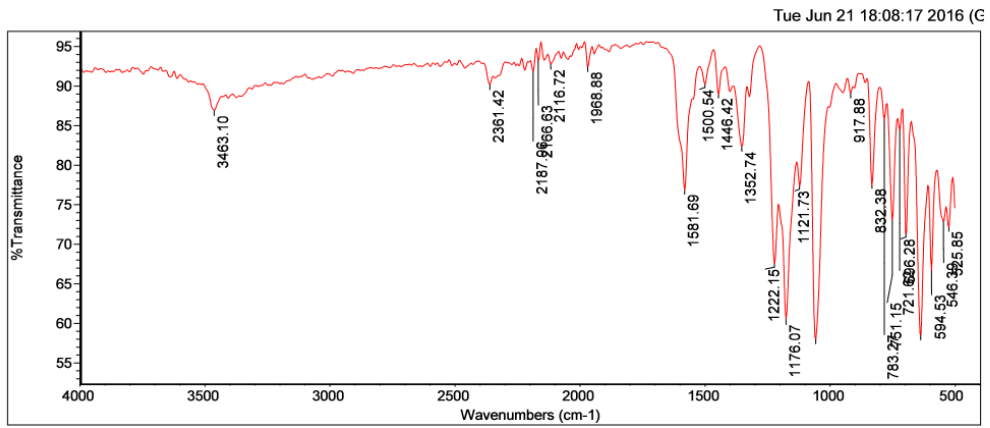
FT-IR Methylene Blue Solid.



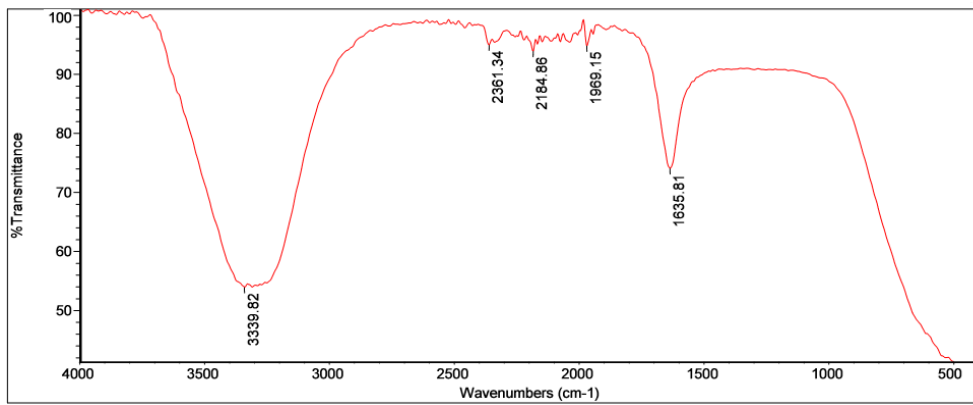
FT-IR Methylene Blue Solution B (1.5 Absorbance).



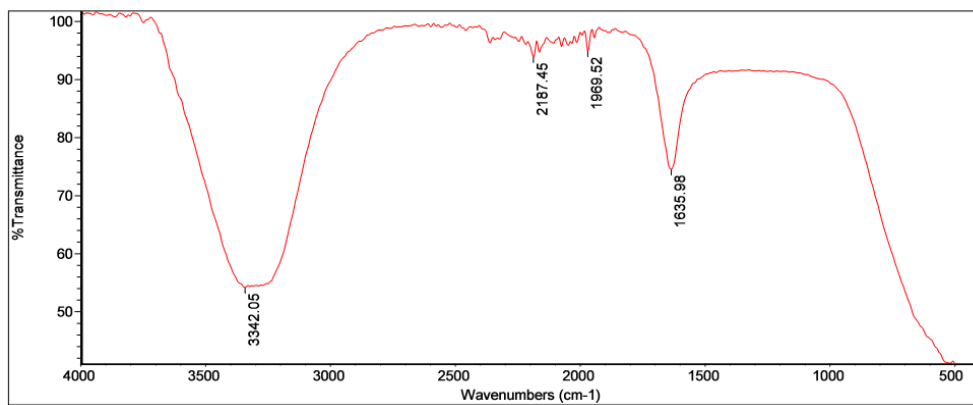
### FT-IR Methylene Blue Solution B (1.5 Absorbance).



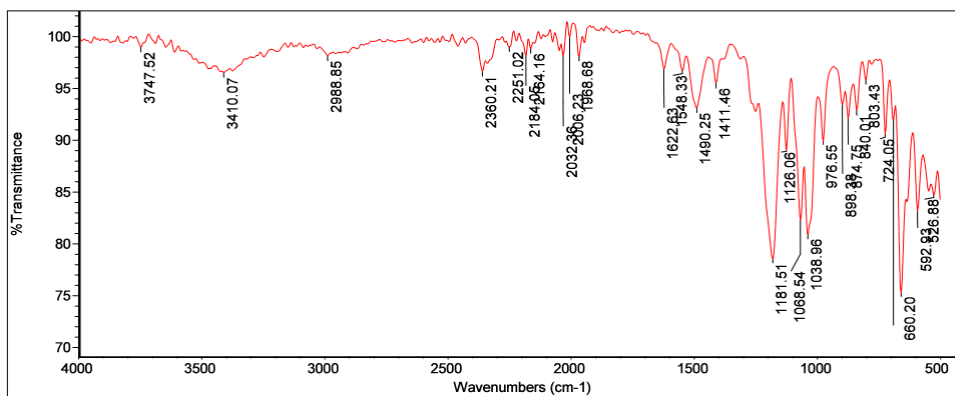
### FT-IR Congo Red Solid.



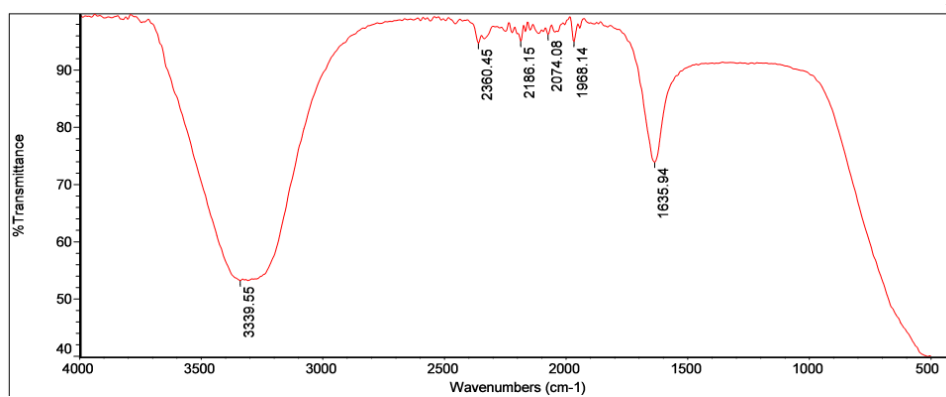
### FT-IR Congo Red Solution B (1.5 Absorbance).



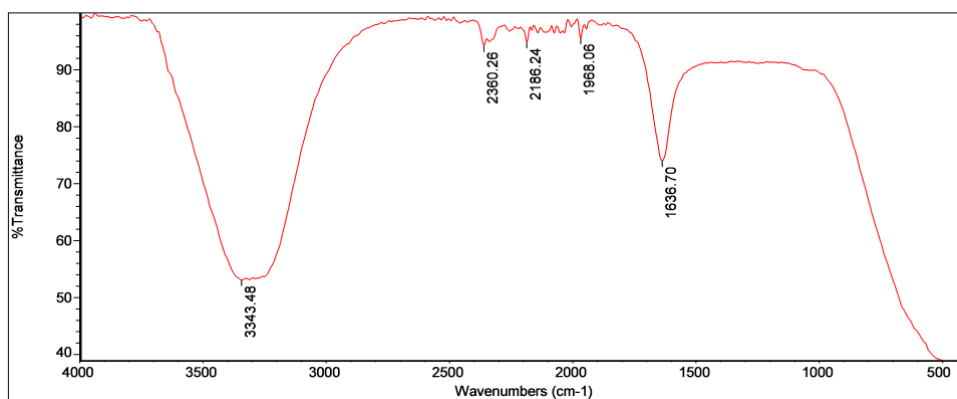
### FT-IR Congo Red Solution A (0.5 Absorbance)



FT-IR Allura Red AC Solid.



FT-IR Allura Red AC Solution B (1.5 Absorbance).



FT-IR Allura Red AC Solution A (0.5 Absorbance).